INFORMATION TO USERS

This manuscript has been reproduced from the microfilm master. UMI films the text directly from the original or copy submitted. Thus, some thesis and dissertation copies are in typewriter face, while others may be from any type of computer printer.

The quality of this reproduction is dependent upon the quality of the copy submitted. Broken or indistinct print, colored or poor quality illustrations and photographs, print bleedthrough, substandard margins, and improper alignment can adversely affect reproduction.

In the unlikely event that the author did not send UMI a complete manuscript and there are missing pages, these will be noted. Also, if unauthorized copyright material had to be removed, a note will indicate the deletion.

Oversize materials (e.g., maps, drawings, charts) are reproduced by sectioning the original, beginning at the upper left-hand corner and continuing from left to right in equal sections with small overlaps. Each original is also photographed in one exposure and is included in reduced form at the back of the book.

Photographs included in the original manuscript have been reproduced xerographically in this copy. Higher quality 6" x 9" black and white photographic prints are available for any photographs or illustrations appearing in this copy for an additional charge. Contact UMI directly to order.

UMI

A Bell & Howell Information Company
300 North Zeeb Road, Ann Arbor MI 48106-1346 USA
313/761-4700 800/521-0600

KINETICS OF OCTADECYLTRICHLOROSILANE SELF-ASSEMBLY ON SILICON OXIDE SURFACES: AN EXPERIMENTAL AND NUMERICAL STUDY

by

SRINIVASAN KRISHNAN

A dissertation submitted to the Graduate Faculty in Engineering in partial fulfillment of the requirements for the degree of Doctor of Philosophy, The City University of New York

1999

This manuscript has been read and accepted for the Graduate Faculty in Engineering in satisfaction of the dissertation requirement for the degree of Doctor of Philosophy.

1/28/99 — Alexander Couzis

Date — Professor Alexander Couzis, Chair of Examining Committee

1/28/1999 — Mumtaz K. Kassir

Date — Professor Mumtaz K. Kassir, Acting Executive Officer

Professor Charles Maldarelli

Professor Leslie Isaacs

Professor Carol Steiner

Professor Chris Durning

Supervisory Committee

THE CITY UNIVERSITY OF NEW YORK

Om Sai Ram

To the memory of my beloved grandmother, Mrs. K.A. Mangalam

ABSTRACT

KINETICS OF OCTADECYLTRICHLOROSILANE SELF-ASSEMBLY ON SILICON OXIDE SURFACES: AN EXPERIMENTAL AND NUMERICAL STUDY

by

Srinivasan Krishnan

Advisor: Dr. Alexander Couzis

In this work, we present and discuss the results of our *in-situ* study on the kinetics and mechanism of self-assembly of octadecyltrichlorosilane (OTS) onto a silicon oxide surface. FTIR-ATR is the technique used to monitor the self-assembly process. The surface coverage of the adsorbing OTS, Γ_{ads}, is determined using the molar absorptivity of adsorbed OTS, ε_{ads}. The rate of adsorption and the final Γ_{ads} increase with increasing concentration of OTS, and also with increasing flow rate of the OTS solution over the silicon ATR surface. The effects of water, both at the substrate surface and in the solvent are investigated. We present proof of the ordering occurring in the adsorbing layer. First, the position of the absorption peak, characteristic of the asymmetric -CH- stretch of the -CH_2- moiety in the adsorbate shifts to lower wavenumber with increase in time. In addition, *in-situ* polarized FTIR-ATR data of OTS self-assembly offers evidence for the changes occurring in the conformation and ordering of the adsorbate molecules at the solid/liquid interface. The crystalline ordering occurring in the adsorbing layer, as evidenced by the shift in the peak position, is also supported by the crystalline split occurring in the -CH_2- bending moment at 1460 cm^{-1}. By using a silicon wafer

sandwiched to a germanium ATR crystal we extend the useful spectral range beyond 1600 cm^{-1}.

Also for the first time, we have described the adsorption over the entire time scale of our experiment with a single mathematical model. This model accounts for an activation energy for adsorption, $(E_A)_{ads}$, that varies as a function of the surface coverage. The dependence of $(E_A)_{ads}$ on Γ_{ads} is due to the interactions between the hydrocarbon chains of the surfactant molecules on the solid surface. As a result every incoming surfactant molecule has to overcome an increasingly larger energy barrier in order to adsorb onto the substrate. This energy barrier, which is dependent on the surface coverage, assigns a probability for the adsorption of an incoming surfactant to the substrate surface, with the probability being the greatest at the beginning of the process and decreasing as the surface coverage increases.

Acknowledgements

During my stay at the City College of New York pursuing my doctorate degree, there have been a number of people that have contributed to the success of this thesis. As a starting point, I would like to express my gratitude to Dr. Alexander Couzis, my mentor for his constant encouragement, support and advice. He has been easily approachable and his advice, be it professional or personal has always been available. I am also indebted to Dr. Charles Maldarelli for his valuable suggestions and encouragement throughout my doctoral study.

Thanks are also due to the rest of the students in the research group, and in particular to Rajeev Subramanyam for many useful discussions about research.

I would also like to thank my parents, Usha and Venkatraman Srinivasan. Without their love, sacrifice, the values they inculcated in their children, and their constant support, especially when separated by such a large distance, I would have accomplished very little in my life. My brother, Balaji deserves a special word of thanks for always being there to talk to and sort difficult matters out. His outrageous sense of humor has often provided comic relief in many a stressful situation.

Last, but certainly not the least, thanks are due to all my friends at the temples in Flushing, New York. Their support and encouragement have been a great source of moral strength during the entire duration of my doctoral study. They have enabled me to have enjoy the comforts of a home away from home.

Contents

List of Figures

List of Tables

Chapter 1 Adsorption of Surfactants at Solid/Liquid Interfaces

1.1 Introduction

The surface properties of a material control the extent of its interaction with its surroundings. Most often, it is difficult to find materials with the right combination of bulk and surface properties. It is under these circumstances that the modification of a material's surface properties gains importance. One of the earliest techniques adopted to modify surfaces involves the coating of a substrate surface with another material that possesses the required surface properties. Coating of a surface can be achieved via a number of methods of which one is adsorption from solution. The technological, environmental and biological importance of adsorption of organic material such as surfactants or polymers from solution onto a solid surface cannot be overestimated. When a surfactant molecule adsorbs at a solid/liquid interface, there are various phenomena occurring at the interface that include competing intermolecular, molecular-substrate and molecular-solvent interactions, which affect ordering & growth of the adsorbing layer, and the resultant adhesion and wetting properties of the modified surface.

The impact of such phenomena on our everyday lives is obvious in areas such as food science, packaging, detergency, the extraction of petroleum resources, lubrication, the use of paints, inks, adhesives and protective coatings, magnetic recording media, optics, delayed drug release and artificial organs in medicine. Each of these applications, and many more that involve the stability of colloidal dispersions, modification of solid surfaces for the control of wetting and lubrication, would be difficult if not impossible in the absence of the effect of adsorbed polymers, surfactants and stabilizers at the solid-

liquid interface. The presence of these materials on the solid-liquid interface can alter significantly phenomena related to wetting, adhesion, lubrication, friction, wear, and corrosion. Additionally, the adsorption of surfactants and polymers can greatly affect subsequent rewetting properties (fabric waterproofing, car waxes), electrical properties (antistatic agents and fabric softeners), or the ability of the solid surface to adsorb other solutes (dyeing modifiers). Surfactant systems that offer us the ability to achieve these goals have recently been the focus of intense research. Self-assembled monolayers or SAMs have in particular, attracted a great deal of attention due to their reasonably well ordered structure in spite of the simple procedures required to produce them.

1.2 Self-Assembled Monolayers

Self-assembled monolayers are molecular assemblies that are formed spontaneously when certain surfactant molecules chemisorb from solution onto an appropriate solid substrate and form ordered assemblies on it. The first study on SAMs was reported in 1947 by Zisman[1], who observed that dilute solutions of eicosyl alcohol in n-hexadecane did not wet the walls of the Pyrex, glass-stoppered, flask. This was an indication that the surface of the flask had been modified. However, it wasn't until the pioneering work done by Sagiv and his coworkers[2-6], who studied OTS adsorption onto hydroxylated surfaces, that interest in SAMs exploded. The formation of these SAMs is driven by three primary energetic contributions[7]. First among these is the strong interaction of the surfactant head group with the adsorbing substrate resulting in chemisorption, the most exothermic process. These very strong molecular-substrate interactions result in an apparent pinning of the head group to a specific site on the surface of the substrate. These interactions can be one of the following types:

- A covalent Si-O linkage in the case of alkyltrichlorosilanes on hydroxylated surfaces.
- A covalent, but slightly polar, Au-S bond in the case of alkyl thiols on gold
- An ionic $-CO_2^-Ag^+$ bond in the case of carboxylic acids on AgO/Ag or Al_2O_3.

The energy associated with chemisorption is of the order of tens of kcal/mol. As a result of the exothermic head group-substrate interactions, molecules try to occupy every available binding site on the solid surface, and in the process they push together molecules that are already on the surface. The second of these energy contributions is the van der Waals interaction of the alkyl chain, which is of the order of a few (<10) kcal/mole. The last of these energy contributions is due to the surfactant's terminal functionality, which in the case of a simple alkyl chain is just a methyl (CH_3) group. These groups are thermally disordered at room temperature. The energy (~0.7 kcal/mol) associated with this interaction is much smaller than the other contributions (of the order of a few kTs, k: Boltzman's constant; T: Absolute temperature). These forces are schematically represented in figure 1.1.

There are three main types of SAMs that have attracted the interest of researchers. These include carboxylic acids on native oxidized silver[8] and aluminum oxide surfaces[9,10], alkyl thiols on gold surfaces[11], long chain siloxanes on hydroxylated surfaces (i.e.) SiO_2/Si, Al_2O_3/Al, glass[2,12], chemically treated mica[13]. In particular, SAMs of organosilane compounds on solid substrates like silica[2] offer an elegant approach to the design of molecularly sized microstructures. As a result, SAMs have been investigated for use as ion-selective membranes[14-16], in the fabrication of bio-sensor arrays[16-18], in friction control[19,20], in adhesion promotion[21], and as surface coupling agents in the treatment of silica for chromatographic applications[22]. In order to

realize these applications on an industrial level, we need to have control over the ordering in our adsorbing layers. However, with most of the techniques presently available, there exists the problem of multilayer formation. This results in reduced ordering in the adsorbed layers. Hence, our ability to use them for the various applications detailed earlier is also reduced. However, by appropriately modifying both the head and tail groups of these self-assembling surfactant molecules, we can get a fundamental understanding of these phenomena. As a result, we can precisely engineer the surface properties of materials for applications like bio-sensing, non-linear optics, in the manufacturing of molecular scale electronic devices and permeation membranes. In the next section we give a brief overview of the procedure for making organosilane SAMs on hydrophilic substrates.

1.3 Preparation of Self Assembled monolayers of OTS on solid substrates

Sagiv[2] reported the first study on self-assembled monolayers of octadecyltrichlorosilane on a hydroxylated silicon substrate. A typical procedure for formation of these SAMs involves immersing a hydroxylated substrate with surface hydroxyl groups in a dilute solution of OTS (~1mM). It is important to note that the cleanliness of the substrate plays an important role in the quality of the monolayer. After a certain amount of time, the substrate is withdrawn and either rinsed in other solvents or wiped with a Kimwipe® tissue, presumably to remove the excess OTS that is physisorbed on the substrate surface. With most of the techniques presently available for producing SAMs, one must adopt some of these post treatment procedures to remove the excess layers. The procedure for *ex-situ* analysis of SAMs is schematically represented in figure 1.2.

One of the immediate effects of the OTS adsorption is the drastic change in the wettability of the surface. Hydrophilic surfaces modified with SAMs of silanes, when withdrawn from the solution are not only hydrophobic, but are also autophobic (i.e.) they emerge dry from the deposition solution. It has been suggested that during adsorption, Si-Cl bonds react with the OH groups on the surface of the SiO_2/Si substrates[23] (and with trace amounts of water which we know is adsorbed on the hydrophilic silanol surface[24]) to form a network of Si-O-Si bonds[25]. The early studies by Sagiv et al.[2,4-6] suggested that the OTS molecules bind to the silanol sites on the surface of the substrate in addition to cross linking amongst themselves. This structure is schematically represented in figure 1.3a. However, this picture has changed considerably in recent years[26-28] and it is now believed that the OTS molecules do not form a bond with every silanol molecule on the surface. Instead, they react with the layer of water that is physisorbed onto the silicon surface, and they are anchored to the substrate surface only at a few points. This view is schematically represented in figure 1.3b.

Most of the studies on organosilane SAMs have focussed on the chemical and physical interactions that control the formation, structure, and properties of these molecular assemblies[2,29-32]. These SAMs are affected by factors such as deposition time, substrate cleanliness, substrate hydration and several other process conditions. These are reviewed in greater detail in chapter 4. However, very little is known about the mechanism of formation and growth of organosilane SAMs. Kinetic studies offer considerable insight into the growth mechanism of SAMs.

The kinetics of alkanethiol adsorption on gold[33-35] and those of carboxylic acids onto glass and aluminum substrates[36,37] have been very widely studied. It has been found

that the final coverage of the monolayer on the substrate is dependent on various factors such as solvent, surfactant concentration, quality of substrate, and the deposition time. In addition, the rate of adsorption is found to depend on the concentration of the surfactants in the bulk solution. The adsorption seems to occur in two stages, an initial rapid adsorption of an imperfect assembly followed by a much slower second stage during which the disordered structure reorganizes into a more perfectly ordered monolayer[11]. Most authors[36,37] [33,34] have used the Langmuir kinetics model to describe the self-assembly process. These studies are reviewed in detail in chapter 5.

In comparison to the thiols and carboxylic acids system, it is surprising that there are very few kinetic studies that have been reported on OTS adsorption onto hydroxylated surfaces. The chlorosilane SAM system has always been a difficult system to study due to several reasons. The primary difficulty lies in the extremely high reactivity of the chlorosilane groups, both in the bulk solution and at the interface, and this is discussed in the following sections.

1.4 Reactivity of siloxane surfactants in solution

The hydrolysis of trisiloxane surfactants in the bulk was studied by Kessel et al.[38], and is shown below

$$C_{18}H_{37}-\underset{|}{\overset{|}{Si}}-Cl+H_2O\xrightarrow{k_1}C_{18}H_{37}-\underset{|}{\overset{|}{Si}}-OH+HCl \qquad (1.1)$$

$$C_{18}H_{37}-\underset{|}{\overset{|}{Si}}-Cl+HO-\underset{|}{\overset{|}{Si}}-C_{18}H_{37}\xrightarrow{k_2}C_{18}H_{37}-\underset{|}{\overset{|}{Si}}-O-\underset{|}{\overset{|}{Si}}-C_{18}H_{37}+HCl \qquad (1.2)$$

$$C_{18}H_{37}-\underset{|}{\overset{|}{Si}}-OH+HO-\underset{|}{\overset{|}{Si}}-C_{18}H_{37}\xrightarrow{k_3}C_{18}H_{37}-\underset{|}{\overset{|}{Si}}-O-\underset{|}{\overset{|}{Si}}-C_{18}H_{37}+H_2O \qquad (1.3)$$

It is apparent that, in the case of siloxane surfactants there is reaction of the active surfactant, not only at the substrate surface but also in the bulk. Hence, it can be seen that the ability to obtain non-cross-linked silanols will depend on the relative rates of the three reactions. If k_2 and k_3 are very small relative to k_1, then it might be possible to obtain a solution of silanetriol/trisilanol that would have a finite useful time for use in self-assembly work. In the case of chlorosilanes, steps one and two result in production of acid, which catalyses the subsequent reactions and leads to gel formation very quickly[38]. Thus, it is necessary for us to have a greater control over the water content in the system, especially in the case of the trichlorosilane surfactants. Various research groups have also studied the hydrolysis/condensation of the siloxane molecules at the air/water interface and these results are discussed in the following section.

1.5 Hydrolysis and Condensation of Siloxane surfactants at air/water interface

Langmuir films of different amphiphiles have traditionally been used to study different molecular transitions at the liquid/vapor phase boundary[39]. The kinetics of polymerization reactions was first studied by this technique by Beredjick et al.[40] Until recently, Si29NMR technique was mostly used to map the hydrolysis and condensation reactions of alkoxide silanes[41] in bulk solutions. Recently[42-44] the Langmuir technique has been used to study the hydrolysis and condensation of organosilanes at the air water interface.

The polymerization of triethoxysilane amphiphiles at the air-water interface was reported for the first time by Ariga et al[42]. The authors spread a monolayer of the surfactant at the air-water interface, and monitored the shape of the π-A isotherm at various subphase pH values. They found that there was a radical change in the shape of

the isotherm as the subphase was made more acidic. While the isotherms revealed the existence of a liquid expanded-liquid condensed (LE-LC) coexistence region at a pH of 5.6, there was none at a pH of 2, indicating that the amphiphiles had polymerized on the surface, and were incapable of undergoing a phase transition.

The hydrolysis and condensation of alkylmethoxysilanes at the air/water interface has recently been reported by Sjöbolm et al.[44] They used the Langmuir Blodgett technique[39] to monitor the kinetics of these reactions by spreading octadecyltrimethoxysilane(ODTMS) and octadecyldimethoxysilane (ODDMS) from a solution of chloroform on an aqueous subphase whose pH was varied. They then compressed the monolayer to a preset surface pressure, and then recorded the relaxation in area due to the polymerization on the surface. The hydrolysis and condensation reactions varied with pH. They also found that ODTMS, which could form trimers, achieved a more condensed state than the ODDMS, which could form just dimers.

More recently, the 2-dimensional gelation of octadecyltrimethoxysilane ODTMS at the air/water interface has been reported by Lindén et al.[43] They studied the hydrolysis and condensation of monolayers of ODTMS as a function of pH by means of in-situ fluorescence microscopy, surface potential and compression isotherms. Condensation occurred immediately after the hydrolysis of the methoxy groups, and the time required before gelation varied between a couple of minutes at extreme pH values, to several hours at intermediate pH. In comparison to the alkoxysilanes, there have been few studies that have been reported on OTS hydrolysis and condensation at the air/water interface. Thus it is apparent that there is a great need to understand the kinetics of the self-

assembly of OTS. We report the results of our study on the kinetics of OTS hydrolysis and condensation at the air/water interface in chapter 3.

1.6 Kinetics of siloxane self-assembly on hydrophilic surfaces

Most of the kinetic studies that have been reported for OTS SAMs are for batch adsorption kinetics. In these experiments, the substrates are immersed in the deposition solution and withdrawn after a certain amount of time. These modified substrates are then characterized *ex-situ* using various techniques like FTIR, Ellipsometry, XPS and contact angle goniometry. Sagiv[2] reported adsorption isotherms by doing batch adsorption studies of OTS on ATR elements. He reported an increase in surface coverage with time and the existence of a critical bulk solution concentration for monolayer formation. In another batch adsorption study, Wasserman et al.[29] report the kinetics of adsorption of tetradecyltrichlorsilane (TTS) from a hexadecane solution. A plateau was reached in the adsorption of TTS after about 40 minutes. A fast initial rate of adsorption (~80%) was observed followed by a much slower rate of further adsorption of TTS at the surface until monolayer coverage is attained.

In most of the studies discussed above, *ex-situ* analysis of the substrate surface is performed before and after its modification to understand the self-assembly process. While *ex-situ* strategies obviously offer a measure of versatility, they leave to speculation the rates of reaction and the solution-surface interactions responsible for the observed results. In order to fully understand the self-assembly process, it is extremely important to study the adsorption process in the presence of the solvent. It will then be possible to see the effects, if any, that solute-solvent interactions may have on the self-assembly process. *In-situ* measurements have the advantage that they are conducted with the monolayer in

contact with the solvent/solution and thus eliminate the ambiguities associated with the removal and drying of surfaces. The *in-situ* studies of OTS self-assembly on hydroxylated planar surfaces that will be conducted in this project will help accomplish this.

A number of experimental techniques have been proposed over the years for the in-situ study of adsorption phenomena at the fluid-solid interface. These include attenuated total reflection Fourier transform infrared spectroscopy (ATR-FTIR),[45-49] atomic force microscopy,[50] second harmonic generation[51,52], sum frequency generation[53,54], quartz crystal microbalance[33,34], and surface plasmon resonance spectroscopy[35,55]. In this study we use attenuated total reflection spectroscopy, ATR-FTIR. This technique also referred to as internal reflection spectroscopy (IRS), is a method of obtaining the infrared spectrum of species located near the surface of a solid substrate. Harrick[56] first developed the method. Its capability is attributed to the presence of an evanescent wave of light that is created when total reflection occurs at the interface of two materials with different indices of refraction. This technique, when utilized in in-situ measurements, has the distinct advantage of identifying spectral features characteristic of the interfacial species in question and quantifying them with a high degree of sensitivity and specificity. In the next chapter, we describe the principles of the technique of ATR-IR.

1.7 Outline

In this project, we study the kinetics of formation of OTS SAMs on hydrophilic surfaces. We have adopted a three-pronged approach for the same. We conduct experiments to understand the effects of deposition time, solution aging time or

incubation time, solvent, concentration and water content in the system on the quality of the self-assembled layer. We also conduct experiments to monitor the hydrolysis of OTS at the air-water interface. These experiments at the air-water interface give us an understanding of the kinetics of OTS hydrolysis in the bulk. The mathematical modeling of the adsorption process will give us an insight into the mechanism of self-assembly.

Three main chapters (#3,4,5) that describe the experimental and theoretical results concerning the kinetics of self-assembly of OTS onto hydrophilic surfaces comprise the thesis. There is also a chapter that describes in detail the novel experimental technique used to conduct in-situ measurements. Finally chapter 6 recaps the results and conclusions from this work and closes with suggestions for future work that will tackle questions and issues that arose from the current work.

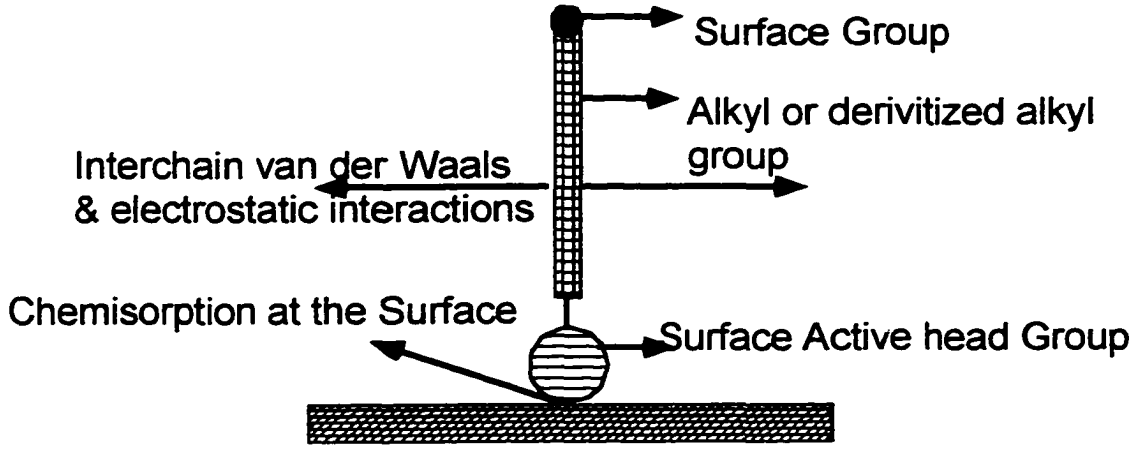

Figure 1.1: Adsorption of Surfactants at Solid/Liquid Interfaces

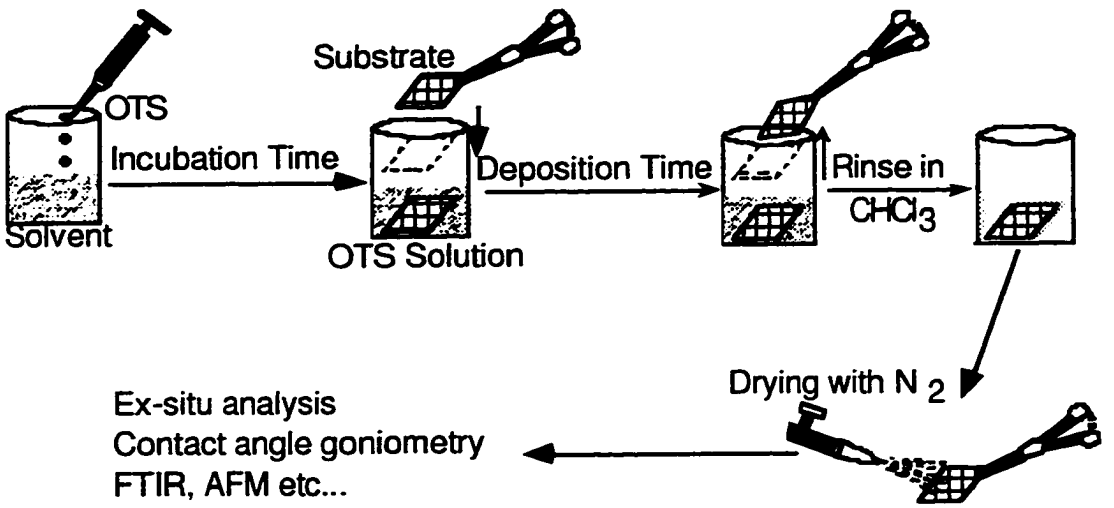

Figure 1.2: Ex-situ Analysis of OTS SAMs

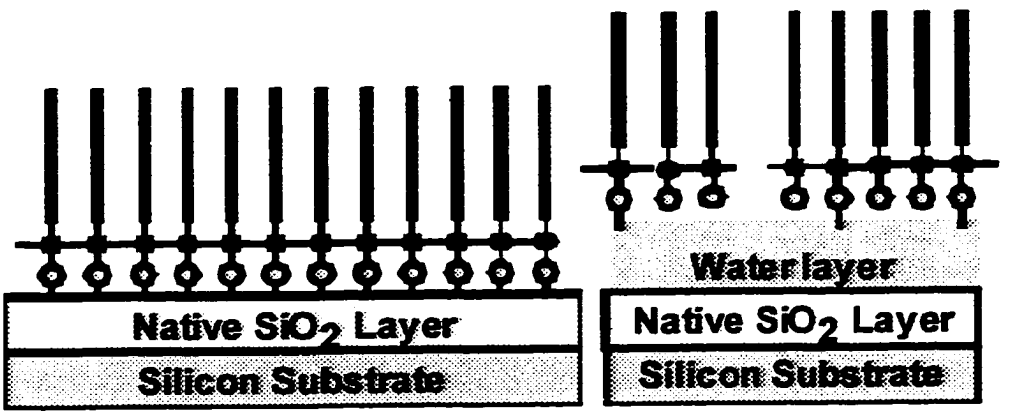

Figure 1.3: Structure of OTS SAM : a: Sagiv et al. (1980); b: Silberzan et al.(1991)

Chapter 2 Experimental Section: Materials and Methods

2.1 Materials

Octadecyltrichlorosilane (95%), Chloroform (>99.9%, HPLC) and Carbon tetrachloride (>99.9%, HPLC) were purchased from Aldrich Chemicals. Acetone (AR grade), Acetonitrile (>99.9%, HPLC), Sulfuric acid (95-98%) and Nochromix® crystals (GODAX labs Inc.) were purchased from Fisher. All chemicals were used as received without further purification. Silicon and germanium internal reflection elements, IREs, (50 x 10 x 3 mm^3, with the beveled edge cut at 45°) were obtained from Spectral Systems, New York. Silicon wafers were obtained from WaferNet Inc., California. The ZnSe and the KBr windows used in the liquid cell were obtained from International Crystal Labs, NJ. The water used in all experiments was purified by passing tap water through a Milli-Q filter system that is fitted with an Organex-Q column to remove trace surface active impurities (Millipore®, Malborough, MA). Argon and industrial grade N_2 gases were purchased from T.W. Smith Corporation, New York.

2.2 Cleaning protocol

It is important to ensure that the substrates used for the adsorption process are clean. This sub-section describes in detail the cleaning protocol adopted during all experiments to eliminate impurities, specially the surface active ones. The glassware was first sonicated in freshly prepared Nochromix® solution for 30 minutes. The Nochromix® solution was prepared by dissolving the Nochromix® crystals in sulfuric acid and stirring the solution until it becomes clear. Rinsing the glassware with water and subsequent sonication in water for 30 minutes followed the Nochromix® treatment.

Cleaning of the silicon substrates involved three steps that focused on removing organic contaminants without stripping the native oxide layer. The first step involved sonication in acetone for 30 minutes. The second step is the same as that used for cleaning glassware. In the third step each side of the substrate was treated in a plasma cleaner (Harrick Scientific Corporation, model PDC - 32G) for 10 minutes. The plasma treatment was performed using argon at a power of 100 W and this is done to ensure the removal of organic contaminants from the substrate surface. In addition, this surface treatment guaranteed the presence of a thin film of silicon oxide on the silicon substrate. The ZnSe and KBr windows used in the liquid cell for measurement of FTIR spectra in transmission mode were sonicated in acetone for 15 minutes and then each side was plasma treated for 15 minutes. The Nalgene® polypropylene tweezers were cleaned by rinsing them with the Nochromix® solution, and then with water before plasma etching them. The cleaned tweezers were then used to handle all apparatus.

2.3 Silanization of Glassware

All glassware used in these experiments was silanized with OTS, since OTS reacts with the Si-OH groups present on the glass surface. As a result the bulk concentration of OTS is reduced. The pre-silanization procedure is given below. The glass surface was contacted with a 30 *mM* solution of OTS in chloroform for 14 hours. Experiments in our lab have shown that these conditions are sufficient for all Si-OH groups on the surface of the glass to react. In fact there exists the possibility of some physisorbed OTS in addition to the chemisorbed layer. To remove this physisorbed layer we sonicated the glassware twice in fresh chloroform. Each sonication was done for 30 minutes. The removal of the physisorbed OTS was monitored by checking for

hydrocarbon related peaks in the FTIR spectrum of the sonicated chloroform, which was measured in transmission mode using ZnSe windows and a ICL PRES-N-LOK liquid cell (International Crystal Labs, New Jersey). 150 μl of the sonicated chloroform was spread on one of the ZnSe window. After 10 minutes, which was sufficient time for the chloroform to evaporate, the other ZnSe window was placed on top of the first one and the spectrum was measured. To complete the pre-silanization process, the glass apparatus were heated at 120 ^{o}C for 1 hour.

2.4 Attenuated Total Reflection Infrared Spectroscopy

2.4.1 Introduction

Infrared Spectroscopy is an analytical technique used to determine molecular structure, molecular behavior, and identification of chemical substances and their mixtures. As every other spectroscopic technique, infrared spectroscopy is based on the interaction of radiation and mass. When infrared radiation strikes a molecule then vibrational transitions of specific bonds within the molecule take place. These transitions will be detectable if the net change in the dipole moment of the molecule, caused by the transitions, is non-zero.[57]

Attenuated Total Reflection Spectroscopy (ATR) or Internal Reflection Spectroscopy (IRS) is a method of obtaining an infrared spectrum of species located near the surface of a sample. It was first developed by Harrick[56] and is also one of the most frequently used tools for surface characterization of polymers. The capability of ATR spectrometry is attributed to the penetrating nature of light when total reflection occurs at an interface of two materials[56]. Moreover, because in ATR reflectivity is measured and

not absorbance, spectra of highly absorbing or opaque materials can be obtained without the need of very small cell path lengths.

Although ATR infrared spectrometry has been familiar as a convenient surface analytical method, it has mostly been applied for qualitative purposes. Over the past decade, the capability of the ATR to analyze very thin films has been examined[48,49,58-61]. In addition to ATR-IR, techniques such as ellipsometry, viscometric and magnetic resonance techniques are also used in studying the adsorption of polymers and surfactants at the solid-liquid interface. However, in comparison to other methods, ATR-IR has the ability to provide information about the bond between the adsorbed species and the substrate and also distinguish between the adsorbed molecules and those that are in the vicinity of the interface. Furthermore, it provides the ability to conduct measurements *in-situ*, thus allowing kinetic studies in the presence of the solvent. The ATR method has been applied successfully for the study of surfactant adsorption[58,59], biopolymer adsorption[62] and polymer adsorption[49,63].

The capabilities and advantages offered by ATR are strongly influenced by the geometry adopted[56]. Today, there are two types of set ups commercially available for ATR spectroscopy. One is of flat geometry in which case experiments with polarized light are possible for the study of the conformation of adsorbed species on interfaces[64]. It also allows the investigator to use various angles of incidence. The flat geometry also gives great flexibility in adjusting the depth of the evanescent wave, permitting the direct investigation of the adsorbing interface. The other geometry is cylindrical[58,59,65], which allows much better sealing of the liquid sample holder, but does not allow changes on the

various parameters effecting the scanning capabilities of the system. Schematic figures of the two geometries is shown in figure 2.1.

2.4.2 Internal Reflection Principles

In this section the analysis first presented by Harrick[56] will be discussed. Total internal reflection is a familiar phenomenon, observed in every day life. When a light beam propagating in an optical medium with a refractive index of η_1, strikes a surface of another material, with a refractive index η_2, then a portion of the beam will be reflected and a portion will be partially transmitted in the second medium. The transmitted beam, shown in figure 2.2, is refracted according to Snell's law:

$$\eta_1 \sin\theta = \eta_2 \sin\varphi \tag{2.1}$$

When the light approaches the interface from a denser medium ($\eta_1 > \eta_2$) and the angle of incidence is greater than the critical angle defined by equation (2.2)

$$\theta > \theta_{critical} = arcsin\left(\frac{\eta_2}{\eta_1}\right) \tag{2.2}$$

then total reflection takes place, i.e., there is no transmitted portion of the incident beam. When total reflection takes place at an interface, then a standing wave is established near the interface, on the denser medium side. In the rarer medium an evanescent wave is created, that has an exponentially decreasing amplitude:

$$E = E_0 e^{-z/d_p} \tag{2.3}$$

E_0 is the amplitude of the electric field at the interface, in the rarer medium and can be calculated from the following equations:

$$E_{yo} = \frac{2\cos\theta}{\left(1-\eta_{21}^2\right)^{1/2}} \tag{2.4}$$

$$E_{x0} = \frac{2\left(sin^2\theta - \eta_{21}^2\right)^{1/2} cos\theta}{\left(1-\eta_{21}^2\right)^{1/2}\left[\left(1+\eta_{21}^2\right)sin^2\theta - \eta_{21}^2\right]^{1/2}} \tag{2.5}$$

$$E_{z0} = \frac{2\,sin\theta\,cos\theta}{\left(1-\eta_{21}^2\right)^{1/2}\left[\left(1+\eta_{21}^2\right)sin^2\theta - \eta_{21}^2\right]^{1/2}} \tag{2.6}$$

The electric field amplitude near the reflecting interface, for total internal reflection, can be seen in figure 2.3.

The distance from the interface required for the electric field to drop to e^{-1} of its value at the surface, is defined as the penetration depth and is given by:

$$d_p = \frac{\lambda_1}{2\pi\left(sin^2\theta - \eta_{21}^2\right)^{1/2}} \tag{2.7}$$

λ_1 is the wavelength of the incident beam, in the denser medium, $\lambda_1 = \lambda/\eta_1$.

The interaction of the evanescent wave with the adsorbing rarer medium causes a loss of reflection. The stronger the interaction the greater the loss of reflectivity. Reflectivity is defined as the ratio of the reflected light intensity to the intensity of the incident light:

$$R = \frac{I}{I_0} \tag{2.8}$$

For small absorption losses (<10%) the strength of interaction can be expressed in terms of an effective thickness, d_e, in a manner similar to the path length used in transmission spectroscopy, as already discussed in the previous section:

$$R = \frac{I}{I_0} = e^{-\alpha d_e} \xrightarrow[\alpha d_e < 0.1]{} R = \frac{I}{I_0} \approx 1 - \alpha d_e \tag{2.9}$$

In order to calculate the effective thickness two distinct cases must be considered: (i) the bulk material approximation; (ii) the thin film approximation.

2.4.3 Effective Thickness for Bulk Materials

In this case the thickness of the rarer medium is greater than the penetration depth of the evanescent wave as defined in equation (2.7). The effective thickness is calculated from:

$$d_e = \frac{\eta_{21}}{cos\theta}\int_0^\infty E^2\,dz \rightarrow d_e = \frac{\eta_{21}E_0^2 d_p}{cos\theta} \tag{2.10}$$

As discussed earlier, the amplitudes of the electric field at the interface in the rarer medium are different for perpendicular and parallel polarization. Hence, the effective thicknesses are different for the two polarizations:

$$\frac{d_{e\parallel}}{\lambda_1} = \frac{\eta_{21}\,cos\theta}{\pi\left(1-\eta_{21}^2\right)\left(sin^2\theta-\eta_{21}^2\right)^{1/2}} \tag{2.11}$$

and

$$\frac{d_{e\perp}}{\lambda_1} = \frac{\eta_{21}\,cos\theta\left(2\,sin^2\theta-\eta_{21}^2\right)}{\pi\left(1-\eta_{21}^2\right)\left[\left(1+\eta_{21}^2\right)sin^2\theta-\eta_{21}^2\right]\left(sin^2\theta-\eta_{21}^2\right)^{1/2}} \tag{2.12}$$

From equations (2.11) and (2.12) it is obvious that the effective thickness is a function of the wavelength of the incident beam. This results in a weighting of the infrared spectrum towards lower wavenumbers (longer wavelengths).

2.4.4 Effective Thickness for Thin Film Materials

When the thickness of the rarer medium is much less than the penetration depth of the evanescent wave, the electric field can be assumed to be constant within the film. The effective thickness, d_e is now given by:

$$d_e = \frac{\eta_{21} E_0^2 d}{\cos\theta} \tag{2.13}$$

In the thin film approximation the system consists of three media as shown in figure 2.4. The electric field is controlled by media 1 and 3 rather than media 1 and 2, as is the case for bulk materials, even though total reflection is taking place at the 1-2 interface.

The electric field in the thin film is then given by:

$$E_\perp = \frac{2\cos\theta}{\left(1-\eta_{31}^2\right)^{1/2}} \tag{2.14}$$

$$E_{//} = \frac{2\cos\theta\left[\left(1+\eta_{32}^4\right)\sin^2\theta - \eta_{31}^2\right]^{1/2}}{\left(1-\eta_{31}^2\right)^{1/2}\left[\left(1+\eta_{31}^2\right)\sin^2\theta - \eta_{31}^2\right]^{1/2}} \tag{2.15}$$

Substituting equations (2.14) and (2.15) into the expression for the effective thickness (equation (2.13)), we get the effective thickness for the two polarizations:

$$d_{e\perp} = \frac{4\eta_{21} d\cos\theta}{\left(1-\eta_{31}^2\right)} \tag{2.16}$$

and

$$d_{e//} = \frac{4\eta_{21} d\cos\theta\left[\left(1+\eta_{32}^4\right)\sin^2\theta - \eta_{31}^2\right]}{\left(1-\eta_{31}^2\right)\left[\left(1+\eta_{31}^2\right)\sin^2\theta - \eta_{31}^2\right]} \tag{2.17}$$

When the thin film approximation is used then there are some significant differences over the bulk material approach. The effective thickness does not become infinite as the angle of incidence approaches the critical angle, $\sin^{-1}\eta_{31} = \theta_c$. Spectra obtained near the critical angle are not distorted or displaced. Finally, because the effective thickness does not vary with the wavelength of the incident radiation, the

spectra obtained are not weighted towards the longer wavelength. The spectra obtained with internal reflection of thin films resemble those obtained via transmission spectroscopy.

The foregoing discussion has been given for the case where the surfactant molecules adsorb directly onto the ATR surface. However, a major drawback of the silicon ATR is that it is opaque to infrared radiation beyond 1600 cm^{-1}. Tripp et al.[31,66-70] overcame this problem by studying the adsorption of chlorosilanes onto fumed silica. Since the surface area of fumed silica is several orders of magnitude larger than that of planar silica, the authors were able to investigate the region beyond 1600 cm^{-1}. However, our studies are performed on low surface area silica, (i.e.) planar Si/SiO_2 surfaces. Claassen[71] has shown that when a thin Si crystal is in optical contact with a Ge IRE, the useful spectral range can be extended beyond 1600 cm^{-1}. For our experiments, we used a freshly cleaned Si wafer of ~400μ thickness, and placed it in contact with a Ge ATR. Adsorption of the surfactant occurred on the Si wafer. In figure 2.5, we show the cartoon depicting the difference in the two cases, the Si ATR, and the Si wafer/Ge ATR. By adopting the above procedure, we have a larger range of spectral data (i.e.) 4000-600 wavenumbers available for analysis. The representative spectra from the two methods are shown later in chapter 4.

2.4.5 Quantitative Analysis Using ATR

The amount of light adsorbed for every reflection, A/N, per unit area and thickness of dz in the rarer medium, when total reflection is taking place at the interface with an optically denser medium, is given by[56]:

$$d\left(\frac{A}{N}\right)=\frac{1}{cos\theta}\alpha E^2 dz \tag{2.18}$$

Integrating from $z=0$ to $z=\infty$, we get the absorbance per reflection:

$$\frac{A}{N}=\frac{1}{cos\theta}\int_0^{\infty}\alpha E^2 dz \Rightarrow \frac{A}{N}=\frac{E_0^2}{cos\theta}\int_0^{\infty}\alpha e^{-\frac{2z}{d_p}}dz \tag{2.19}$$

The above equation has been developed independently by a number of investigators[72-75]. The absorption coefficient, α, contains both the effects of concentration, C, and molar absorptivity, ε (i.e.) $\alpha=C\varepsilon$. Thus substituting into equation (2.19), the following equation relates quantities that are measured to quantities of interest:

$$\frac{A}{N}=\frac{E_0^2}{cos\theta}\varepsilon\int_0^{\infty}C(z)e^{-\frac{2z}{d_p}}dz \tag{2.20}$$

From equation (2.20) we can then calculate the surface excess of an adsorbing molecule[58]. To do so we define the following concentration profile:

$$C(z)=\begin{cases}C_{bulk}+C_i & for\ 0<z<\ell \\ C_{bulk} & for\ \ell<z<\infty\end{cases} \tag{2.21}$$

The above profile is schematically depicted in figure 2.6. In equation (2.21) l is the thickness of the adsorbing layer, and C_{bulk} and C_i are the concentration of the surfactant in the bulk and in the adsorbed layer respectively. Substituting into equation (2.20) and integrating results to an equation that relates the total absorption measured to the bulk solution concentration and the surface excess, $\Gamma_i = C_i \ell$.

$$\frac{A_{total}}{N}=\varepsilon_{bulk}C_{bulk}d_e+\varepsilon_{ads}\left(\frac{2d_e}{d_p}\right)\Gamma_{ads} \tag{2.22}$$

Equation (2.22) has been used, throughout this study for calculating the surface excess of adsorbing polymers and surfactants at the solid-liquid interface. In the above equation, there are 3 other quantities, ε_{bulk}, ε_{ads} and N, which have to be determined before we can determine Γ_{ads}. The determination of N and ε_{bulk} is described in following sections. In an earlier study[76] we have shown that ε_{ads} is different from ε_{bulk} and hence it was measured separately. The procedures adopted to measure ε_{ads} are described in the following chapter.

2.5 Determination of N, number of reflections

The procedure adopted by Sperline et al.[58] was used to determine the number of reflections occurring in the ATR element, N. At the end of the kinetics run, the cell was flushed with pure solvent. Without disturbing the existing set-up, pure water was passed through the flow cell in order to collect a spectrum of water to be used as background. After collecting the spectrum of pure water, a dilute aqueous solution of acetonitrile (ACN) was flown through the cell.* The spectra of these solutions were collected as interferograms. All spectra were converted to absorbance files by referencing them to the spectra of pure water. As suggested by Sperline et al.[58], the integrated absorbance, A, of the peak characteristic of the C≡N absorption peak was found by numerically integrating the spectra between 2282 cm^{-1} and 2231 cm^{-1}. Clearly equation (2.22) is applicable to the spectra of aqueous ACN too, albeit simplified. Since ACN does not adsorb onto the solid

---

* It has been shown earlier that ACN is not surface active[58] and hence it will not adsorb on the either the silicon ATR or on the OTS layer.

surface, the contribution to the integrated absorbance is entirely due to the ACN in the bulk solution (i.e.)

$$\frac{A}{N} = \varepsilon_{bulk\_ACN} C_{bulk\_ACN} d_e \qquad (2.23)$$

In order to measure ε_{bulk_ACN}, dilute solutions of ACN were prepared in water at different concentrations, C_{bulk}. The spectra of these solutions were measured using a liquid cell in the transmission mode. ZnSe windows with a 0.05-mm spacer were used. The actual spacing, *t*, in the cell was found from the interference pattern of the empty liquid cell[77]. The integrated absorbance, A, was calculated for the C≡N stretch in the region of 2259 cm^{-1}. ε_{bulk_ACN} (for the C≡N stretch) is determined from the slope of the graph of A vs. C_{bulk}*t, and is equal to 498 L/mol/cm^2. With the knowledge of ε_{bulk_ACN}, de and the slope of the A/C_{bulk} graph, we can determine N. It should be noted here that N is dependent on several factors such as the position of the IRE in the flowcell, the angle of incidence of the incident IR beam at the beveled edge surface and the actual path length of the beam in the IRE. However, in all our experiments the N was about 6.5 ± 0.5. This is in good agreement with the value calculated theoretically[78], which is approximately 7. A sensitivity analysis was performed to verify that the difference in the values of N, as discussed above, did not introduce any significant errors in the calculation of the Γ.

2.6 Infrared Measurements

IR spectra were measured using a Bio-Rad FTS 175 spectrometer. The sample chamber was purged with nitrogen. The detector used was a narrow band, linearly amplified, liquid nitrogen cooled Mercury-Cadmium-Telluride (MCT) detector. Spectra

were taken as interferograms with a resolution of 2 cm^{-1} and Fourier transformed with triangular apodization. All spectra were averaged over 100-500 scans. The substrate was carefully checked for hydrocarbon contamination before each experiment. Spectra of bulk compounds were obtained as transmission spectra using KBr windows. Experiments were conducted using unpolarized light. We checked to see that our FTIR had no preferred polarization. The check was conducted by measuring the intensity of the infrared beam as a function of the wavenumber with a wire grid rotating polarizer placed in the path of the infrared beam, one which can be oriented to produce parallel and perpendicular polarization. The intensities for the two polarizations were measured as a function of wavenumber and we found marginal difference between the two (ratio of intensities for the parallel and perpendicular polarizations ranged from 0.9 - 1.0 over the entire wavenumber range). If the FTIR had induced a preferred polarization, then the intensities at a given wavenumber would have been different for the two polarizations used.

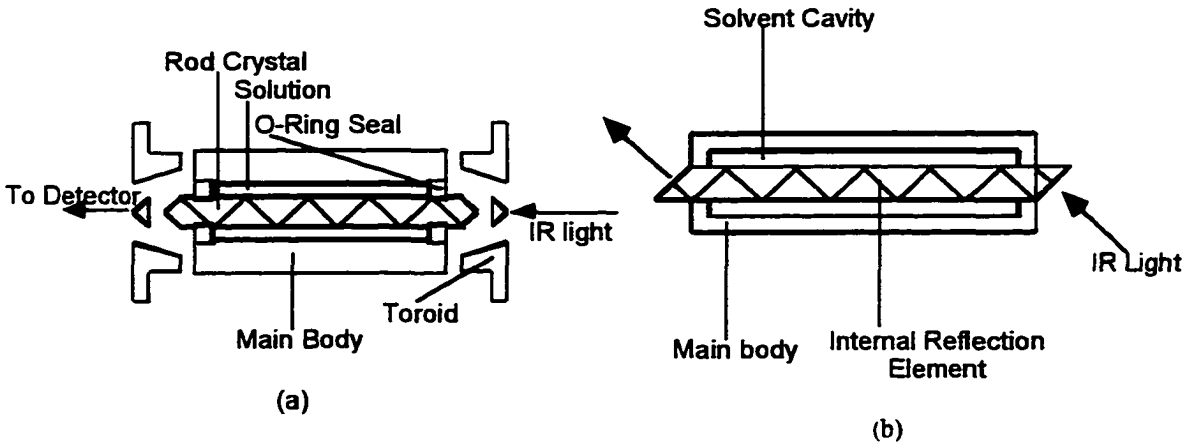

Figure 2.1: ATR geometry: a: cylindrical; b: flat geometry

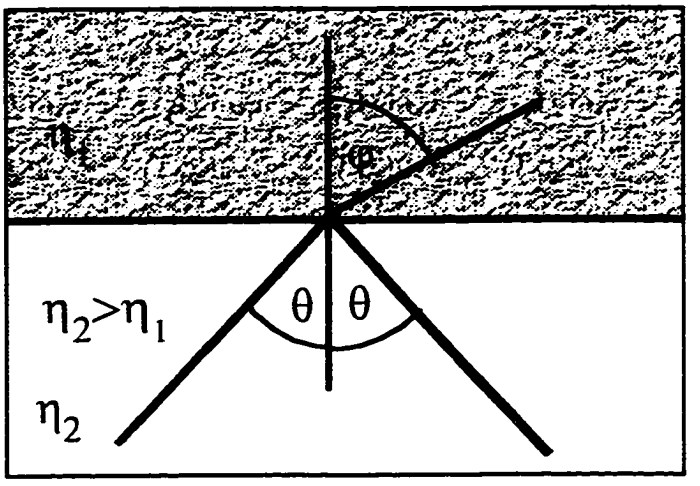

Figure 2.2: Internal Reflection Principles

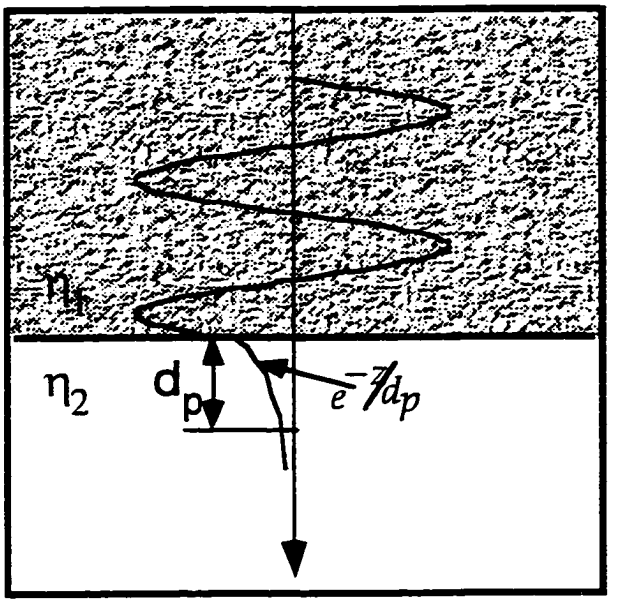

Figure 2.3: The electric field amplitude at the reflecting interface

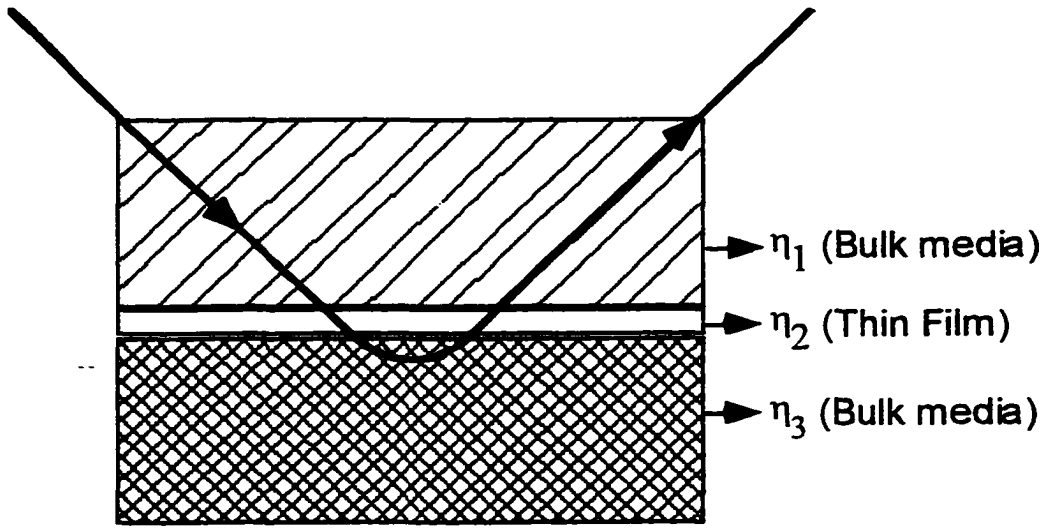

Figure 2.4: Measurements of Thin Films via Internal Reflection Spectroscopy

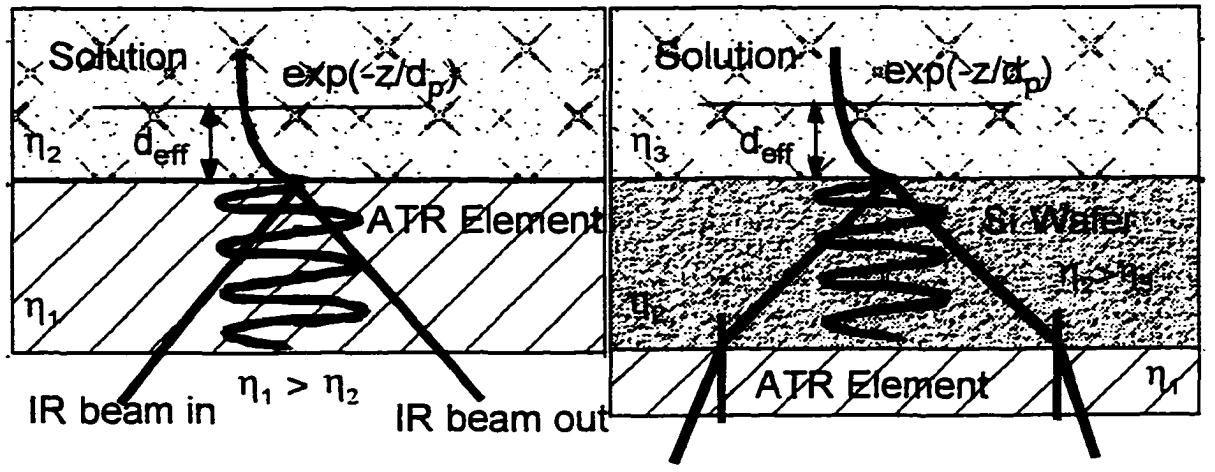

Figure 2.5. The technique of Sandwiching

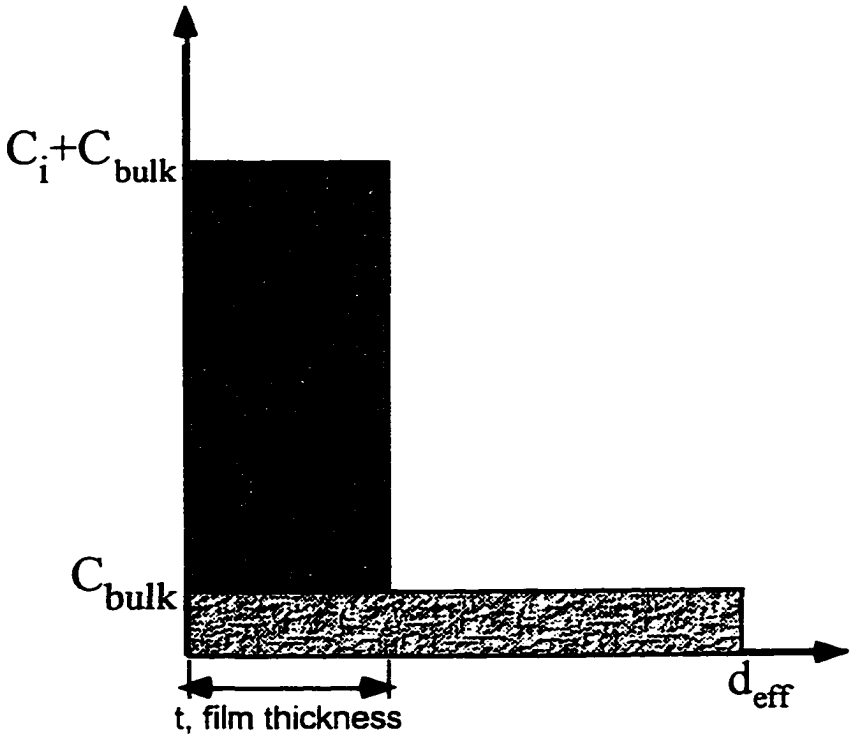

Figure 2.6: Concentration Profile

Chapter 3 Measurement of molar absorptivity of OTS adsorbed onto Silicon

3.1 Introduction

Infrared spectroscopy[57,77,79-81] is a widely used technique for the analysis of organic species, both in the bulk and in the adsorbed states. In order to derive the concentration of the adsorbing species directly from the infrared spectra, one needs to know the the molar absorptivity, ε, of the infrared active band of the adsorbing species of interest. The molar absorptivity, ε, depends on the environment of the species[57] that is absorbing the IR radiation. The immediate environment of the species in the adsorbed state is different from that in its free state and therefore it is reasonable to expect that ε_{bulk} (ε values for various species in the bulk) will be different from ε_{ads} (the ε of the adsorbed species). Earlier studies[12] have shown that the position of the peak characteristic of the methylene asymmetric stretch (in the region of 2920 cm^{-1}) is different when the species is in the adsorbed state than when it is in its free state. In addition, it has also been shown that the packing of molecules in an adsorbed layer affects the position of the above-mentioned peak[9,10,82-84]. Thus, one may also expect ε_{ads} to vary with the surface concentration of the adsorbing species, Γ. Values of ε_{bulk} for different chemical species have been reported in the literature[58,59,80]. On the other hand, there is little data available on ε_{ads}. Two approaches have been reported in the literature for determining surface coverages. The first approach has been to use ε_{bulk} values[46,47,49,58,83,85-87] in place of the appropriate ε_{ads}. The second approach is to compare the IR spectra of the species with

unknown surface concentration, Γ, with that of a reference sample[37,38,88] of known surface concentration, Γ_{ref}. This approach is accurate only for the case when $\Gamma = \Gamma_{ref}$. The possible variation of ε_{ads} with change in surface concentration necessitates a study to obtain ε_{ads} over varying surface concentrations.

The objective of this study is to measure ε_{ads} of a surfactant species adsorbed onto a solid substrate. This will enable one to determine surface coverage of molecules adsorbed on a solid substrate from their IR spectra. We believe that this is the first complete study of its kind to calculate the molar absorptivity as a function of surface coverage. The ε_{ads} that we determine is for the -CH- asymmetric stretch of the methylene group, and is reported on a per $-CH_2-$ basis. Earlier studies have shown that the absorbance of this band increases linearly with the number of $-CH_2-$ groups in the molecule.[37,57,89] Hence, it is reasonable to expect that $\varepsilon_{TOT} = N_{CH2} * \varepsilon_{CH2}$. Therefore, the ε_{ads} that we determine can be used to accurately estimate the surface concentration of adsorbates possessing at least one $-CH_2-$ group. Our calibration involves transferring a monolayer of a reference adsorbate at a known surface coverage from the air/water interface onto a solid substrate using the Langmuir-Blodgett technique.[39] The IR spectrum of each transferred monolayer is then measured. The integrated absorbance, A, for the methylene asymmetric stretch in the region of 2920 cm^{-1} is determined for various surface coverages of the adsorbate by integrating our spectral information in the range of 2945-2902 cm^{-1}. ε_{ads} is then determined using the absorbance and the known value of the surface concentration Γ. In order to obtain ε_{ads} as a function of Γ, the adsorbate should be capable of exhibiting a wide range of surface coverage at the air/water interface.

Furthermore, the surface coverage of the adsorbate on the substrate needs to be known accurately, which is possible only for a adsorbate capable of forming a robust film on the substrate.

We chose OTS as the adsorbate for our study because its π-A isotherm exhibits a large surface concentration range (20-55 $\AA^2/molecule$) for which the surface pressures are sufficiently large (> 5 mN/m)[90,91]. At these surface pressures we can accurately transfer the monolayer from the air/liquid interface onto a solid substrate by the Langmuir-Blodgett technique. Earlier studies[90-93] have shown that in order to attain this wide range of surface coverages we must minimize the extent of polymerization of the OTS monolayer at the air/water interface. As part of our study we have developed a set of experimental conditions that minimize the polymerization of OTS and allow us to utilize the π-A isotherm for our ε_{ads} calculations. This set of experimental conditions is discussed in detail in the following sections.

3.2 Formation of Films

A 0.3 ± 0.03 mg/ml solution of OTS in chloroform was prepared. 200 μl of this solution was immediately spread onto the subphase (Millipore® water, 18 $M\Omega$) maintained at 18.6 ^oC and a pH of 5.6. A Langmuir film balance (Lauda Model D, Lauda-Konigshofen, Germany) was used for all our experiments. The initial surface coverage was 100 $\AA^2/molecule$. The monolayer was compressed one minute after spreading (to allow the chloroform to evaporate). The monolayer was transferred onto Si substrate by the Langmuir-Blodgett technique.[39] The transfer speed was varied in order to ensure a transfer ratio of 1 ± 0.05. The monolayer transfer was conducted at five different surface

concentrations of OTS. The IR spectrum of the transferred film on the silicon substrate was then measured in the transmission mode.

3.3 Infrared Measurements

If I_o is the intensity, or radiant power, of monochromatic radiation entering a sample, and I is the intensity transmitted by the sample, then the absorbance A is given by:

$$A = ln\left(\frac{I}{I_0}\right) = \varepsilon bc \tag{3.1}$$

where b is the sample cell thickness, c is the concentration of the absorbing component, and the constant ε is the molar absorptivity which could be a function of concentration when the concentrations are high enough for the absorbing molecules to interact with one another. When b is negligible, the product of c and b, is a measure of surface concentration of the absorbing molecules (i.e. Γ). Then equation (3.1) can be rewritten as

$$A = \varepsilon(\Gamma) * \Gamma \tag{3.2}$$

The integrated absorbance, A, for the methylene asymmetric stretch at 2920 cm^{-1} was determined by integrating our spectral information in the range of 2945-2902 cm^{-1}. The symmetric methylene peak and asymmetric methyl peak are all clearly noticeable in our spectra and in each spectrum we check that these peaks always lie outside the integration region of 2945-2902 cm^{-1}. An example is given in figure 3.1. With the choice of the region of 2945-2902 cm^{-1}, which avoids the strong peaks, we had a baseline that did not intersect the spectra and thus accurate values of the integrated absorbance could

be obtained. Following this selection of a baseline the integrated absorbance was numerically calculated.

3.4 Results and Discussion

3.4.1 Surface pressure isotherms of OTS

Surface pressure (π-A) isotherms of OTS have been studied recently[90,91]. These studies have shown that the shape, and hence the range of surface coverage, of the isotherm depends on the extent of polymerization of OTS. The polymerization of OTS proceeds in two steps, the hydrolysis of the chlorosilane groups (reaction A) and the condensation of the silanol groups (reaction B).

$$C_{18}H_{37}-\underset{|}{\overset{|}{Si}}-Cl+H_2O\xrightarrow{k_1}C_{18}H_{37}-\underset{|}{\overset{|}{Si}}-OH+HCl \qquad \text{(A)}$$

$$C_{18}H_{37}-\underset{|}{\overset{|}{Si}}-OH+HO-\underset{|}{\overset{|}{Si}}-C_{18}H_{37}\xrightarrow{H^+}C_{18}H_{37}-\underset{|}{\overset{|}{Si}}-O-\underset{|}{\overset{|}{Si}}-C_{18}H_{37}+H_2O \qquad \text{(B)}$$

It has been shown that reaction B, which is acid catalyzed[41], is the rate limiting step. When the extent of reaction B is small the surface-pressure isotherm has been shown to exhibit three regions, a liquid expanded (LE) phase, a liquid condensed (LC) phase, and a LE - LC coexistence phase. On the other hand when the extent of reaction B is large a pressure response is seen only at high surface coverage. The negligible (~ 0 *mN/m*) pressure response at low surface coverage has been attributed to the presence of isolated, polymerized islands in the monolayer[91].

The polymerization can occur both at the air/water interface (surface) as well as in the spreading solution (bulk). Studies[90,91] thus far have only accounted for surface polymerization. Specifically, subphase *pH* and $t_{surface}$ (time for which OTS monolayer remains on the surface before being compressed) have been shown to affect the surface

polymerization. The condensation of the silanols, which is acid catalyzed, is greater in the case of a subphase at pH 2 as compared to a subphase at pH 5.7. Moreover, the extent of silanol condensation is found to increase with $t_{surface}$.[91] Based on the results that have been discussed thus far, we believe that V_c (compression speed) also affects the surface polymerization. Moreover t_{bulk} (time for which OTS remains in the spreading solution before being applied on the surface) and C_b (concentration of OTS in bulk) affect the polymerization in the spreading solution.

The effect of t_{bulk} on the π-A isotherm of OTS is shown in figure 3.2. The experimental conditions used were similar to those used by previous investigators[90] (0.3 *mg/ml* OTS in chloroform, compression speed of 20 cm^2/min, a subphase temperature and pH of 18.6 ^oC and 5.7 respectively). At small t_{bulk}, the isotherm exhibits a LE, LE-LC and LC phase in agreement with earlier studies.[90,91] This isotherm is characteristic of an unpolymerized monolayer. Moreover, when the monolayer was compressed beyond the LC phase, a cusp was seen in the isotherm, indicative of a phase transition. This second transition has not been reported earlier for π-A isotherms of OTS. However, a similar transition has been shown to occur in the π-A isotherm of Octadecyltrimethoxysilane (OTM).[43] It has been suggested that this transition is one from the LC state to the LS state. It can also be seen from figure 3.2 that at large t_{bulk}, a pressure response is seen only at high surface coverage, characteristic of a polymerized monolayer.[91,92] This indicates that OTS has undergone progressive polymerization in the bulk solution. This is reasonable, since chloroform has dissolved water[94] which promotes the hydrolysis of OTS[26] and thus results in the formation of HCl. This acid catalyses the silanol condensation (reaction B) resulting in the formation of polymeric structures in the bulk.[41]

This result clearly shows that bulk polymerization effects are important in determining the isotherm.

The effect of C_b on the isotherm is shown in figure 3.3. A comparison of the isotherms clearly indicates that OTS (in the spreading solution) is relatively more polymerized at higher concentrations. This is reasonable since we expect the extent of polymerization to increase with an increase in the concentration of the reacting species. Furthermore, the amount of dissolved H_2O in chloroform[94] is in excess of the stoichiometric requirement for the completion of the hydrolysis (reaction A), true for the concentrations (0.3 *mg/ml* ~ 0.77 *mM*; 0.8 *mg/ml* ~ 2.06 *mM*) used in this study. The hydrolysis results in the formation of HCl, which acidifies the spreading solution. Assuming that all the chlorosilane groups are hydrolyzed, the HCl concentration in the spreading solution is 2.31 *mM* at the lowest C_b and 6.18 *mM* at the highest C_b. As discussed earlier the condensation of the silanols is catalyzed by acid (reaction B). Since the HCl concentration increases with increase in C_b, the rate and therefore the extent of polymerization is greater at the higher C_b. This result further underscores the importance of bulk polymerization effects in determining the isotherm.

Figures 3.2 and 3.3 indicate that conditions in the spreading are as important in determining the π-A isotherm as the previously documented conditions at the air/water interface.[91] By conducting the experiments at low values of t_{bulk} and C_b, we can minimize the effects due to polymerization in the bulk. Furthermore, the earlier studies have only reported the effect of subphase *pH* and $t_{surface}$ on the polymerization of OTS at the air/water interface. We hypothesize that the compression speed, V_c, which is a direct

measure of the residence time for OTS molecules at the air/water interface, affects the extent of surface polymerization as well.

The effect of V_c on the isotherm is shown in figure 3.4. Clearly the compression speed, within our experimental range, has no apparent effect on the shape of the isotherm. This is in agreement with an earlier study which investigated the effect of V_c on the surface pressure isotherm of OTM.[44] The similarity of the two isotherms would seem to indicate that the extent of polymerization of the two monolayers is similar. However, the residence time of the monolayers is different in the two cases, (viz.) 5 and 35 minutes for the compression speeds of 150 and 20 cm^2/min respectively. Hence we expect the composition of the reactive species (monomeric and polymeric OTS amphiphiles) in the monolayers to be different. In order to qualitatively compare the composition of the OTS monolayer (at the air/water interface) at the two speeds of compression, the surface area was monitored as a function of time while maintaining surface pressure constant. In such studies, referred to as "surface relaxation", the rate of change of surface area is a measure of the rate of surface polymerization.[40,95] If the rate of change of surface area of different Langmuir monolayers is equal, it would indicate similar rates of surface polymerization and thereby comparable composition of the reactive species in the monolayer.

The variation of surface area as a function of time at the two compression speeds is shown in figure 3.5. In both cases the surface pressure of the monolayer was maintained at 30 mN/m following the compression of the monolayer at two different speeds of 150 cm^2/min and 20 cm^2/min. Comparing the two curves it is evident that the rate of decrease in area is higher for the monolayer which is compressed at 150 cm^2/min, indicating that this monolayer has a higher composition of reactive OTS.

The results of figures 3.4 and 3.5 indicate that during polymerization of a monolayer at the air/water interface, the π-A isotherm could be the same although the monolayer composition is different. This is reasonable since the experimental pressure observed is a function of the surface pressure of both monomer and the polymer species.[40] In addition, it has been shown in an earlier study that partially polymerized monolayers of methacrylate derivatives undergo a phase transition.[96] The authors suggested that the mobility of the alkyl chains, which participate in the phase transition, was not restricted by the polymerization occurring in the head group of the amphiphile. Hence, these hydrophobic tail groups are able to interact when the monolayer is compressed and thereby undergo a phase transition.

From figures 3.2 and 3.4 it can be inferred that the extent of polymerization of OTS molecules is higher in the spreading solution than at the air/water interface. While a t_{bulk} of 60 minutes resulted in enough polymerization to lose the LE-LC transition, a residence time of 35 minutes at the air/water interface, the time required for full compression at 20 cm^2/min, had no effect on the isotherm. (However, our surface relaxation experiments that have already been discussed (figure 3.5) indicate that there is still a difference in the extent of polymerization at the air/water interface at the compression speeds of 20 cm^2/min and 150 cm^2/min) Although the residence time on the surface was shorter than t_{bulk}, we believe the difference in the extent of polymerization may also be due to the higher rate of polymerization of the OTS in the spreading solution relative to that on the surface. This difference in rate is attributed to the locally lower pH in the spreading solution compared to the pH of the subphase. As discussed earlier the condensation of the silanols is catalyzed by acid (reaction B). The subphase at pH 5.7

has an H^+ concentration of $10^{-5.7} M$. This value is lower than the H^+ concentration in the bulk which is as high as $2.31*10^{-3} M$ at the lowest concentration. Therefore the extent of polymerization, which is mainly determined by the condensation reaction, proceeds to a greater degree in the bulk than at the surface.

From the foregoing discussion we believe that the optimal conditions for obtaining an OTS isotherm with a large range of surface coverages are those which minimize bulk and surface polymerization. Based on this we decided to conduct further experiments at the following experimental conditions, (viz.) $C_b \sim 0.3\ mg/ml$, $t_{bulk} \sim$ 5 minutes, $t_{surface} \sim$ 1 minute, compression speed = 150 cm^2/min and pH ~ 5.7.

3.4.2 Transfer of OTS films from air/water interface onto the silicon substrate

We used the Langmuir-Blodgett (LB) technique to transfer the OTS monolayer from the air/water interface to the Si substrate. This procedure involves immersing the Si substrate in the subphase of the Langmuir trough and thereafter spreading OTS on the subphase. Subsequently, the monolayer is compressed until the predetermined surface pressure is attained. At this point the OTS monolayer is transferred onto the Si substrate by vertically lifting the substrate through the interface at a constant speed, known as the transfer speed. During the transfer process the surface pressure is held constant and the area of the trough is monitored as a function of time. The film transfer is considered successful if the transfer ratio (TR), defined as the ratio of the area of the transferred film to the geometrical area of the substrate,[39] is 1 ± 0.05. In the case of bulk-insoluble and non-polymerizing monolayers, the calculation of TR is straightforward since the area of the transferred film is the same as the decrease in the trough area. However, in the case of polymerizing monolayers like OTS Langmuir films, the decrease in the trough area is not

only due to the transferred film but also due to the surface polymerization. Hence, to obtain accurate values of TR one needs to minimize the effects of surface polymerization.

Surface relaxation studies were undertaken to monitor the polymerization of OTS at the air/water interface. The result one such study at a surface pressure of 30 *mN/m* is shown in figure 3.6. Expectedly, the area of the trough decreases with time due to the surface polymerization of OTS. As suggested earlier in order to obtain an accurate TR one needs to minimize the effect due to surface polymerization. This can be easily achieved by choosing to transfer the OTS film at a speed such that the change in area due to surface polymerization is negligible. The change in area during the LB transfer of the OTS film is also shown in figure 3.6. The transfer was conducted at a surface pressure of 30 *mN/m* and a transfer speed of 125 *mm/min*. Clearly, during the transfer process, the change in trough area due to surface polymerization is negligible. The transfer speeds chosen and the TR achieved for the various transfer pressures used are listed in Table 3.1. From Table 3.1 we can clearly see that for the transfer speeds chosen, the TR in the case of all of the transferred films is 1±0.05.

In addition to obtaining an acceptable TR during the transfer process, one also needs to verify that the packing of the film on the solid substrate is similar to that at the air/water interface. IR spectroscopy has proved to be a useful tool in studying the packing of molecules in adsorbed films. It has been shown that the packing of molecules in the adsorbed layer affects the peak position of the asymmetric methylene stretch.[9,10,83,84] These studies suggest that a lower value of the peak position indicates a more compact and ordered adsorbed layer in which the aliphatic chains of the adsorbate are in the trans state. The IR spectra of the OTS films transferred onto the Si substrate were measured.

The variation of the peak position with the surface coverage of the transferred layer is shown in figure 3.7. An initial sharp drop is followed by constant value of the peak position. This suggests that as (ads increases, the packing of the OTS molecules becomes increasingly ordered and then reaches a limit. This is similar to what is observed at the air/water interface, where the packing of the OTS molecules is initially amorphous when they are in the LE region, and become increasingly ordered as the monolayer is compressed from the LE to LC and finally to the LS phase. This indicates that the packing of OTS molecules on the Si substrate is similar to that at the air/water interface.

3.4.3 Calculation of ε_{ads}

The integrated absorbance, **A** for the asymmetric methylene stretch in the region of 2920 cm^{-1} was determined from the IR spectra of the LB films. The variation of the integrated absorbance, **A**, with surface coverage of OTS, Γ_{ads} is shown in figure 3.8. We have only included points corresponding to one phase (i.e.) LE, LC or LS so that the surface is homogenous with only one phase. It is evident from figure 3.8 that **A** varies linearly with Γ_{ads} until the end of the LC phase, suggesting that ε_{ads} is independent of Γ_{ads} for the LE and the LC phases. The ε_{ads} obtained for the LE and LC phases is equal to $1.7*10^6$ *cm/mole/-CH_2- group*. However ε_{ads} is different in the LS phase.

The fact that ε_{ads} is the same in the LE and the LC phases was further confirmed by transferring a monolayer in the LE-LC coexistence region (Π=16.5 *mN/m*, Γ~ 4.4 $\mu moles/m^2$) and measuring its IR spectrum. The integrated absorbance for the asymmetric methylene stretch in the region of 2920 cm^{-1} was measured and was found to be 0.026. The integrated absorbance can also be calculated using

$$A = X_{LE}\left(\varepsilon_{ads}\right)_{LE}\Gamma_{LE} + X_{LC}\left(\varepsilon_{ads}\right)_{LC}\Gamma_{LC} \qquad (3.3)$$

where X_{LE} and X_{LC} are the surface area fractions of the LE and the LC phases respectively and Γ_{LE} is the surface coverage of the LE phase at the onset of the LE-LC coexistence phase and Γ_{LC} is the surface coverage of the LC phase at the end of the LE-LC coexistence phase. From figure 3.4, these values are 45 $\AA^2/molecule$ for Γ_{LE} and 28 $\AA^2/molecule$ for the Γ_{LC}. Since the ε_{ads} is the same for the LE and the LC phases, eqn. (3.3) can be rewritten as

$$A = \varepsilon_{ads}\left(X_{LE}\Gamma_{LE} + X_{LC}\Gamma_{LC}\right) \qquad (3.4)$$

where the bracketed term in eqn. (3.4) is the average surface coverage measured on the trough, $4.4*10^{-10}$ $moles/cm^2$. From eqn. (3.4) the calculated value of the integrated absorbance for the monolayer transferred in the LE-LC coexistence phase is 0.027, which is in good agreement with the measured value.

It is important to compare this value of ε_{ads} for the LE and LC states to the molar absorptivity of dissolved OTS (i.e. ε_{bulk}). To measure ε_{bulk}, dilute solutions of OTS were prepared in CCl_4 at different concentrations (C_{bulk}). The spectra of these solutions were measured using a liquid cell in the transmission mode. KBr windows with a 0.05-mm spacer were used. The actual spacing, t, in the cell was found from the interference pattern of the empty liquid cell.[77] The integrated absorbance, A was calculated for the asymmetric methylene stretch in the region of 2920 cm^{-1}. The variation of A with $C_{bulk}*t$, is shown in figure 3.9. As expected, A varies linearly with $C_{bulk}*t$. ε_{bulk} (for the asymmetric methylene stretch) is determined from the slope of the line and is equal to $1.1*10^6$ $cm/mole/\text{-}CH_2\text{-}\ group$.

The difference in the numerical value of ε_{ads} and ε_{bulk} can be explained as follows. When OTS is dissolved dilutely in a solvent, there is no interaction between OTS molecules to affect the absorptivity. Moreover, we believe the CCl_4 solvent molecules do not affect the absorptivity, because the molecular interaction between the OTS' methylene groups and the solvent molecules are not strong enough to affect the bond vibrational stretch. On the contrary, if the difference in the molar absorptivity is due to solvent effects, then our dried monolayer film and the exact same film in the presence of our solvent should exhibit differences in peak position and absorptivity due to the interaction of the solvent with the monolayer. To prove that this is not the case, we successively measured the spectra of the film in the absence and presence of CCl_4. The spectra are shown in figure 3.10. It is clear that no changes in peak position and integrated absorbance can be attributed to the absence or presence of CCl_4. In addition, this increase between the solution and surface molar absorptivity has been observed in the literature. Furthermore, it is well established in the literature that CCl_4 is often used as the solvent of preference for the recording of spectra of hydrocarbon species because it does not affect their IR spectra.

When the OTS molecules are adsorbed on the surface, their hydrocarbon chains develop van der Waals interactions and become closely packed, and it is this interaction which is the reason for the change in the molar absorptivity of adsorbed OTS relative to OTS dilutely dissolved in a solvent. This interaction also gives rise to differences in the absorptivity of different adsorbed states of the OTS molecule; we note that the absorptivity, while the same in the LE and LC states, is different in the more condensed LS state where the molecules are most closely packed and the interaction the strongest

(see Figure 3.8). So while it is the environment of the molecules that accounts for the difference between ε_{bulk} and ε_{ads}, it is more specifically the fact that when dissolved dilutely in a solvent, the solvent molecules do not exert an effect on the absorptivity since there is no strong interaction between the OTS molecules and the solvent as discussed above. However, on the surface, the close-packed hydrocarbon chains in the adsorbed layer (rather than the surrounding air) affects this absorptivity.

3.5 Conclusions

In this paper we have reported a protocol for the measurement of the molar absorptivity (in the IR range) for a species adsorbed onto a solid substrate. We have used OTS as a model adsorbate and have transferred monolayers of known surface coverage from the air/water interface onto a silicon substrate with its native oxide layer. The infrared spectra of the transferred films were measured and the integrated absorbance was determined for the methylene asymmetric stretch in the region of 2920 cm^{-1}. The ε_{ads} was calculated using the surface coverage and the integrated absorbance and was found to be independent of the surface coverage for monolayers transferred in the LE, LC and the LE-LC coexistence phases. This absorptivity was measured to be $1.7x10^6$ *cm/mole per -CH_2- group*. It differs from ε_{bulk}, which was measured to be $1.1x10^6$ *cm/mole per -CH_2- group*. The absorptivity was found to be dependent on the surface coverage in the LS state.

The determination of the surface coverage at the air/water interface necessitates the minimization of OTS polymerization both at the air/water interface and the spreading solution. OTS polymerization in the spreading solution is initiated because of dissolved water and was minimized by spreading relatively low OTS concentration solution (≤ 0.3

mg/ml solution) within 5 minutes of the its preparation. The aqueous sublayer initiates polymerization of the monolayers at the air/water interface; the extent of this polymerization is reduced by compressing the monolayer at relatively high compression speeds (≤150 cm^2/min) so as to decrease the residence time of the monolayer at interface. This measurement can be used in conjunction with infrared spectroscopy methods to determine the surface coverage of a surfactant adsorbing from solution onto the solid-liquid interface.

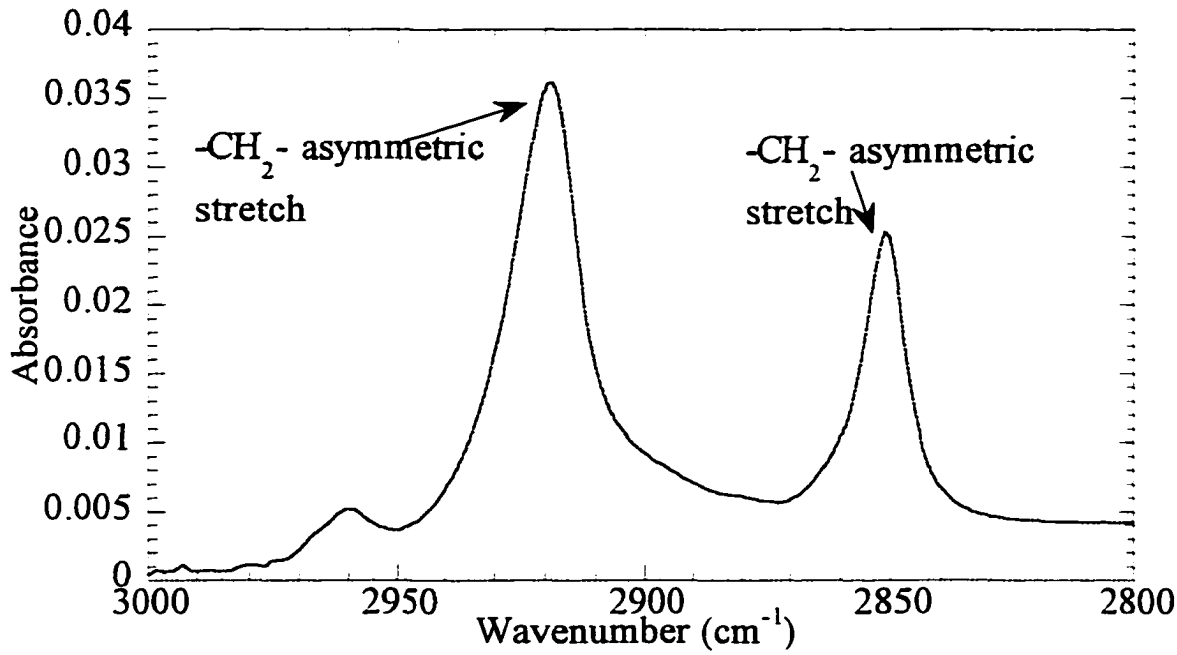

Figure 3.1. Typical IR Spectrum

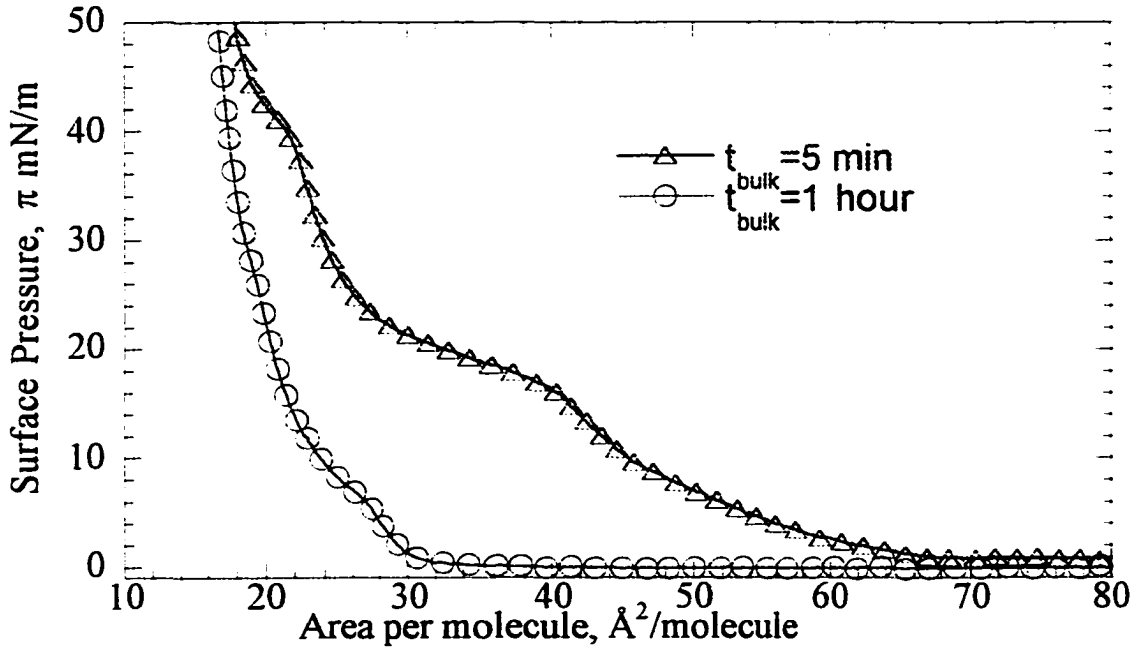

Figure 3.2. Effect of t_{bulk} on the π-A isotherm of OTS

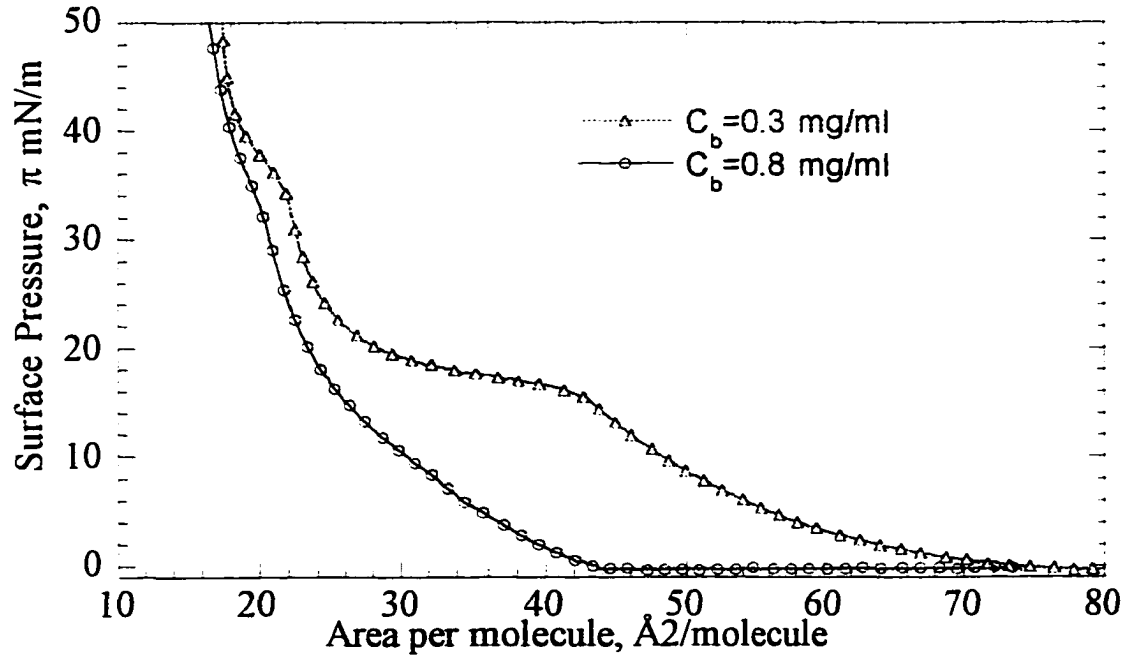

Figure 3.3. Effect of C_b on the π-A isotherm of OTS

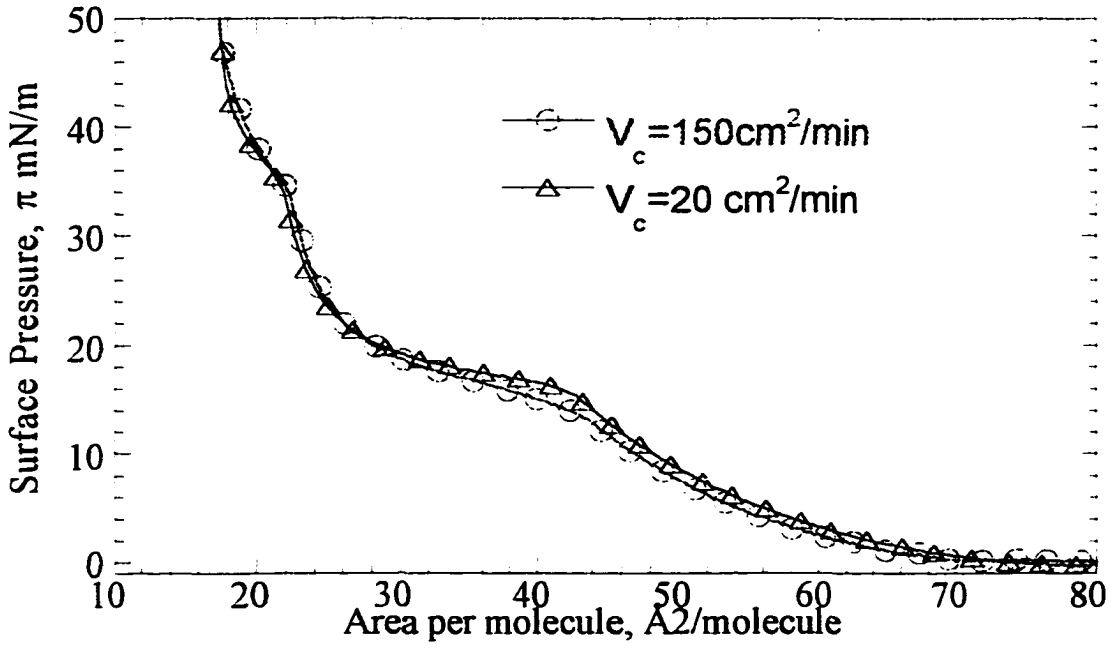

Figure 3.4. Effect of V_C on the π-A isotherm of OTS

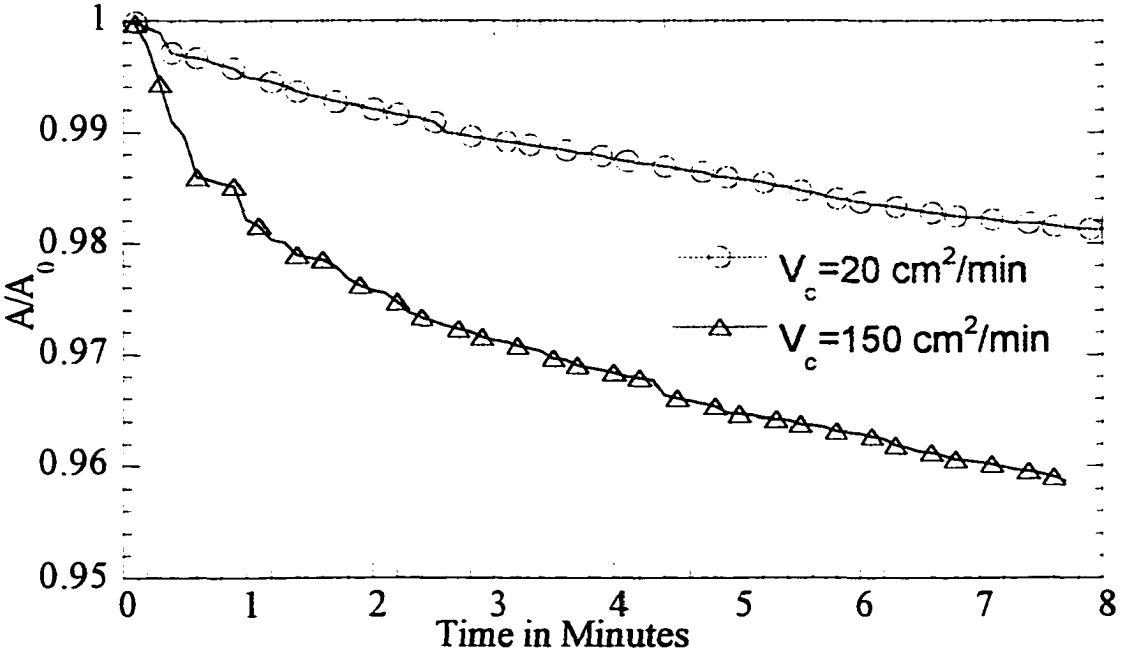

Figure 3.5. Surface area relaxation: Effect of V_C

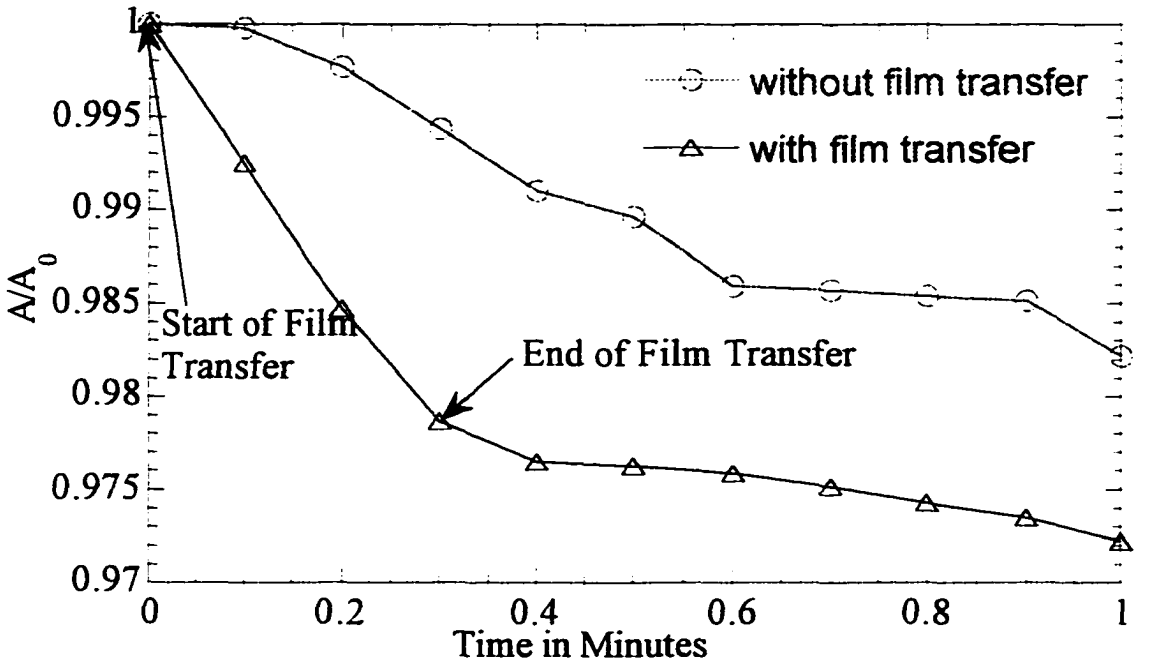

Figure 3.6. Constant surface pressure relaxation of OTS monolayers

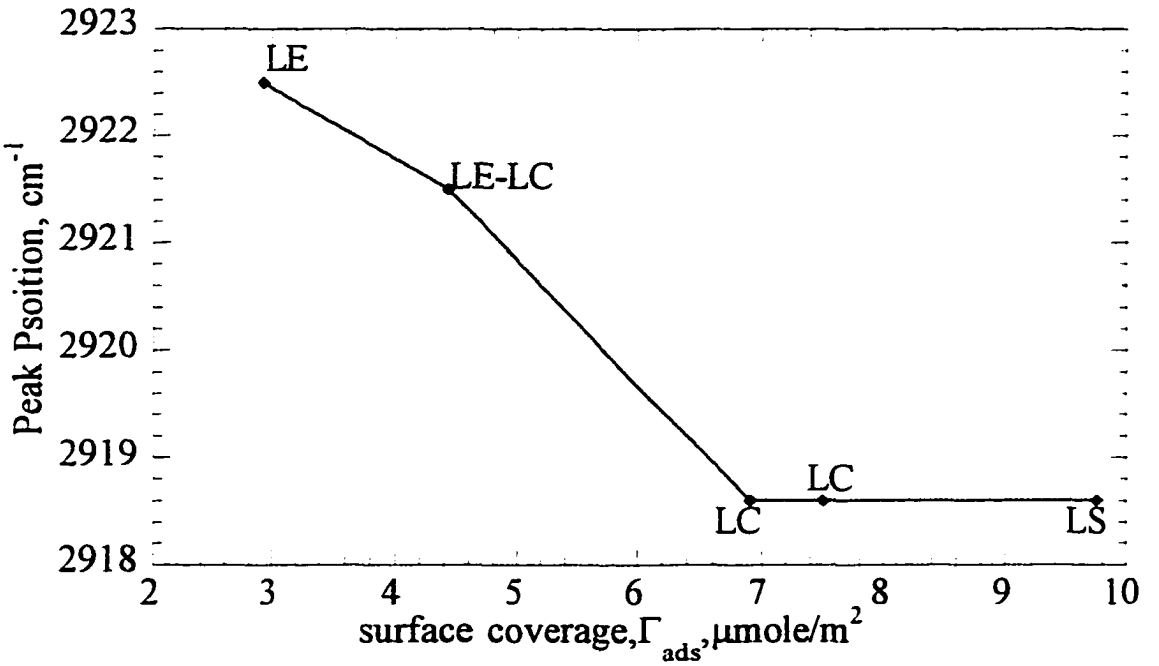

Figure 3.7. Effect of Γ_{ads} on the position of the methylene asymmetric stretch peak

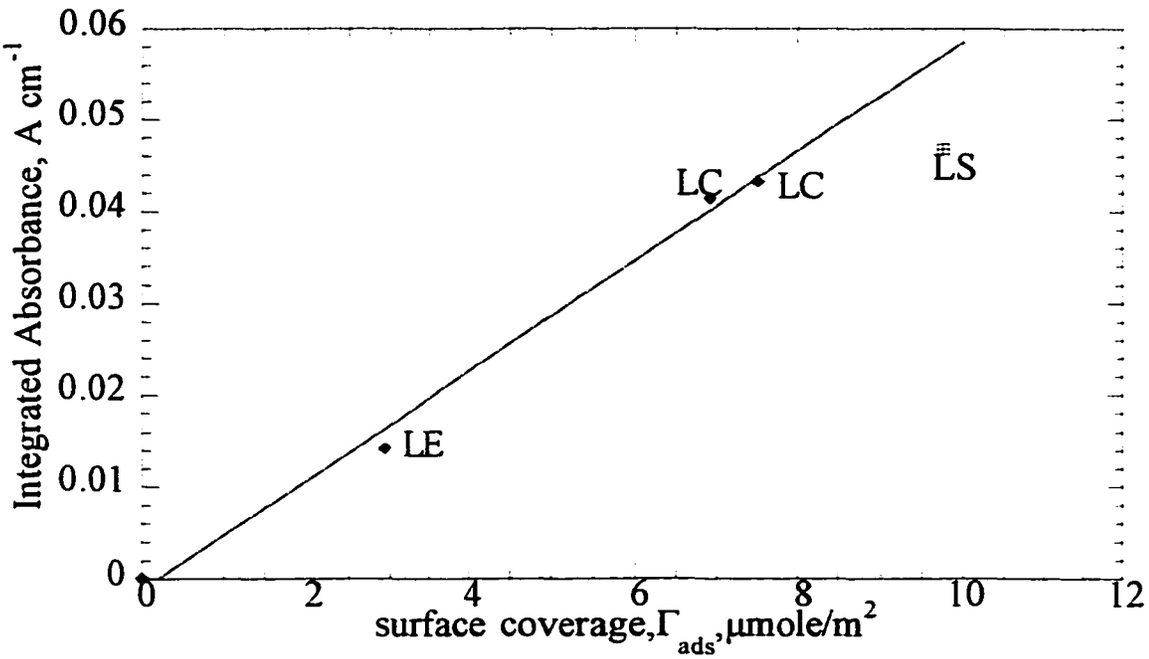

Figure 3.8. Calculation of ε_{ads} by IR measurements

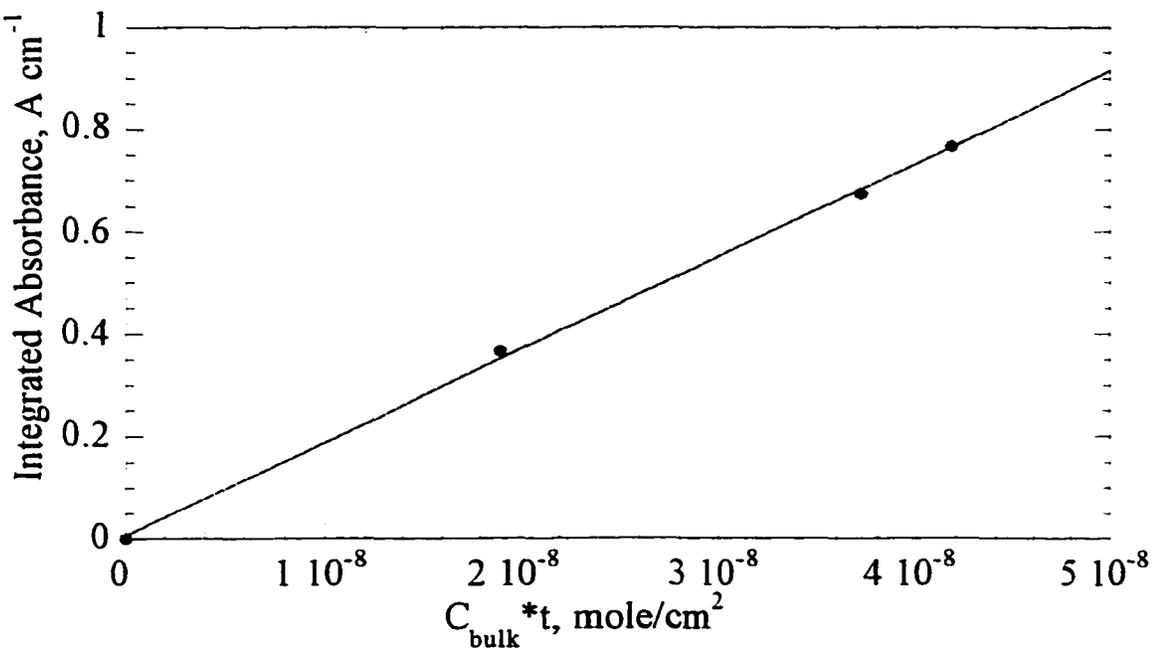

Figure 3.9. Calculation of _bulk by IR measurements

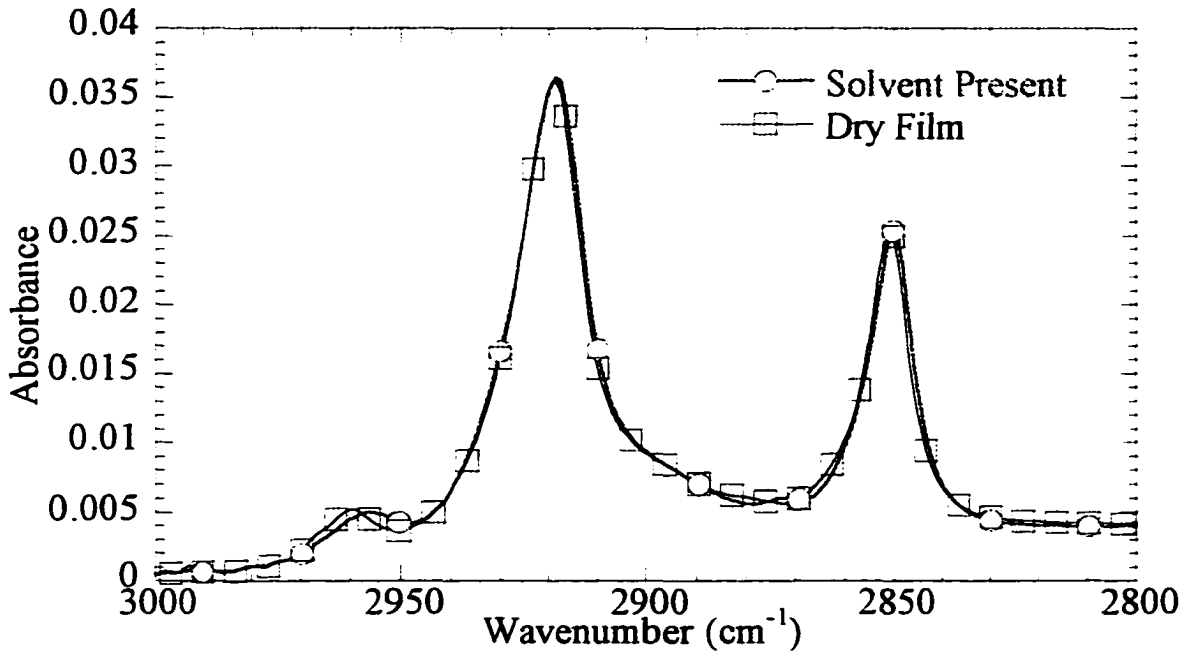

Figure 3.10 Spectra of adsorbed OTS in the presence and absence of the solvent, CCl_4

Pressure, π mN/m	8.5	16.5	23.0	30.0	48.0
Surface coverage, $\Gamma*10^{10}$ moles/cm^2	2.92	4.43	6.91	7.51	9.75
Transfer speed, mm/min	50	125	125	125	250
Transfer Ratio, TR	1.04	1.04	0.95	0.97	0.97

Table 3-1. Transfer Speed Used and TR Obtained during LB Transfer

Chapter 4 An *In-situ* Fourier Transform Infrared Study Octadecyltrichlorosilane Self-Assembly

4.1 Introduction

The study of thin organic monolayer films has attracted a great deal of attention over the past decade. Self-assembled monolayers (SAMs) are a class of thin organic films anchored to the substrate, usually by means of a chemical bond. They are formed via an adsorption process when an appropriate substrate is immersed in a solution containing the self-assembling surfactant. They are similar in organization and packing to Langmuir-Blodgett[39] films. SAMs of organosilane compounds on solid substrates like silica[2,29,31,32,97] and gold[12] offer an elegant approach to the design of molecularly sized microstructures. As a result, SAMs have already found use as ion-selective membranes[14-16], in the fabrication of bio-sensor arrays[16-18], in friction control[19,20], in adhesion promotion[21], and as surface coupling agents in the treatment of silica for chromatographic applications[22]. Earlier studies on organosilane SAMs have dealt with the chemical and physical interactions that control the formation, structure, and properties of these molecular assemblies[2,12,29-32,97]. We provide a brief overview of these studies in the following sections.

4.1.1 Structure and Physical Characteristics of Organosilane SAMs : *Ex-situ* Studies

The early studies of Sagiv et al.[2,4-6] have provided considerable information about the structure and physical properties of these SAMs. In particular, the authors postulated that the OTS molecules bind to the silanol sites on the surface of the substrate in addition to cross linking amongst themselves. This structure is schematically

represented in figure 1.3a, and was discussed earlier in chapter 1. However over the years this picture has changed considerably. First, Wasserman and his coworkers[29,98] using an array of techniques that included ellipsometry, x-ray photoelectron spectroscopy and low angle x-ray reflectivity showed that the OTS molecules bind to a layer of water that exists on the silicon oxide surface, and do not form direct linkages with the surface silanol. This result was further confirmed by the work of Angst et al.[26] and Tripp et al.[31]. Angst et al.[26] using ellipsometry and ATR-IR spectroscopy showed the lack of any OTS-surface silanol linkages. Tripp et al.[31] using IR spectroscopy showed that the adsorption of the OTS molecules onto high surface area silica occurred neither with the surface silanols nor with the 1st layer of the physisorbed water, but with the 2nd layer of water that was physisorbed on the silanol surface. The authors also showed that the cross condensation among the OTS molecules does not occur at room temperature. This view is schematically represented in figure 1.3b.

In addition to spectroscopic studies, scanning probe microscopy work has elucidated the self-assembly mechanism further. Schwartz et al.[99] and Britt et al.[100] performed ex-situ AFM studies on the adsorption of OTS from bicyclohexyl solutions onto mica surfaces and found that the growth of the monolayer follows a nucleation and growth mechanism. Bierbaum et al.[101] conducted similar measurements of OTS SAM formation from bicyclohexyl solutions onto silicon substrates and observed that the nucleation and growth mechanism, proposed by Schwarz et al.[99], appeared to govern the self-assembly of the OTS layer.

4.1.1.1 Effect of Solvent

McGovern et al.[102] have shown that the nature of the solvent used in the adsorption process has an effect on the time of formation, as well as the structure of the monolayer. The authors attributed the observed differences to the ability of the solvent to extract surface water into the bulk phase, where the OTS molecules undergo hydrolysis. In addition, when they used dioxane (a solvent with excess water) the authors observed that OTS molecules undergo extensive hydrolysis, which facilitates polymerization of the intermediate silanetriol, directly in competition with the surface adsorption of this triol.

CCl_4 is used in our adsorption studies as the solvent, due to its low water solubility when compared to other solvents that are used for self-assembly[94] and also because it does not adsorb IR radiation in the region of interest. In a study of silane adsorption on silica, Tripp et al.[31,69] compared the adsorption characteristics of OTS and TCMS onto fumed silica. The authors observed that both the hydrolysis and condensation of OTS are more difficult than for TCMS since it is easier for the latter to obtain a favorable orientation for hydrolysis with water and also for condensation and polysiloxane formation. The authors also postulated that the difference between the reaction of TCMS and OTS could be in part due to the partitioning of the alkyltrisilanol between the surface and the CCl_4 suggesting that octadecyltrisilanol would be more soluble in CCl_4 than methyltrisilanol. For the above-mentioned reasons we have used CCl_4 as our solvent of choice. However, we have performed adsorption studies with other solvents too, and these will be discussed later in this chapter.

4.1.1.2 Effect of Surface Hydration

The effect of the water present on the substrate has been investigated by several research groups[26,27,31,68]. Angst and Simmons[26] have also reported that the amount of

water on the substrate surface is vital for the formation of a complete monolayer. They were able to obtain a tightly packed monolayer on a fully hydrated silicon wafer, whereas reaction with a dry silicon wafer gave a disordered monolayer with low surface coverage. In a study by Le Grange et al[27], it was found that the OTS coverage increased with increase in hydration of the silica surface. However, the authors also report that a fully hydrated surface was not required for complete coverage of the substrate indicating that not every silane group is bonded to the surface. Tripp et al.[31] showed that the use of super saturated fumed silica as the substrate resulted in the formation of a polymerized OTS layer. Tripp et al.[31,68] also showed that the in the case of dehydrated substrates they observed the absorption of bulk water, (i.e.) water dissolved in the solvent, by the substrate surface. Finklea et al[12] report a study of OTS SAMs formation on gold, an oxide free surface, suggesting again that OTS SAMs can be obtained on a hydroxyl free surface. In a recent study by Allara et al[103], the authors proved that organosilane SAMs prepared on vastly different surfaces like hydrolyzed gold and oxidized silicon have similar IR spectra, and thus the SAM structure is the same irrespective of the presence or absence of silyloxy links at the surface. The above studies seem to suggest an adsorption mechanism in which the first step in the adsorption of the SAM is adsorption of a water film. This is followed by the physisorption of the silane to this water film. The last step in this process is the chemical reaction on the water film linking the silanes together and anchoring the net to the film. We report the results of our investigation on the effect of surface hydration on monolayer formation later in this chapter.

Even though all of the above mentioned studies provide a great deal of detail regarding the structure of the final monolayer they do not elucidate on the formation

mechanism and growth dynamics of the monolayers. Adsorption kinetic studies are required for such a task. Most of the early kinetic studies on organosilane self-assembly[2,4-6,29,30] have been confined to determining the change in surface properties by examination of the substrate surface before and after exposure to the adsorbate solution (i.e.) *ex-situ* analysis of the SAMs. While *ex-situ* strategies obviously offer a measure of versatility, they leave to speculation the rates of reaction and the solution-surface interactions responsible for the observed results.

4.1.2 *In-situ* Studies of OTS SAMs

In-situ measurements have the advantage that they are conducted with the monolayer in contact with the solvent/solution and thus eliminate the ambiguities associated with the removal, the associated drying of surfaces and their subsequent characterization. Banga et al.[104] used IR spectroscopy and AFM and have observed such differences between their *ex-situ* and *in-situ* studies, in terms of the times of formation and structure of their monolayers. The authors reported that less time is required for monolayer formation in the *ex-situ* studies when compared to their *in-situ* experiments. They attribute this difference to the varying amounts of water available in the two cases. They also suggest that the exposure of the substrate to atmospheric humidity when the experiments were conducted *ex-situ* may have affected the results. In view of these problems associated with *ex-situ* measurements, it is surprising that only a few studies[45,51,104] have investigated the process of organosilane self-assembly at interfaces using *in-situ* techniques.

Guyot-Sionnest et al.[51] used the technique of sum-frequency generation to monitor OTS adsorption *in-situ* onto fused silica, from a mixed solvent system (carbon

tetrachloride, chloroform, hexadecane). The authors followed the absorption by monitoring the intensity of the sum-frequency signal and observed that there was no change in the same after approximately 10 minutes of contact time. In a later study, Cheng et al.[45] used the technique of FTIR-ATR to characterize *in-situ*, the adsorption of OTS, from its solution in bicyclohexyl, onto a germanium surface. The authors characterized the adsorption by monitoring the increase in the integrated absorbance of absorption peaks characteristic of CH_2 bending motion.[45] The authors observe an exchange between the solvent, and the adsorbing OTS at the solid/liquid interface. Again, they observe no change in their IR signal, for times larger than 500 minutes. In both of the above-mentioned studies, there was no attempt to quantify the amount of OTS adsorbed on the substrate surface. Banga et al.[104] studied the adsorption of OTS from its solution in deuterated toluene onto a silicon ATR element. Again, the authors report no changes in the IR signal for times larger than approximately 140 minutes. They also calculated the Γ_{ads} of OTS from the integrated absorbance of their spectrum using the molar absorptivity of OTS in the bulk state. They found that the limiting surface concentration of OTS on the surface was 24±2 $Å^2$/molecule. In comparison, Wasserman et al.[29,98] have shown that the limiting surface coverage of an OTS self-assembled monolayer is 21±3 $Å^2$/molecule. When all three AFM studies are compared, the most striking fact is their disagreement with respect to the time needed for the adsorbed amount to reach a plateau, clearly showing that it is not possible to compare the kinetics of adsorption between different solvent and substrate systems. This observation is in agreement with the results of McGovern et al.[102] who have shown that the solvent used

has an effect on the time of formation as well as the structure of the monolayer (as discussed earlier in this chapter).

4.1.2.1 Experimental techniques for in-situ studies

A number of experimental techniques have been proposed over the years for the *in-situ* study of adsorption phenomena at the fluid-solid interface. These include attenuated total reflection Fourier transform infrared spectroscopy (ATR-FTIR)[45,48], atomic force microscopy[50], second harmonic generation[51], sum frequency generation[54], quartz crystal microbalance[33], and surface plasmon resonance spectroscopy[35]. In this study we use attenuated total reflection spectroscopy, ATR-FTIR. ATR-FTIR or internal reflection spectroscopy (IRS) is a method of obtaining the IR spectrum of species located near the surface of a solid substrate. The method was first developed by Harrick[56] and its principles been described in detail in chapter 2. This technique, when utilized in *in-situ* measurements, has the distinct advantage of identifying spectral features characteristic of the interfacial species in question and quantifying them with a high degree of sensitivity and specificity.

4.1.3 Current Work

From our kinetic measurements we observe that Γ_{ads} increases with time without reaching a plateau value. The adsorption seems to occur in two steps, a fast initial step and a second much slower step. The final surface coverage as well as the rate of adsorption are found to increase with increasing concentration of OTS in the bulk solution. Increasing the flow rate of the solution over the silicon ATR surface also increases the rate of adsorption. In addition, it is also observed that OTS molecules, when

adsorbing from a lot water content solvent like CCl_4 do not undergo self-condensation. However, when the same molecules adsorb from their solution in chloroform, which has a higher water content[94], the OTS molecules polymerize in solution. Furhtermore, we offer proof that ordering is occurring in the adsorbing layer as the surface coverage increases from zero to its final value. Moreover, by using a Si wafer sandwiched to a Ge ATR (as described earlier in chapter 2), we are able to overcome the shortcomings of the Si ATR and thereby extend the useful spectral range to beyond 1600 cm^{-1}. The spectral data obtained by using the $Ge/Si/SiO_2$ system provides evidence for the ordering occurring in the adsorbing OTS layer (i.e.) as there is an increase in the surface coverage, there is a splitting of the methylene bending moment at 1460 cm^{-1}. In addition, *in-situ* polarized FTIR-ATR data of OTS self-assembly from solution offer further proof of the conformational changes and ordering occurring among the adsorbate molecules at the solid/liquid interface.

4.2 Adsorption Studies

The adsorption of OTS onto the native silicon oxide of the silicon IRE surface was monitored *in-situ* using FTIR spectroscopy in the ATR mode. A schematic of experimental setup is shown in figure 4.1. The silicon IRE, with dimensions of 50x10x3 mm^3, was clamped between the two Teflon® blocks, each of which has a flow channel machined into it. This arrangement constituted the flow cell. Only one of the flow channels was used. The dimensions of the flow channel are 38.1x3.1x1.3 mm^3. Figure 4.2 shows a schematic of the flow cell. After assembly, the flow cell was mounted on a variable angle ATR attachment purchased from Harrick Scientific. The "set-angle" on the ATR attachment was locked at 45°. The angle of incidence at the silicon IRE/OTS film

interface is 45°, and is greater than the critical angle for this system, which is calculated to be ~23° [56].

After priming the system, a constant, predetermined flow rate for the solvent/solution was used throughout the experiment. By using a Y-connector at the inlet, it was possible to flow either surfactant solution or pure solvent without disrupting the flow setup. The experiments were conducted under ambient laboratory conditions (T~23^{0}C, ambient humidity). First, the pure solvent was passed through the cell, which allowed us to check for leaks and also to collect a spectrum to be used as a background. A freshly prepared OTS solution was used for every experiment. After the background spectrum of the pure solvent was collected, the OTS solution flow was started and spectra collected. Each spectrum was averaged over 100 scans. The time required for each spectrum was approximately 36 seconds (@2cm^{-1} resolution, interferogram scan, double sided symmetry). The spectra were collected at intervals of 36 sec for the first hour and every 600-sec thereafter. The interferograms were converted into absorbance files by referencing them to the spectrum of pure solvent. The adsorption of OTS was monitored by monitoring the absorption peak characteristic of the asymmetric -CH- stretch of the CH_2 moiety in the adsorbing OTS.

4.3 Results and Discussion

4.3.1 *In-situ* studies of OTS self-assembly

In figure 4.3, a typical series of spectra in the CH stretching range of the adsorbing OTS can be seen. Clearly, there are changes occurring in the relative intensities and positions of the absorption bands with time. These changes are indicative of the increasing amount of surfactant adsorption, and also the change in the ordering of the

adsorbate species. The spectra of the adsorbing OTS, as shown in figure 4.3, were numerically integrated between 2902 cm^{-1} and 2945 cm^{-1} to obtain the integrated absorbance. The calculation of the surface coverage, Γ_{ads}, from the integrated absorbance has been described earlier in chapters 2 and 3.

In figure 4.4 we observe the variation of surface coverage, Γ_{ads}, with time for different bulk concentrations of OTS. Clearly, Γ_{ad} increases with time, and also with increasing bulk concentration of OTS. For all the concentrations, the rate of adsorption changes considerably over time. For short times, the rate of adsorption is high, while for long times, the rate is reduced considerably. These results are similar to those obtained by others in the study of carboxylic acids adsorption onto glass surfaces[36,37], adsorption of thiols onto gold[11] and more recently in the adsorption of silanes onto silica surfaces[104]. The high initial rate of adsorption has usually been attributed to the large number of surface sites available for adsorption at the early stages of the process[11]. However, as the adsorption process continues, the number of available sites is reduced and further adsorption is limited by the rate of rearrangement of the molecules already adsorbed onto the surface[11]. Hence the rate of adsorption is substantially reduced in the later stages. In addition, we also observe that OTS continues to adsorb even at the end of 14 hours without ever reaching a saturation surface coverage, at least within the time range of our experiments.

In figure 4.5, the integrated absorbance of the two bands at 2850 and 2920 cm^{-1} (i.e.) the symmetric and the asymmetric stretch of the methylene group in the adsorbing OTS, are graphed as a function of time. The behavior of the integrated absorbance of the two bands is similar, an expected result, since they represent the same functional group of

the adsorbing surfactant. The ratio of the absorbance of these bands, also shown in figure 4.5, suggests a similar conclusion.

Earlier studies in our lab[76], also described in chapter 3, have shown that the limiting coverage of an OTS monolayer at the air/water interface is 18±1 $Å^2$/molecule. These results agree well with low angle X-ray reflection data[98]. It is evident from figure 4.4 that a monolayer coverage (i.e.) 18±1 $Å^2$/molecule (~9.2±0.6 μmole/m^2) is attained for the highest concentration. However, for the lower concentrations, monolayer coverage is not attained even after 14 hours. This is in contrast to other *ex-situ* studies[2,29] that suggest that a monolayer is attained within minutes. However, our results are in agreement with those of Banga et al.[104], a study that was discussed extensively in the introduction of this chapter. We also believe that this difference in monolayer formation times can be attributed to the different experimental conditions, mainly different solvents, employed by the different groups[2,76,104].

In order to investigate the difference in monolayer formation times between *in-situ* and *ex-situ* studies, we performed *ex-situ* studies of OTS adsorption from CCl_4 (solution concentration ~3 mM, 14 hours deposition time) onto silicon wafers in our lab. Contact angle measurements were made on these samples with water and methylene iodide as the probe fluids. We observed that the water contact angles on these substrates was 105°±2°, and methylene iodide contact angles were 63°±2°. In comparison, the water contact angles measured on the substrate at the end of the *in-situ* adsorption experiments was 103°±2°, and methylene iodide contact angles were 60°±3°. Available data in the literature[2] suggest that a complete monolayer of OTS exhibits a water contact angle of

112°±1°. This leads us to believe that the coverage on the substrate is indeed sub-monolayer, and not otherwise.

In figure 4.6 we have graphed Γ_{ads} as a function of time for two different flow rates, and for two different concentrations. It is evident that the rate of OTS adsorption is dependent on the flow rate of the surfactant solution across the silicon ATR surface. In the case of the higher concentration of ~23 mM, the rates of OTS adsorption are similar for the short times. (≤ 600 seconds). There is however a clear difference in the surface coverage from that point on until the end of the adsorption experiment, where the two surface coverages seem to match. However, in the case of the lower concentration of ~3mM, the difference in the rates of adsorption are distinct from the start of the adsorption process, indicating that the adsorption at short times is more dependent on convection at lower concentrations. At long times, both the curves seem to reach similar surface coverage. These results seem to suggest that flow rate effects are important, especially at short times.

4.3.2 Structural Changes in the adsorbing layer

Figure 4.3 also gives us useful information about the ordering occurring in the adsorbing layer. In particular, the peak position of the absorption band characteristic of the asymmetric C-H stretch of the CH_2 moiety is shifting towards lower wavenumbers and is also increasing in intensity with time. This shift in the position of the above mentioned peak, typically in the range of five to six wavenumbers, has been observed earlier,[76,82,84] and has been attributed to the change in the packing order of the surfactant molecules in the adsorbate layer. In addition to the absorption bands characteristic of the CH_2 groups at 2920 cm^{-1} and 2850 cm^{-1}, we also observe that the band characteristic of

the asymmetric C-H stretch of the CH_3 moiety (at about 2960 cm^{-1}) is increasing with time. In figure 4.7, in addition to the shift of the above-mentioned peak, we also observe that the peak characteristic of the methylene bending mode at ~1460 cm^{-1} undergoes a split with increasing surface coverage. This split in the bending mode peak is indicative of increasing crystallinity in the adsorbing layer. The latter spectra were obtained using the sandwiching technique described in chapter 2.

4.3.3 Water Effects on SAM formation rates and structure

As discussed earlier in section 1.4, the presence of trace amounts of water in the solvents is required to hydrolyze the chlorosilane groups in the OTS molecule[26,27,31,38,102,105]. The insufficiency of this water of hydrolysis in the solvent would reduce the rate of OTS self-assembly since the OTS molecules. Thus the water content in the solvent/substrate system plays a crucial role in determining the formation rates and structure of SAMs. In the following sections we present the results of our studies on the effect of surface hydration and water content in solvent on the SAM structure and formation.

4.3.3.1 Effect of Surface Hydration

In figure 4.8, we have shown the variation of the integrated absorbance (of the asymmetric methylene stretch) with time for three different cases of surface hydration. Varying the time for which the substrate was kept under water before being assembled into the flow cell controlled the surface hydration. We can clearly see that the rate of adsorption is dependent on the extent of surface hydration, and increases with increase in surface hydration. This is an expected result and is in agreement with earlier studies[27,31,68]. In another study performed in our research group[106], it has been observed

that when a solvent is made to flow over a hydrated substrate, it removes some of the water from the substrate, a result that is in agreement with McGovern et al.[102]. As was stated earlier in our experimental section, as part of the experimental protocol, the pure solvent is passed over the substrate surface before the start of the adsorption process in order to check for leaks in the system and also to obtain a reference spectrum. We believe that this experimental step in the adsorption process, albeit wholly a necessary component of the study, results in a depletion of the surface hydration, and could be a reason for the relatively slow rates of adsorption that we observe in this study, in comparison to other published results.[1] It is also known that among the following solvents, hexadecane, chloroform, toluene and carbon tetrachloride, carbon tetrachloride has the lowest water solubility[94]. The low water content of CCl_4 also contributes to the increased time for the formation of the OTS monolayer in our study, as compared to its adsorption from other solvents[2,32,102,104,105].

4.3.3.2 Effect of water content in solvent

In figure 4.9, we have shown the effect of the solvent on the adsorption of OTS. The solvents in this case were $CHCl_3$ and CCl_4. It has been shown earlier that $CHCl_3$ has a higher water content in comparison to CCl_4[94]. We observe that the OTS molecules have polymerized when they adsorb from a solution in $CHCl_3$. The peaks characteristic of the Si-O-Si linkages[68,107] in the bulk solvent occur at 1070 and 1020 cm^{-1}. These peaks are clearly visible when the solvent used in $CHCl_3$ and absent when the solvent is CCl_4.

---

[1] This result has been independently verified by *in-situ* AFM measurements performed in our research group, the results of which are to be published soon.

Moreover, when the adsorption occurs from CCl_4, the peak at 898 cm^{-1} that is characteristic of the Si-OH stretch of the molecules in the bulk[68], is observed. This provides evidence for the fact that when dissolved in a solvent of low water content like CCl_4, the chlorosilanes are hydrolyzed, but do not undergo condensation. Thus, the surfactant species are predominantly monomeric when the adsorption occurs from a low water content solvent like CCl_4. In addition, the formation of any Si-O-Si linkages among the adsorbed molecules can be detected by the appearance of IR peaks at 1007 cm^{-1}. This peak characteristic of the strained Si-O-Si stretch, results from self-condensation among the molecules in the adsorbed layer. We observe that this peak characteristic of the cross-condensed species is not observed even at the end of 24 hours. This peak starts to appear after the monolayer is allowed to cure at room temperature for over 48 hours (not shown). Thus, it is apparent from the foregoing discussions that the OTS species adsorbed from CCl_4 onto the SiO_2 surfaces have not undergone cross condensation. These results are in agreement with the results of McGovern et al.[102] who studied the effect of the solvent on the self-assembly of OTS. The authors found that when they used dioxane (a solvent with excess water like $CHCl_3$) the OTS molecules undergo extensive hydrolysis, which facilitates polymerization of the intermediate silanetriol, directly in competition with the surface adsorption of this triol.

Recent AFM studies of partially formed OTS monolayers have been performed by several groups[99-101]. These groups have used bicyclohexyl as the solvent of choice, and have reported the formation of fractal patterns in partially formed monolayers. However, the amount of water available in their systems for OTS hydrolysis and polymerization is different from our study, and as discussed earlier, the solvent affects

the monolayer formation times and structure[102]. AFM studies of partially formed monolayers have been performed in our group[106]. We have seen the appearance of fractal like patterns similar to those reported in earlier studies[100,101] when the solvent system (Hexadecane+$CHCl_3$+CCl_4) proposed by Sagiv[2] is used. However when CCl_4 is used as the only solvent, and even for contact times in excess of 30 minutes, we observe the complete lack of fractal like features which are characteristic in the previously mentioned studies. These results further reinforce the effect of the solvent on the self-assembly process.

4.3.4 Interactions among the OTS molecules

The forces that arise due to the van-der Waals' interaction between the hydrocarbon chains of the adsorbing species constitute one of the three main driving forces for the self-assembly of molecules at solid/liquid interfaces. This was discussed in detail in section 1.2. In order to investigate the existence, if any, of these interactions in the case of the OTS species, we studied the behavior of OTS monolayers at the air/water and solid/liquid interfaces, and we present the results of these studies in the following sections.

In an earlier study by our group, we had shown that OTS molecules at the air/water interface exhibit interactions among their hydrocarbon chains, especially when they are in their unpolymerized state[76]. In figure 4.10, the π-A isotherm of the OTS molecules at the air/water interface is shown for two different experimental conditions. Clearly, we can see that the molecules in the unpolymerised state still exhibit lateral interactions among their hydrocarbon chains, as a result of which they undergo the LE-LC phase transition. However, when the OTS molecules are in a polymerized state they

are incapable of undergoing this transition. It is important to note that the limiting coverage of the OTS monolayer is approximately 18 ± 1 $Å^2$/molecule (~9.2 ± 0.6 μmole/m^2). This is in agreement with the surface coverage obtained at the end of the process for the highest concentration (figure 4.4). Having thus established the existence of the interactions between the OTS molecules at the air/water interface, we wanted to prove their existence at the solid/liquid interface too.

In order to verify the existence of interactions among the OTS molecules at the substrate interface, and study the conformation changes occurring in the adsorbate layer, we polarized the incident radiation parallel ($I_{\parallel}$) and perpendicular ($I_{\perp}$) to the plane of incidence, and monitored the adsorption with time. The details of polarized ATR-FTIR spectroscopy are described in detail elsewhere[56,83,86]. We denote the integrated absorbance of the band located at ~2920 cm^{-1}, in the perpendicular and parallel directions, as $A_{\perp}$ and $A_{\parallel}$ respectively. The ratio of $A_{\perp}$ to $A_{\parallel}$ is a measure of the orientation of the adsorbate at the interface[56,83,86].

$$\frac{A_{\perp}}{A_{\parallel}} = \frac{|E_{Y0}|^2}{|E_{X0}|^2 + |E_{Z0}|^2} \tag{4.1}$$

where E_{Y0} is the electric field amplitude in the direction perpendicular to the plane of incidence, and E_{X0} and E_{Z0} are the electric field amplitudes in a direction parallel to the plane of incidence[32,56]. In figure 4.11, we show the variation of $A_{\perp}/A_{\parallel}$ with time, for OTS self-assembling from a 3mM solution. The two curves are for two different flow rates (0.35 ml/hr and 0.15 ml/hr). In both the cases it can be see that the ratio goes through a minimum. This minimum seems to suggest that changes are occurring in the

adsorbing layer. We discuss our explanation for the occurrence of this minimum in the following section.

A surfactant molecule that adsorbs onto the substrate at the beginning of the adsorption process would tend to assume a random orientation on the substrate surface. The methylene asymmetric vibrational mode that we are monitoring is in a direction perpendicular to the plane of incidence. As a result, a molecule at the beginning of the adsorption absorbs a greater amount of $I_{\perp}$ in comparison to $I_{\parallel}$. However, as the adsorption process continues, the hydrocarbon tails interact and the surfactant molecules become oriented with their tails lifted off the substrate surface. As this process is occurring, there is a decrease in the amount of $I_{\perp}$ that is absorbed with a corresponding increase in the adsorption of $I_{\parallel}$. As a result, the ratio of $A_{\perp}$ to $A_{\parallel}$ decreases at first and goes through a minimum. As further ordering occurs in the adsorbing layer in terms of conformational changes, the ratio begins to rise again. Similar transitions have been observed recently in a study of adsorption of thiols on gold[108]. The authors report that when adsorbing from 2-butanol, the thiol molecules initially adsorb on gold with the molecular axis of their hydrocarbon chains oriented parallel to the surface. As the surface coverage increases to near saturation, a two-dimensional phase transition occurs and produces islands composed of molecules with their hydrocarbon axis oriented; 30° from the surface normal.

It can be clearly seen from figure 4.11 that in the case of adsorption occurring from the solution at a flow rate of 0.35 ml/hr, for the first 30 minutes of the adsorption process, the ratio is decreasing. After approximately 30 minutes, we observe that the ratio is increasing. This is indicative of the interactions between the hydrocarbon tails coming

into effect. From figure 4.4, we observe that the surface coverage at the same time, (i.e.) 30 minutes, is approximately 1.6 μmole/m^2. This corresponds to an approximate molecular area of 100 $Å^2$. We can see from figure 4.10 that this is close to the molecular area at which the molecules at the air/water interface begin to interact with one another, as a result of which there is an increase in the surface pressure. Thus the surface coverage at which the minima is occurring at the solid/liquid interface can be likened to the surface coverage at the which the transition from the gaseous to the liquid expanded phase occurs at the air/water interface. It is important to note that the time required for this transition is increasing with decrease in flow rate, (i.e.) 30 minutes at 0.35 ml/hr, vs. 90 minutes at 0.15 ml/hr. This suggests that the transition occurs only when a definite surface coverage is attained on the substrate surface, since the adsorption rate could increase with increase in flow rate.

Moreover, as discussed in earlier chapter 3, it has been shown that polymeric molecules of OTS do not undergo the LE-LC transition at the air/water interface since they are incapable of exhibiting these hydrocarbon tail interactions. By extending these results to the solid/liquid interface, we can conclude that the minima in the $A_{\perp}/A_{II}$ curve is due to the interactions existing between the hydrocarbon tails of the individual molecules at the substrate surface. Hence we can conclude that the adsorbates at the solid/liquid interface consists primarily of monomeric species and not polymerized particles. This is also supported by two other independent observations. First, the shift in the position of the absorption peak characteristic of the asymmetric -CH- stretch and second, the splitting of the peak characteristic of the bending moment of the $-CH_2-$

moiety in the adsorbate. These provide proof of the ordering occurring in the adsorbate layer with increasing surface coverage.

4.4 Conclusions

Experimental results concerning the self-assembly of OTS from its carbon tetrachloride solution onto the native silicon oxide layer of a silicon ATR/wafer are presented. We have shown the effect of bulk solution concentration, surface hydration, water content in solvent and flow rate on the self-assembly of OTS. We have found that Γ_{ads} increases with time without reaching a plateau value. The adsorption occurs in two steps, a fast initial step and a second step that is much slower. The final surface coverage is found to increase with the concentration of OTS in the bulk solution. In addition, the rate of adsorption is found to increase with increasing concentration of OTS in the bulk solution and also with increasing flow rate of the OTS solution over the silicon ATR surface. Our experiments have shown that the rate of adsorption of OTS increases with increase in flow rate, with greater water content in solvent system, and with greater hydration of the substrate surface. In addition, we have also used a Si wafer/Ge ATR system to increase the spectral range available for data analysis. The peak characteristic of the methylene bending moment splits with an increase in the adsorbed amounts. This complements the data from the shift in the position of the asymmetric methylene stretch and is suggestive of the increasing order occurring in the adsorbed layer. We present the first *in-situ* polarized FTIR-ATR data of OTS self-assembly from solution. The data offer qualitative proof of the interactions existing between the hydrocarbon tails of the OTS molecules, and conformational changes occurring during the self-assembly process.

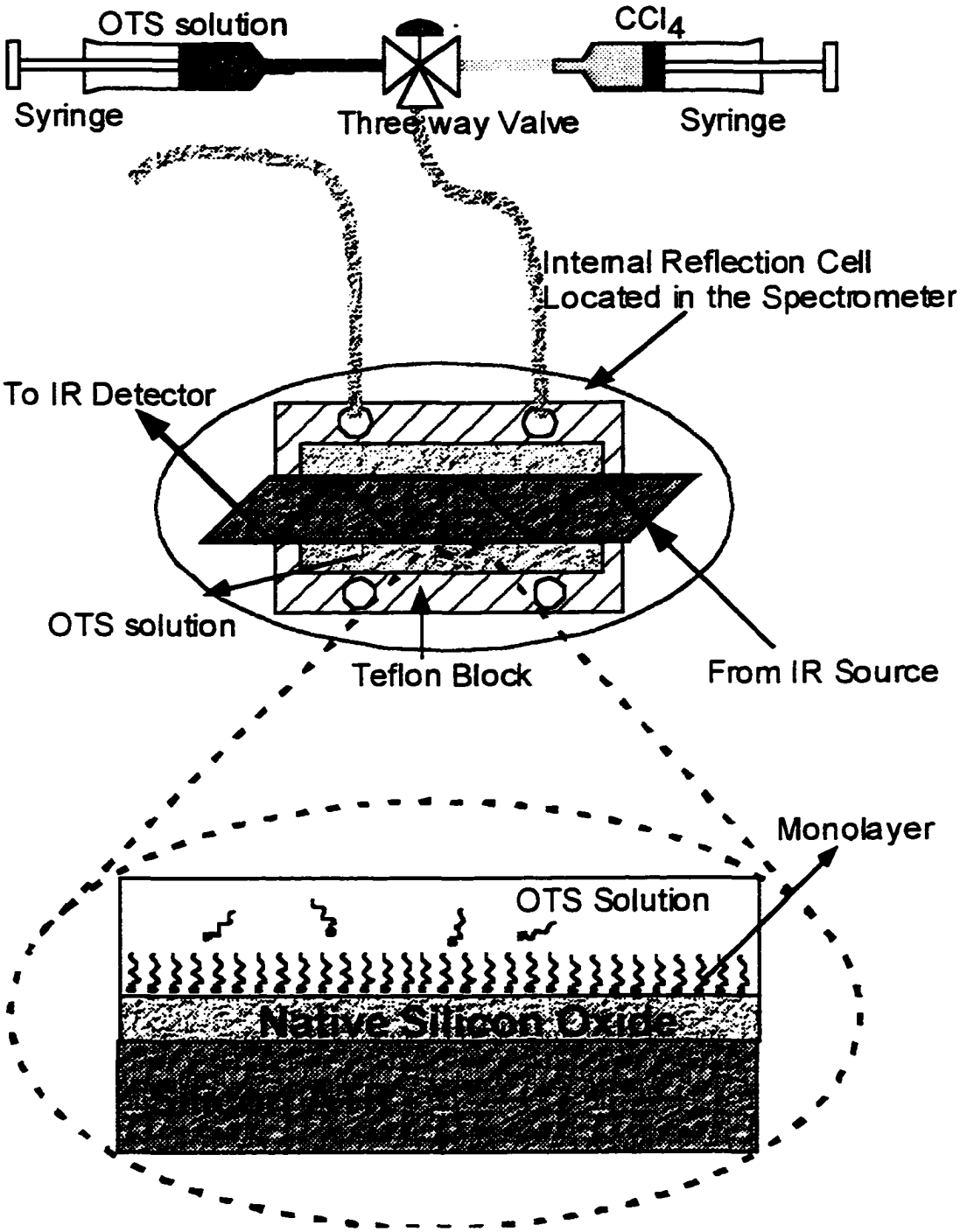

Figure 4.1. Experimental Set-up for *in-situ* monitoring of OTS adsorption

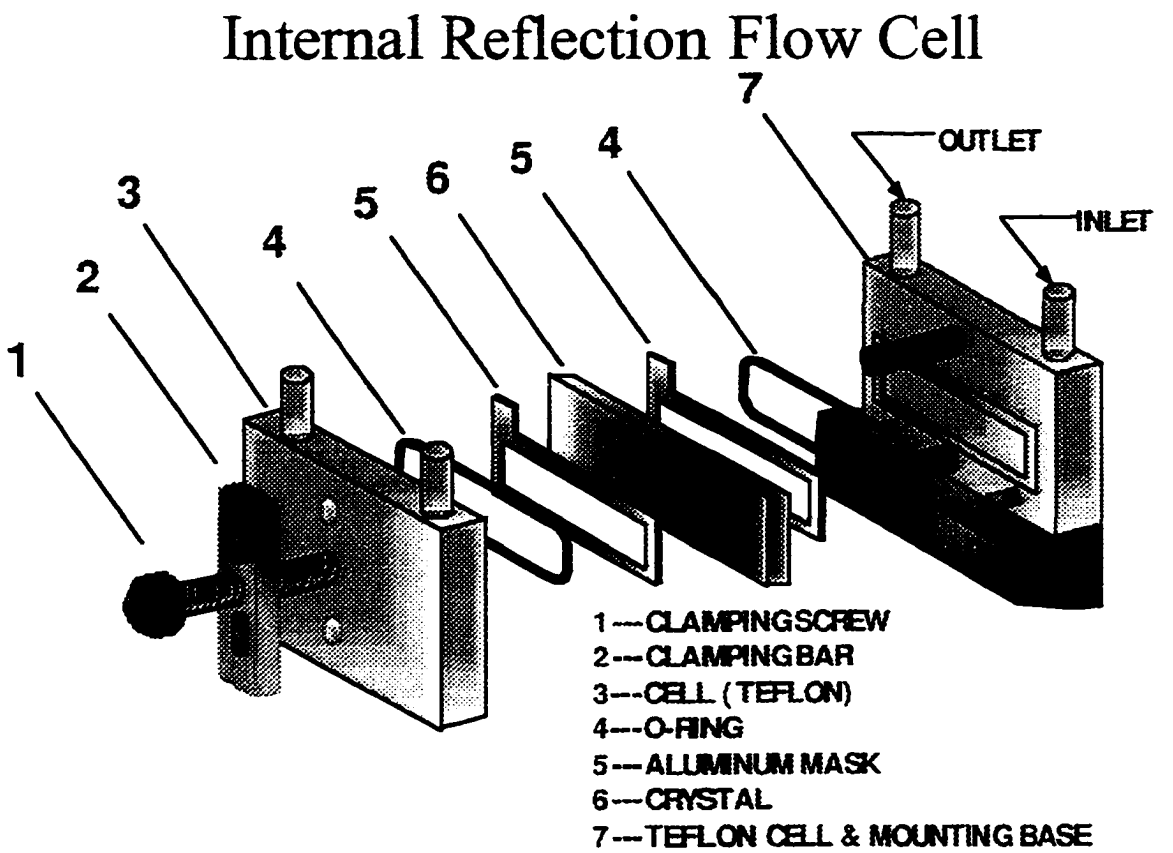

Figure 4.2. Harrick® flow cell for *in-situ* FTIR study.

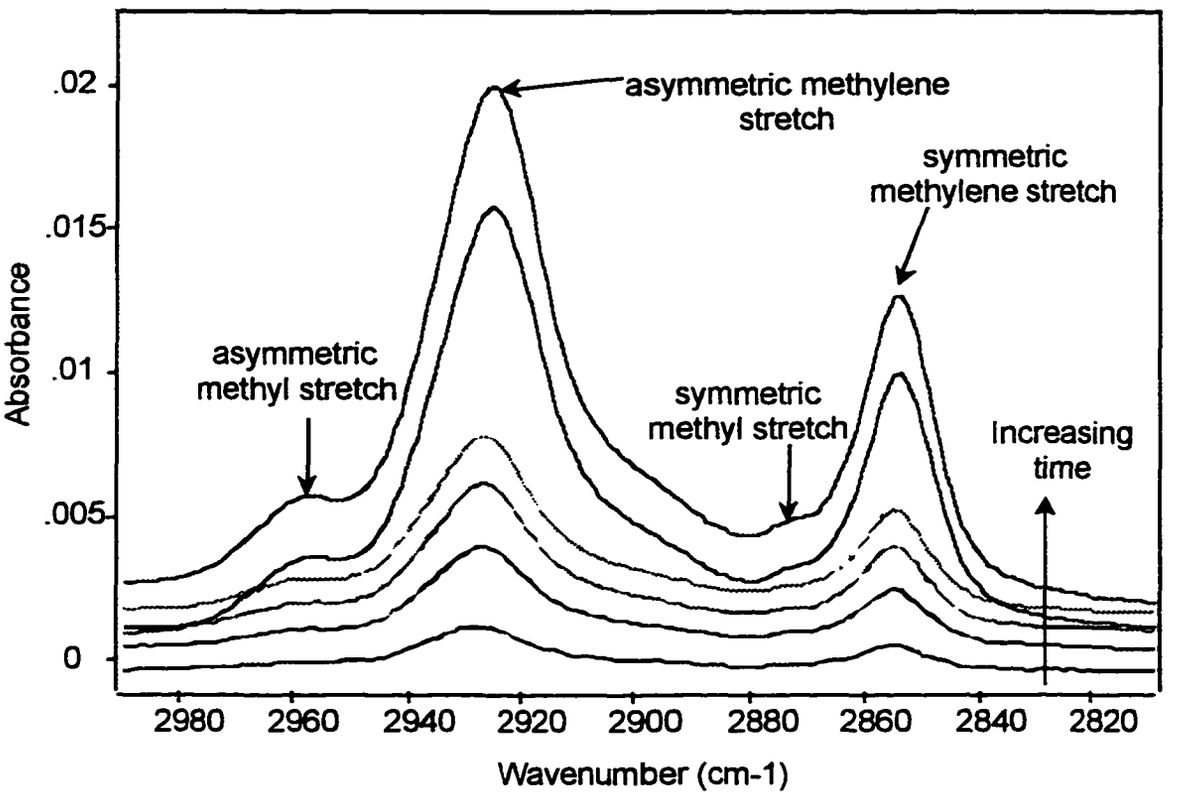

Figure 4.3. Variation of the -CH- stretching region in the IR spectrum of adsorbing OTS with time

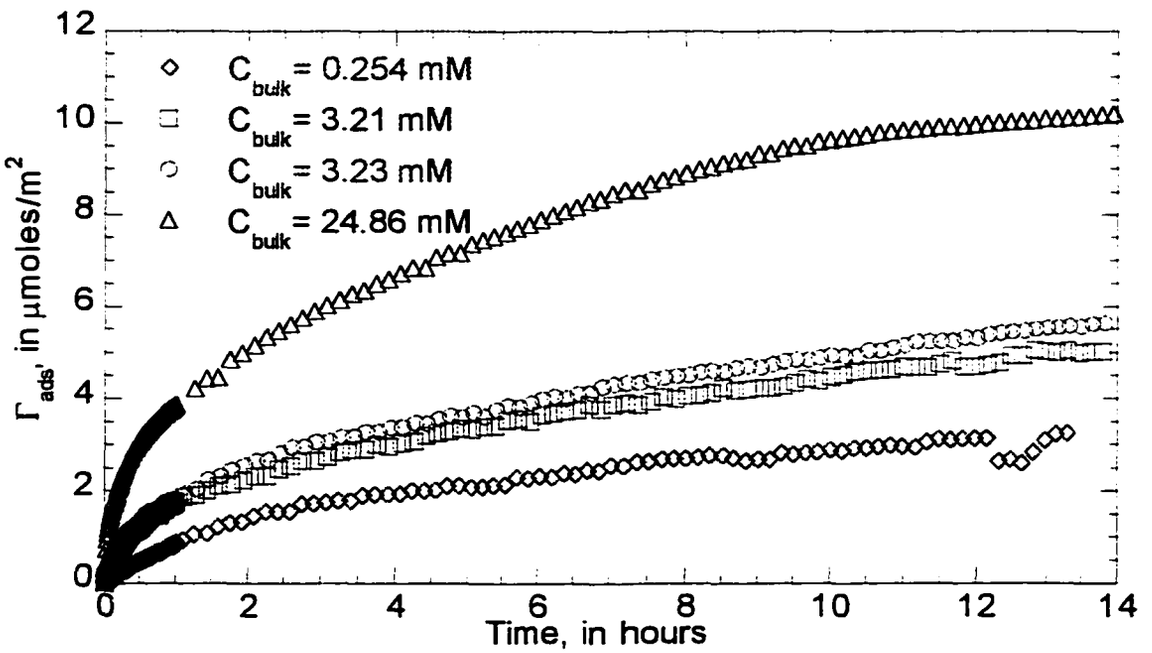

Figure 4.4.Effect of bulk solution concentration on the surface coverage of OTS.

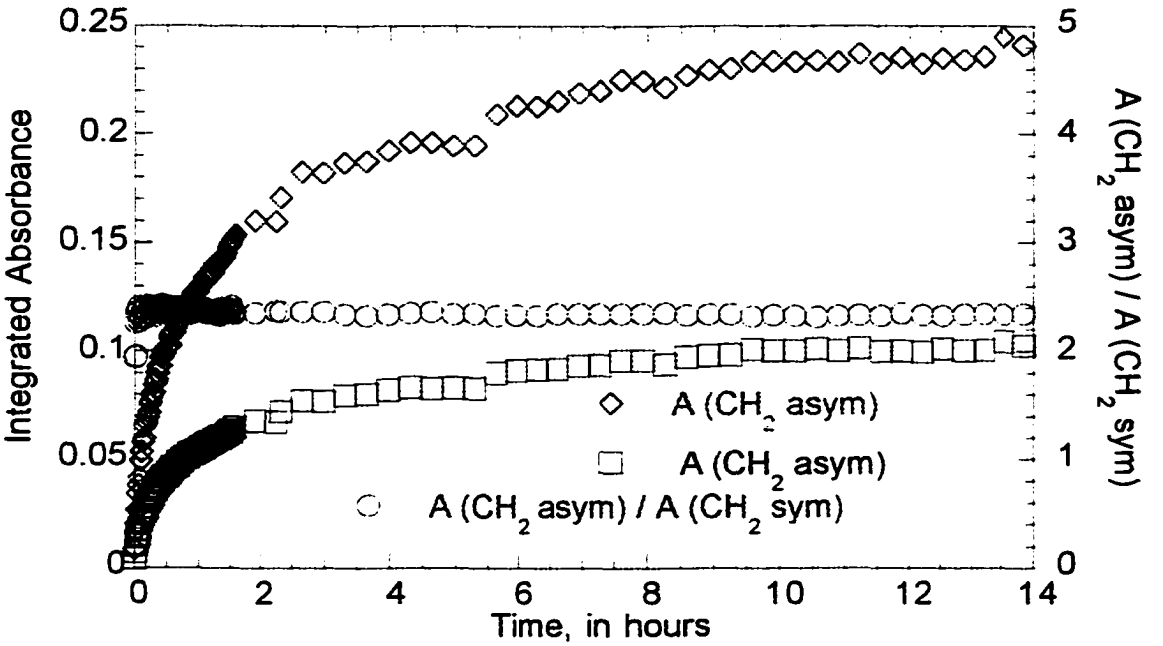

Figure 4.5. Integrated Absorbance of ν_s(CH) and ν_a(CH) of the methylene group in the adsorbing OTS as a function of time.

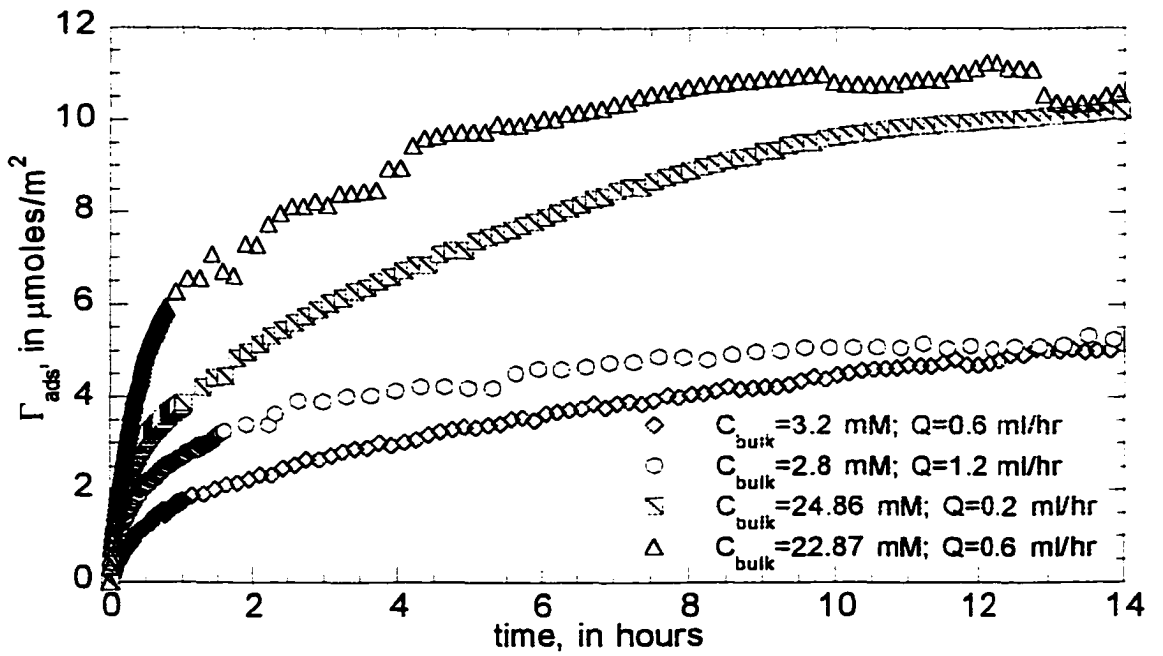

Figure 4.6. Effect of convection on the surface coverage of OTS.

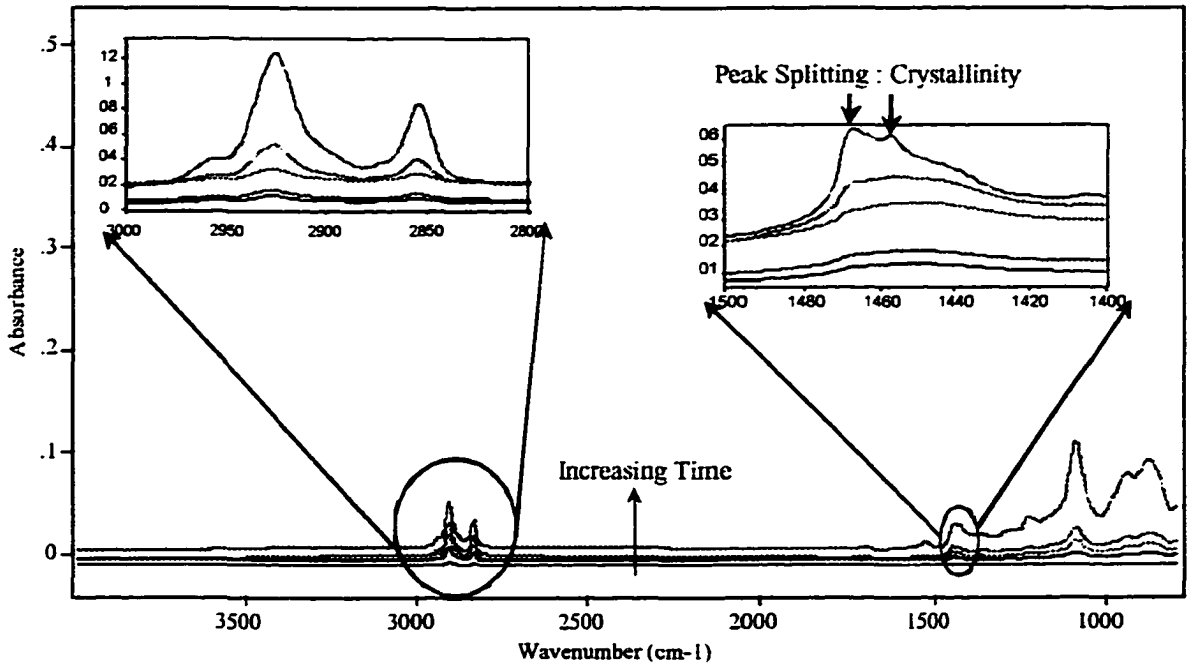

Figure 4.7. Proof of crystallinity in the adsorbed layer: the split of the methylene bending mode peaks & the shift in position of the -CH_2- asymmetric stretch.

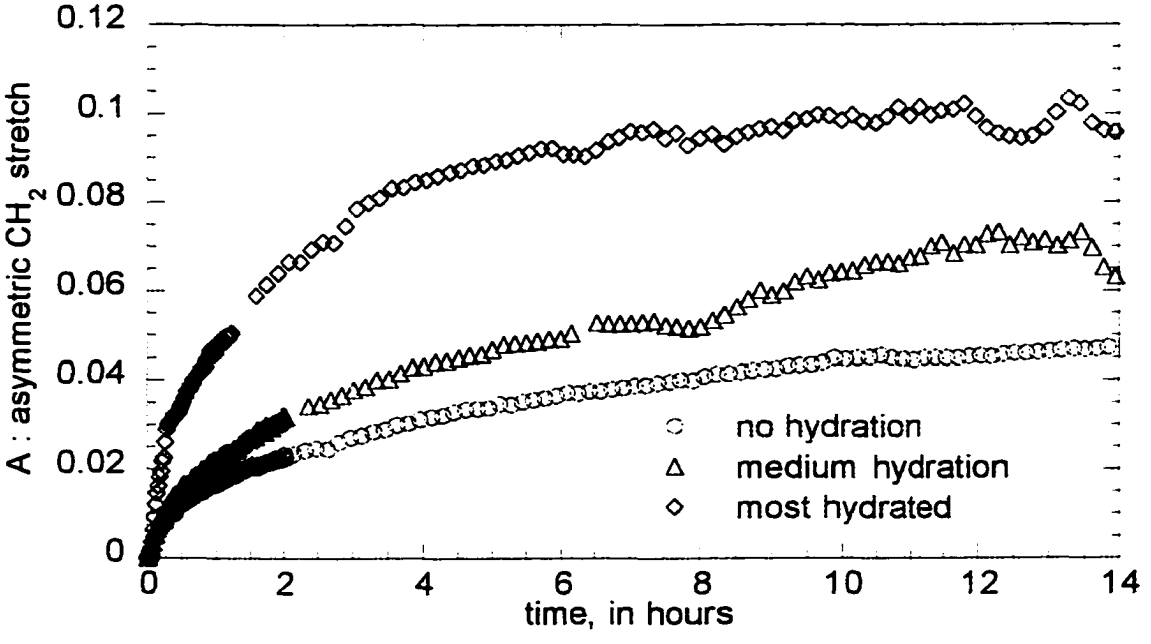

Figure 4.8.Effect of Surface Hydration on the rate of OTS adsorption

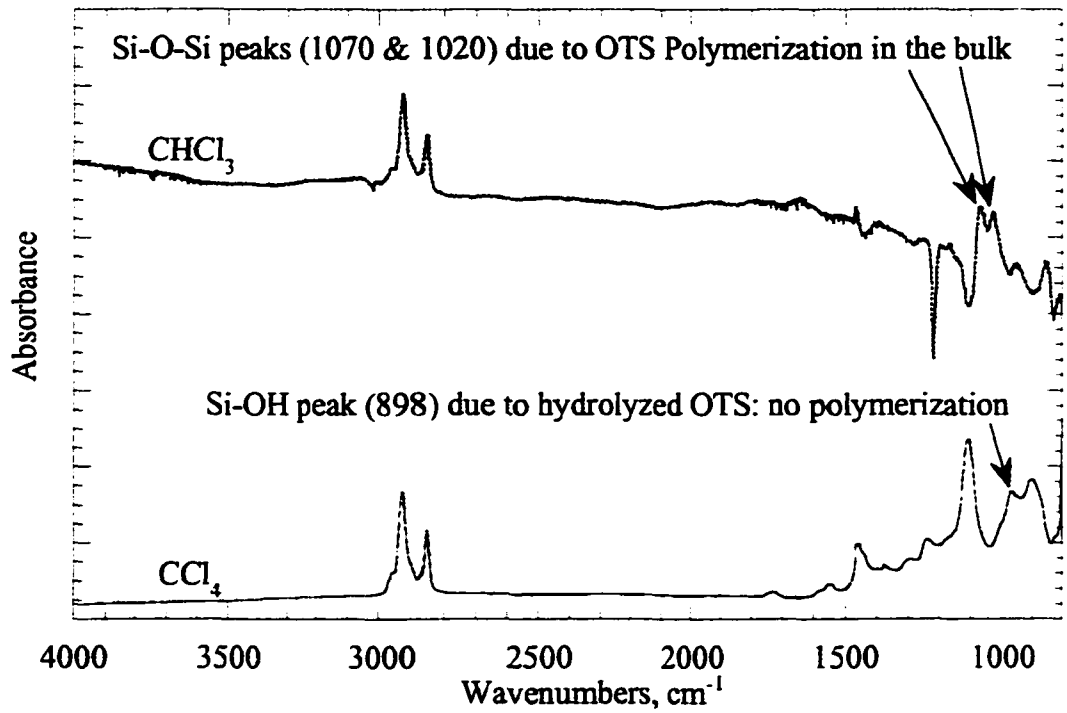

Figure 4.9. IR spectrum of OTS adsorbing onto the Si wafer sandwiched to the Ge ATR. The effect of solvent on the polymerization of OTS species in the bulk.

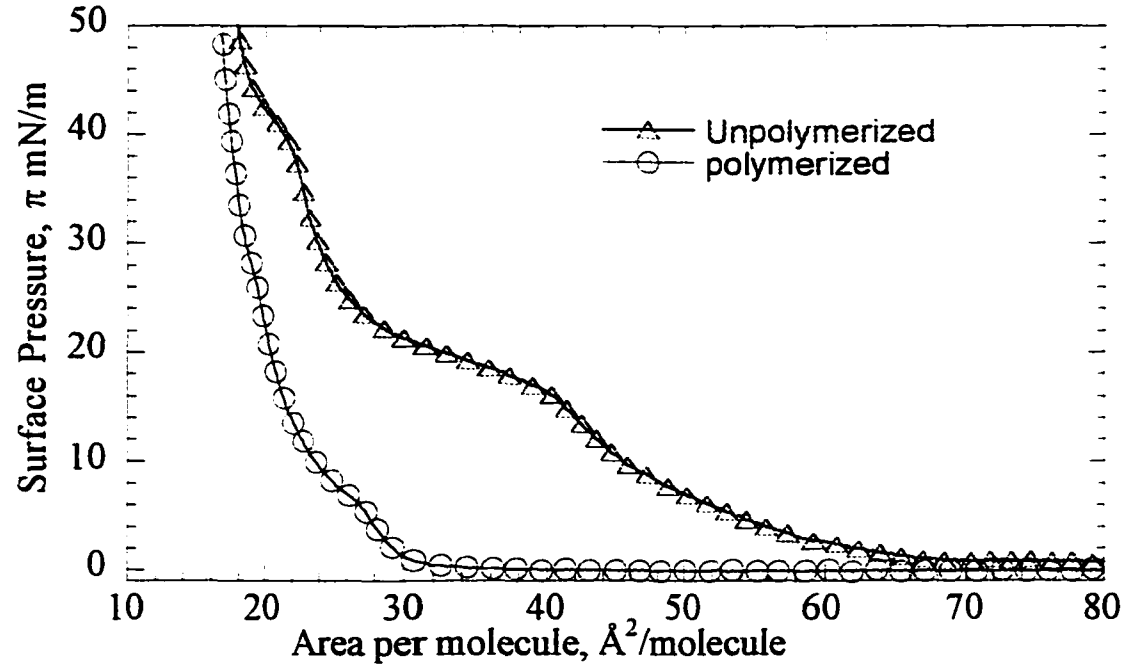

Figure 4.10. π-A isotherm of OTS. The existence of the LE-LC coexistence region has been attributed to the van der Waals interactions of the hydrocarbon tails of the surfactant molecules at the air/water interface (see text). It can be seen that the limiting surface coverage of OTS at the air/water interface is approximately 18 ± 1 Å^2/molecule.

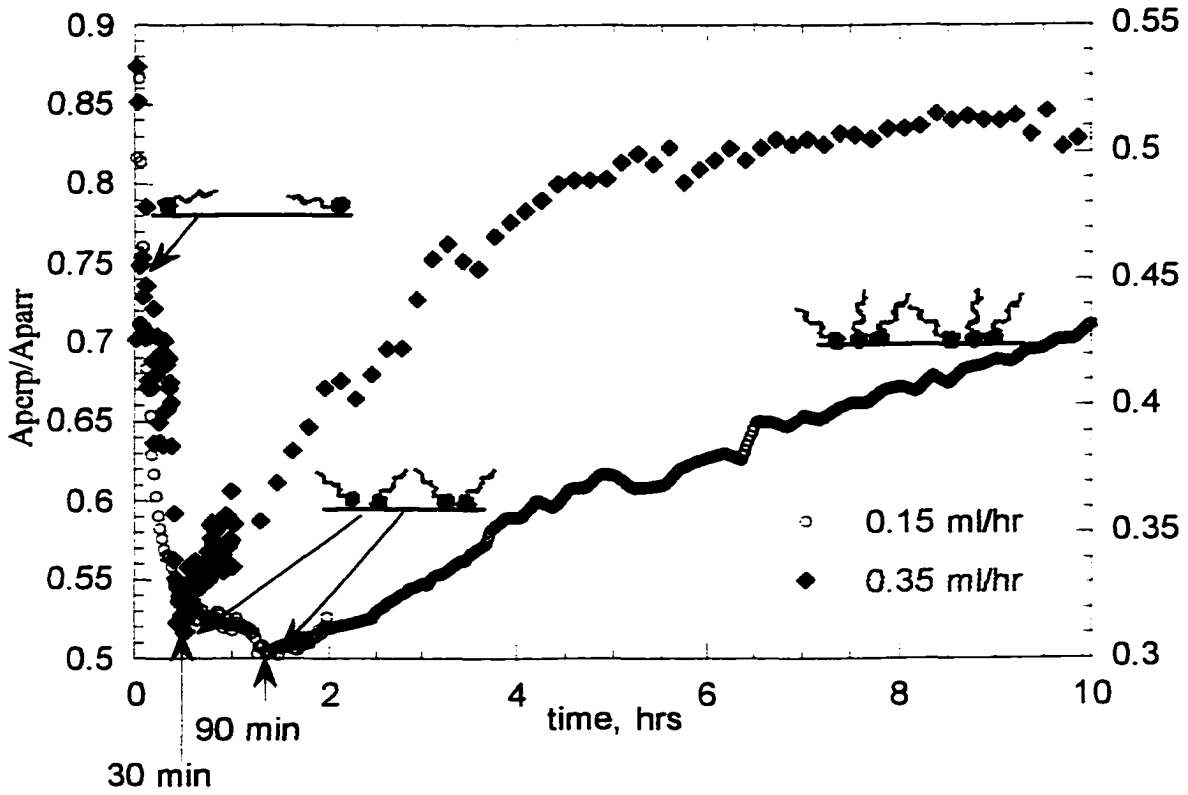

Figure 4.11. In-situ polarized ATR-FTIR spectroscopy of OTS self-assembly. The minimum in the ratio of $A_{\perp}$ to A_{11} is indicative of conformational changes occurring in the adsorbate layer, as indicated by the cartoon. (See text)

Chapter 5 Kinetics & Mechanism Of Octadecyltrichlorosilane Self-Assembly – A Mathematical Model

5.1 Introduction

Several processes of great scientific and technological impact are governed by dynamic mass exchange in liquid mixtures. In particular, the adsorption kinetics of some specific constituents at fluid/fluid or fluid/solid interfaces often play a major role in determining the final results. The adsorption kinetics may be limited by either the transport of the surfactants in the bulk phase, or by their adsorption at the interface. The net rate of adsorption would be a balance between these two phenomena. In the earlier chapter we had presented the results of our study on OTS self-assembly at a Si/SiO_2 surface. As with all other adsorption processes, OTS adsorption, is also governed by both kinetic and transport processes. In this chapter, we will present our mathematical model that describes the kinetics of *in-situ* OTS self-assembly. We will first consider the case where mass transfer limitations can be neglected in the analysis of the adsorption process (i.e.) the process is kinetically controlled. Then we will discuss the effects of including the transport process, (i.e.) diffusion and convection into the mathematical model.

5.2 Kinetically Controlled Adsorption Processes

In the case of adsorption of surfactants at an interface, the kinetics has usually been described using a Langmuir adsorption model. This model makes three main assumptions. First, the surface consists of adsorption sites; second, the adsorbates do not interact with one another; and third, the adsorption is limited to a monolayer[109]. In the case of adsorption at a solid-liquid interface modifications are made to the above

assumptions. Adsorption is still limited to a monolayer, but this layer is now regarded as an ideal two-dimensional solution of equal size solute and solvent molecules. Therefore, the lateral interactions, absent in the site picture, cancel out in the ideal solution layer picture. As a result, differences in adsorption behavior are attributed entirely to difference in adsorbate-solid interactions[109].

In the case of the simple Langmuir adsorption model, based on the number of available surface sites, the rate of surface reaction is given by:

$$\frac{d\Gamma}{dt} = \beta C_b exp\left(-\frac{E_A}{RT}\right)\left(\Gamma_\infty - \Gamma\right) - \alpha\Gamma\, exp\left(-\frac{E_D}{RT}\right) \tag{5.1}$$

where β & α are kinetic constants for the adsorption & desorption processes respectively, R is the gas constant, T is the temperature, Γ & Γ_∞ is the instantaneous and saturated surface coverage respectively, C_b is the bulk solution concentration, and E_A & E_D are the activation energy for the adsorption & desorption processes respectively. E_A & E_D are assumed to be independent of surface coverage since we neglect the presence of any lateral interactions among the adsorbates. Equation (5.1) can now be simplified to obtain the Langmuir model for adsorption onto an interface,

$$\frac{d\Gamma}{dt} = k_a C_b\left(\Gamma_\infty - \Gamma\right) - k_d\Gamma \tag{5.2}$$

where k_a & k_d are the redefined kinetic constant for adsorption and desorption respectively. If we assume that there is no desorption occuring in the adsorbing layer, (i.e.) k_d=0, then equation (5.2) can be expressed as

$$\frac{d\Gamma}{dt} = k_a C_b\left(\Gamma_\infty - \Gamma\right) \tag{5.3}$$

5.2.1 Adsorption Models for Self-Assembly at solid/liquid interfaces

In the case of self-assembly from solution, the mathematical modeling has been approached in a variety of ways. The Langmuir adsorption model, discussed above, has been used to describe the adsorption of thiols onto gold[11,33,34,110], the adsorption of carboxylic acids onto glass[36,37], and the adsorption of silanes onto solid substrates[45,51,104,105]. The model has been fairly successful at short times only. More recently there have been attempts to model the adsorption process over the entire time scale of the experiment using a combination of models[35,55], based on the simple surface-site limited Langmuir adsorption model. In a study of the adsorption of alkyl thiols onto gold surfaces using surface plasmon resonance (SPR) spectroscopy, the authors have monitored the adsorption process *in-situ* for up to 70 hours[35]. The authors characterized the adsorption process by monitoring the thickness of the adsorbing layer, and concluded that there was no single adsorption model that could describe their experimental data, although the combination of the three models predicted the thickness of the adsorbing thiol layer reasonably well. In another study of the thiol adsorption onto a gold surface[55], the authors used a rate law that incorporates two steps in the adsorption process. This two step rate law used a linear combination of two separate Langmuir adsorption models, each with its own kinetic constants.

None of the approaches described earlier accounts for the possibility of a nucleation and growth mechanism. Only Schwartz et al.[99], who have studied the adsorption of OTS from bicyclohexyl onto mica surfaces using AFM, have attempted to describe their data in light of the nucleation mechanism using a two step model. For short

times and partially formed monolayers, the adsorption process is modeled with a diffusion-limited aggregation (DLA) model. This step is followed by an adsorption limited second step that is described by the Langmuir kinetics.

However, none of the models discussed in the earlier sections is successful in describing our experimental data. For example, in figure 5.1, we have used the Langmuir model described by equation (5.3) to fit our experimental data. In this approach we are fitting our data with two parameters. Clearly it is seen that this model is highly inadequate to describe the adsorption of OTS and we will discuss the reasons for the inadequacy of the Langmuir model to describe OTS self-assembly. First, earlier studies on OTS self-assembly have shown that the OTS molecules do not adsorb specifically to the surface silanol groups but adsorb to a layer of water that is physisorbed on the SiO_2 surface[26-28,31,103,111]. Hence, the assumption of surface sites for the Langmuir model is violated. The second and most important reason for our inability to use the existing Langmuir model is the violation of the assumption of the lack of interactions among the adsorbate species. As a consequence of this assumption, E_A & E_D are assumed to be independent of the surface coverage of the adsorbed species. However, it has been shown earlier that adsorption at adjacent surface sites is not independent, due to the interactions between the adsorbate species[112,113]. In chapter 4, we described experiments done in our lab to investigate the existence of inter-molecular interactions, both at the air/liquid and solid/liquid interfaces. It was clearly shown that the hydrocarbon tails of the OTS molecules experienced interactions due to one another. This was reflected in the existence of the LE-LC phase co-existence region at the air/water interface (figure 4.12), and the minima in the graph of $A_{\parallel}/A_{\perp}$ vs. time (figure 4.13). Therefore, any model that is

used to describe the adsorption process will have to include intermolecular interactions in the adsorbate species.

In order to describe the self-assembly of OTS we looked for a single model that would not only describe the process over the entire time scale of the experiment, but one that would also account for the physical interactions existing among the adsorbate molecules. We therefore propose a model that accounts for the van der Waals interaction between the hydrocarbon chains of the surfactant molecules on the solid surface, resulting in a surface-coverage dependent activation barrier.

5.2.2 The Proposed Model

Let us visualize the adsorption process in the event of the existence of these interactions. At the start of the adsorption process, an adsorbate molecule finds a clean surface for adsorption. However, as a result of the van der Waals interactions between the adsorbate species, an adsorbate molecule that adsorbs onto the substrate later in the adsorption process, has to consume energy in accommodating itself into the layer already formed on the substrate. As a result, every incoming adsorbate molecule has to overcome an increasingly larger energy barrier in order to adsorb onto the substrate. This energy barrier which depends on the surface coverage, assigns a probability for the adsorption of an incoming surfactant to the substrate surface, with the probability being the greatest at the beginning of the process and decreasing as the surface coverage increases. Hence, this kinetic barrier becomes larger as the surface coverage increases, and thereby slows down the adsorption process.

MacRitichie et al.[114,115] have shown that the adsorption of molecules, when not limited by the available surface sites, produces an interfacial pressure that gives rise to an

energy barrier. In order for a molecule to enter the film from the bulk phase, it must create a hole at the interface, of an area, ΔA, large enough to accommodate the adsorbing molecule. To do so, this molecule must overcome the compression of the interfacial pressure, π, by doing work equal to $\int \pi d(\Delta A)$. Because this step is generally rapid compared to the rate of change of π, it can be considered to occur at constant π and consequently the work done is simply $\pi\Delta A$. The rate of adsorption will then be equal to the number of molecules striking a unit area of interface per unit time, and having energies in excess of $\pi\Delta A$, and is described below[115].

$$\frac{d\Gamma}{dt} = kC_{bulk} exp\left(-\frac{\pi(\Gamma)\Delta A}{N_{AV}RT}\right) \tag{5.4}$$

The π-A isotherm of an OTS monolayer at the air-water interface is shown in figure 4.12. Clearly, it can be seen that the surface pressure of the monolayer is different at different surface coverage of the OTS molecules at the air-water interface. Therefore, it is reasonable to expect that this behavior can be carried over to the solid-liquid interface too, (i.e.) the activation energy of adsorption will be dependent on the instantaneous surface coverage and will not be a constant throughout the adsorption process. This dependence of the activation energy on the surface coverage is accounted for in our description of the adsorption process, and is represented in the cartoon in figure 5.2. As a result, we can now describe the adsorption of OTS as follows:

$$\frac{d\Gamma}{dt} = k_a C_b exp\left(-\frac{E_A(\Gamma)}{RT}\right) \tag{5.5}$$

In the above equation, we have made three assumptions. First, the adsorption of OTS is not surface site dependent. Second the adsorption is irreversible, an assumption that is supported by the stability tests conducted by Gun et al.[4] and Kumar et al.[116] (hence $k_d = 0$). Third, the activation energy for adsorption, E_A is dependent on the instantaneous surface coverage (i.e.) $E_A=E_A(\Gamma)$.

We can use equation (5.4), which includes the surface pressure isotherm of the OTS molecule at the air/water interface to provide the correction to activation energy, and thereby describe the rate of change of surface coverage. However, as a first approximation, we have assumed that $E_A(\Gamma)= E_A^0 + k_2'\Gamma$, where k_2' is the linear correction to the activation energy of adsorption. Thus we have assumed the existence of a linear isotherm for the adsorption of the OTS at the solid/liquid interface. Using this correction to the activation energy, equation can be modified,

$$\frac{d\Gamma}{dt} = k_a C_b exp\left(-\frac{E_A^0 + k_2'\Gamma}{RT}\right) = k_a' C_b exp\left(-k_2\Gamma\right) \tag{5.6}$$

where C_b is the concentration of OTS in the bulk, and k_a' is the redefined kinetic constant for surface adsorption. Equation (5.6), integrated analytically, gives surface coverage as a function of time:

$$\Gamma = \frac{1}{k_2} ln\left[1 + k_a' C_b k_2 t\right] \tag{5.7}$$

We have used equation (5.7) to model our experimental data. It is important to note that only two parameters are fitted, k_a' and k_2. The best-fit values of k_a' and k_2 were found by minimizing the sum of the differences between the experimental data and the simulation results. MINPACK subroutines, freely available off the Internet, were used for

the fitting routines. The Fortran code for this procedure is given in the appendix. As can be seen from figure 5.3, the activation energy model does a very good job of describing the adsorption process at all times. The values of k_a', and k_2 are given in table 5.1. Evidently, these values are dependent on the concentration of OTS in the bulk, and also on the flow rate of the OTS solution. This suggests that the adsorption process may not be completely described by just the linear correction to the activation energy. (In an earlier study of surfactant adsorption at the air/water interface, Chang et al.[117] used a model similar to the one described above, and obtained kinetic constants that were a function of the bulk solution concentration).

In using the above model we have neglected any mass transfer limitations that may exist in the system, and thereby assumed that the bulk concentration of OTS is a constant throughout the process. However, our experimental results indicate that the flow rate of the solution across the substrate surface has an effect on the rate of adsorption (figure 4.11). It is thus apparent that mass transfer effects will have to be considered in order to model the data accurately. In the following sections, we discuss the effects of including the diffusion of the surfactant in the bulk solution into the mathematical model.

5.3 Diffusion-Kinetic Models

The diffusion of the surfactant molecule in the bulk solution can be described by the Ficks' diffusion law and is given below.

$$D\frac{\partial C^2}{\partial y^2} = \frac{\partial C}{\partial t} \tag{5.8}$$

$$t = 0, \quad C = C_{bulk}, \quad y > 0 \tag{5.9}$$

$$t > 0, \quad C = C_{bulk}, \quad y = \infty \tag{5.10}$$

$$C(0,t) = C_S(t) = 0 \tag{5.11}$$

where D is the diffusion coefficient, C_{bulk} is the concentration in the bulk far from the interface, $C_S(t)$ is the sublayer concentration and y is the direction normal to the plane of adsorption. In figure 5.4 we have shown a brief schematic of our flow channel. For a first approximation we will neglect convection effects in the longitudinal direction, (i.e.) x direction. Equation (5.11) defines the boundary condition at the adsorption interface. This equation is valid for an adsorption process that is diffusion-controlled. However, when the rates of diffusion and kinetics of adsorption are comparable, we use the condition that the diffusive flux at the surface is equal to the rate of change of the surface coverage (i.e.)

$$D\left(\frac{\partial C}{\partial y}\right)_{y=0} = \frac{d\Gamma}{dt} = r_A \tag{5.12}$$

where r_A is the kinetic rate of adsorption of the surfactant at the interface. For diffusion controlled adsorption onto a clean interface, Ward and Tordai[118] solved the bulk diffusion equations by the Laplace transform technique. This results in an integral equation which relates the surface coverage, Γ, to the sublayer concentration $C_S(t)$:

$$\Gamma(t) = 2C_{bulk}\left(\frac{Dt}{\pi}\right)^{1/2} - 2\left(\frac{D}{\pi}\right)^{1/2}\int_0^{\sqrt{t}} C_S(t-\tau)\,d\sqrt{\tau} \tag{5.13}$$

The application of the equation (5.13) to experimental data is not so easy. This is because, using equation (5.13), it is not possible to obtain an explicit analytical solution for $\Gamma(t)$. Therefore Sutherland[119] derived an equivalent relation between Γ and t by taking into account a linear adsorption isotherm, (i.e.) $\Gamma(t)=KC_S(t)$, where $K=\Gamma_\infty/C_{bulk}$. He obtained the following analytical expression:

$$\Gamma = \Gamma_0 \left\{ 1 - exp\left(\frac{Dt}{K^2}\right) erfc\left(\frac{\sqrt{Dt}}{K}\right) \right\} \tag{5.14}$$

The above equation can be used rather simply, but its application range is very small and is restricted to the application range of the linear adsorption isotherm. Adamczyk et al.[120,121] have provided an analytical expression for the solution of equation (5.13) and equation (5.3), for short times. The solution provided by Adamczyk et al.[120,121] is of the form:

$$\theta = \frac{1}{\bar{k}_a}\left[exp\left(\bar{k}_a^2 \tau\right) erfc\left(\bar{k}_a \sqrt{\tau}\right) - 1 \right] + \frac{2}{\sqrt{\pi}}\sqrt{\tau} \tag{5.15}$$

where

$$\theta = \frac{\Gamma}{\Gamma_\infty};\ \bar{k}_a = \frac{k_a \Gamma_\infty}{C_b D};\ \tau = \left(tDC_b^2 \Big/ \Gamma_\infty^2 \right) \tag{5.16}$$

However, for long times, simultaneous numerical solution of equation (5.13) and the equation describing the kinetic process, like equation (5.2),(5.4) or (5.6), provide Γ(t). Miller et al.[122] suggested one could approximate the integral equation (5.13) by a simple algorithm, for example by the trapezoidal rule,

$$\int_0^{\sqrt{t}} C_S\left(t-\tau\right) d\sqrt{\tau} = \sum_{i=1}^{n} \int_{\sqrt{t_i}}^{\sqrt{t_{i+1}}} C_S\left(t-\tau\right) d\sqrt{\tau} \approx \frac{1}{2}\sum_{i=1}^{n} \left(C_S\left(t-t_{i+1}\right) + C_S\left(t-t_i\right) \right) \left(\sqrt{t_{i+1}} - \sqrt{t_i} \right) \tag{5.17}$$

and use equidistant time steps $t_1=0$; $t_i=t_{i-1}+\Delta t$, i=2,3,...,n+1. By some arithmetic rearrangements, we obtain the following recursive formula for calculating the course of the function Γ(t) or $C_S(t)$:

$$\Gamma\left(t_{n+1}\right) = b_1 C_S\left(t_{n+1}\right) + b_2 \tag{5.18}$$

where b_1 and b_2 are constants evaluated at every time step, and are dependent on the values of $C_S(t)$ and $\Gamma(t)$ until the n^{th} time step. Equation (5.18) is now solved simultaneously with the equation describing the kinetic adsorption, (i.e.) equation (5.2) ,(5.4) or (5.6) to obtain $\Gamma(t)$ and $C_S(t)$. The above numerical procedure is tested for accuracy with the analytical expression given by Sutherland[119] (i.e.) equation (5.14). The results of numerical simulation are also compared to the analytical expression given by Adamczyk et al.[120,121] (equation (5.15)). These results are presented later in the chapter.

5.4 Convection-Diffusion-Kinetic Models

As we had discussed in the earlier chapter, the rate of self-assembly of OTS is affected by the flow rate of the solution across the interface. In order to incorporate the effects of convection into the mathematical model, we have used an approach that has been used by several authors[123-128] in the recent past. For flow in the slit like geometry of the flow cell, shown in figure 5.4, we have assumed a fully developed laminar flow. We have neglected diffusion effects in the x (i.e) axial direction and convection effects in the y (i.e.) longitudinal direction[123,126]. The governing equations for the convective diffusive model are given below.

$$\frac{\partial C(x,y,t)}{\partial t}+\gamma\, y\left(1-\frac{y}{b}\right)\frac{\partial C(x,y,t)}{\partial x}=D\frac{\partial^2 C(x,y,t)}{\partial y^2},\ 0\le y\le b,\ 0\le x\le l \qquad (5.19)$$

The following initial and boundary conditions apply to this system.

$$C(x,y,0)=1,\ for\ all\ y,x>0 \qquad (5.20)$$

$$C(0,y,t)=C_{bulk}\ for\ all\ y,t \qquad (5.21)$$

$$C(x,y,t)_{y=b}=C_{bulk} \qquad (5.22)$$

$$D\left(\frac{\partial C(x,0,t)}{\partial y}\right)=\frac{d\Gamma(x,0,t)}{dt}=r_A \tag{5.23}$$

where b is the thickness of the flow chamber, r_A is the intrinsic kinetic rate expression, γ is the wall shear rate. For the case where the process is limited by diffusion, equation (5.23) becomes

$$C(x,0,t)=0,\ for all\ x>0, t\geq 0 \tag{5.24}$$

γ, in the above equations, is calculated assuming fully developed laminar flow[123] within the chamber using:

$$\gamma=\frac{6q}{b^2w} \tag{5.25}$$

where q is the experimentally measured volumetric flow rate, b the thickness, and w the width of the flow chamber. For the experiments performed in our lab, the Reynold's number is in the range (0.1-1). Hence, the assumption of laminar flow is valid. Rewriting the system of equations in dimensionless form yields:

$$\frac{\partial \tilde{C}}{\partial \theta}+Y(1-Y)\frac{\partial \tilde{C}}{\partial X}=\frac{1}{Pe}\frac{\partial^2 \tilde{C}}{\partial Y^2} \tag{5.26}$$

$$\tilde{C}=\frac{C}{C_{bulk}},\ X=\frac{x}{l},\ Y=\frac{y}{b},\ \theta=\frac{t}{\left(l/\gamma b\right)} \tag{5.27}$$

$$\theta=0,\ \tilde{C}=0\ \ for all\ Y, X>0 \tag{5.28}$$

$$X=0,\ \tilde{C}=1\ \ for all\ Y,\theta \tag{5.29}$$

$$Y=1,\ \tilde{C}=1\ \ for all\ X,\theta\geq 1 \tag{5.30}$$

For the boundary condition at the surface, (i.e.) y=0, we will use equation (5.6) to describe r_A:

$$D\left(\frac{\partial C(x,0,t)}{\partial y}\right)=\frac{d\Gamma(x,0,t)}{dt}=k_a' C_S(t)\exp(-k_2\Gamma) \tag{5.31}$$

In dimensionless form the above equations reduce to:

$$\frac{\partial \bar{C}}{\partial Y}=\left(\frac{k_a' b}{D}\right)\bar{C}_S \exp\left(-\bar{\Gamma}\right)=Da\,\bar{C}_S \exp\left(-\bar{\Gamma}\right) \tag{5.32}$$

$$\frac{\partial \bar{\Gamma}}{\partial \theta}=\left(\frac{k_a' b}{D}\right)\left(\frac{lD}{\gamma b^3}\right)\left(\frac{b}{1/k_2 C_{bulk}}\right)\exp\left(-\bar{\Gamma}\right)=\left(\frac{\alpha Da}{Pe}\right)\exp\left(-\bar{\Gamma}\right) \tag{5.33}$$

$$\bar{\Gamma}=k_2\Gamma \qquad \alpha=\frac{b}{\left(1/k_2 C_{bulk}\right)}, \qquad Pe=\left(\frac{\gamma b^3}{lD}\right), \quad Da=\left(\frac{k_a' b}{D}\right) \tag{5.34}$$

The convection-diffusion-kinetic model as described above cannot be solved using the techniques suggested by Miller et al.[122] Instead, equations (5.26)-(5.30),(5.32) & (5.33) were solved numerically using an alternating-direction-implicit (ADI) method[129]. This method involves approximation of the derivatives with a difference formula[129]. The details of the method, and the Fortran code are given in the appendix.

5.5. Mixed Kinetics : Results

In order to verify the results of the numerical simulations, equations (5.8)-(5.12) were solved using the finite difference technique as well as the integral approximation technique[122] and the results compared to the analytical solutions of Sutherland[119] (equation (5.14)) and Adamczyk et al.[120] (equation (5.15)). The results are presented in figures 5.5 and 5.6. Clearly, there is excellent agreement between the numerical simulations and the analytical expressions.

We now proceed to apply the diffusion-kinetic model to our experimental data. We first used equation (5.3) and solved it using the two different numerical procedures. However, the diffusion model with the Langmuir kinetics model was not successful in describing the experimental data. We next proceeded to use the kinetic model in equation (5.6) and solved it using the two different numerical procedures detailed above (i.e.) finite difference approximation and integral approximation. The results are presented in figure 5.7 where we have shown the variation of simulated Γ with time. The model parameters that have been used in the simulation of these curves are also indicated in the figure. We have used the values of k_a' and k_2 obtained from the minimization procedure detailed earlier in section 5.2.4. In addition we have used a value of 5d-10 m^2/sec for the diffusivity*. Clearly, there is no difference between the results of the two numerical procedures. However, the integral approximation procedure is computationally more cumbersome since it involves the evaluation of the sum at every time step. For the large values of time that we have in our experiments (~15 hrs) this method is computationally very intensive. The finite difference code on the other hand gives us the same results in a more efficient manner.

In figure 5.8, we have shown the variation of Γ with time for two different cases. Whereas, in one case, Γ was calculated using just the kinetic expression, in the second case the diffusion-kinetic model was used to calculate Γ. It is surprising to see the incorporation of bulk diffusion to model the kinetics has not really affected the value of

---

* This value of the diffusivity has been used in the past to describe the bulk diffusion of ionic/non-ionic surfactants.[130]

Γ. This result is further confirmed by following the variation of the sublayer concentration, $C_S(t)$, with time. From figure 5.9, we observe that $C_S(t)$ is not really a function of time, and remains close to the value of C_{bulk}. This would suggest that the adsorption process is kinetically limited and is independent of mass transfer limitations. However, we have shown in the earlier chapter that the flow rate of the OTS solution across the interface had a pronounced effect on the initial rates of adsorption. Hence, we proceeded to simulate the adsorption process using the convective-diffusive-kinetic model and compare it to our experimental data.

In figure 5.10, we have shown the variation of Γ with time for the convection diffusion model. The values of the parameters used in the simulation are indicated in the plot. The values of the kinetic constants and the diffusivity are the same as the ones used in the diffusion-kinetic model. The introduction of flow effects into the mathematical model does not appear to affect the adsorption rate or the adsorbed amounts. This is an unexpected result since this is in contrast to our experimental studies that clearly show a dependence of the adsorption rate/adsorbed amounts on the flow rate. In the following section we offer a few possible explanations that could account for these differences.

5.6 Discussion

From figure 5.9, it is clear the sublayer concentration stays close to the value of the bulk concentration at all times in the process. If the process were diffusion limited, then $C_S(t)$ would drop to zero at the beginning of the process, and remain that way at all times, (i.e.)

$$C_S(t)=0 \text{ for all } t \qquad (5.35)$$

On the contrary, in the case of a process that is kinetically limited $C_S(t)$ would be close to C_{bulk} at all times. However, for a process that is governed by mixed kinetics, $C_S(t)$ would drop to zero at the beginning of the process and then climb back to the value of the C_{bulk} with time. The absence of such a behavior leads us to suspect that the process may be kinetically limited. As discussed earlier the experimental results clearly indicate that the self-assembly process is affected by the flow rate of the solution across the interface. We therefore have to look for reasons to resolve this apparent discrepancy. First, the value of the diffusivity, D, that has been assumed for the simulations, is $5*10^{-6}$ cm^2/sec. This value of D has been successfully used to describe the diffusion of monomeric surfactants in the bulk[130]. However, it is possible that the transport limitations are not occurring in the bulk, but in a layer close to the adsorption interface, akin to a boundary layer. The diffusional resistance to the adsorption process may occur in this layer. If we assume that this scenario is true, then the value D would be smaller than the value that has been used in our simulations. In addition, the diffusion process would have to be restricted to a layer close to the interface with a value of D that is lower than its value in the bulk.

Second, the flow profile that has been assumed in the mathematical model is a parabolic one. However, in the actual experiment we have a flow that is, in a sense, impinging onto the Si wafer. It should be mentioned here that with the existing model, the change in the flow characteristics would not really make a difference in our ability to predict the experimental data. This is because, as mentioned earlier the sublayer concentration is close to C_{bulk} at all times, and the mass transfer effects would have no bearing on the process. However, mass transfer effects may make a difference if the

different flow field is incorporated into the model that accounts for diffusional resistance in a layer close to the interface rather than in the bulk.

5.7 Conclusions

In this study, we propose a novel model that describes the adsorption process over the entire time range of the experiment. This model accounts for an activation energy for adsorption, $(E_A)_{ads}$, that varies as a function of the surface coverage. The dependence of $(E_A)_{ads}$ on Γ_{ads} arises due to the van der Waals' interaction between the hydrocarbon chains of the surfactant molecules on the solid surface. As a result of these interactions, a surfactant molecule that adsorbs onto the substrate late in the adsorption process has to spend energy in creating a hole in the existing layer already adsorbed on the substrate. Hence, every incoming surfactant molecule has to overcome an increasingly larger energy barrier in order to adsorb onto the substrate. This energy barrier which is dependent on the surface coverage, assigns a probability for the adsorption of an incoming surfactant to the substrate surface, with the probability being the greatest at the beginning of the process and decreasing as the surface coverage increases. This model is successfully applied to describe the self-assembly of OTS. We have also looked at the transport processes involved in the self-assembly process. For the value of the diffusion coefficient being used for monomeric species, the convection-diffusion-kinetic model does not explain the dependence of the kinetic constants on the flow rates and bulk concentration. This suggests that the self-assembly process cannot be modeled with the assumption of simple surfactant-like behavior.

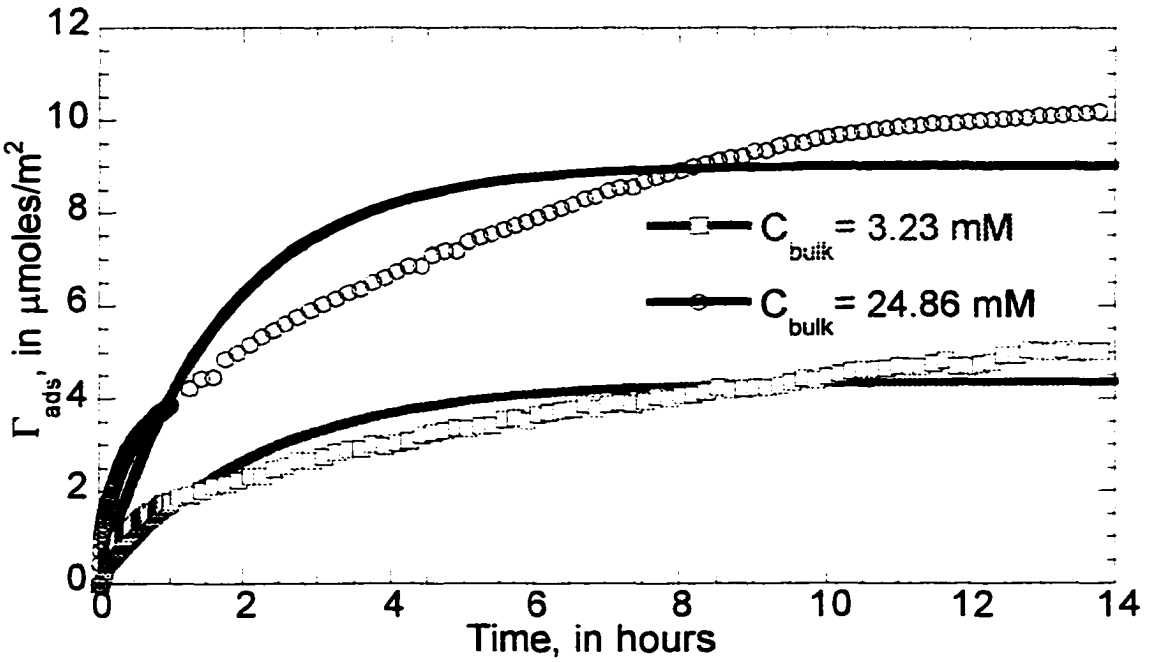

Figure 5.1. Langmuir adsorption model, $\Gamma = k_1[1 - \exp(-k_2 t)]$ fitted to our experimental data. The Langmuir adsorption model, that assumes no interaction between the adsorbate molecules, is inadequate in describing the adsorption process.

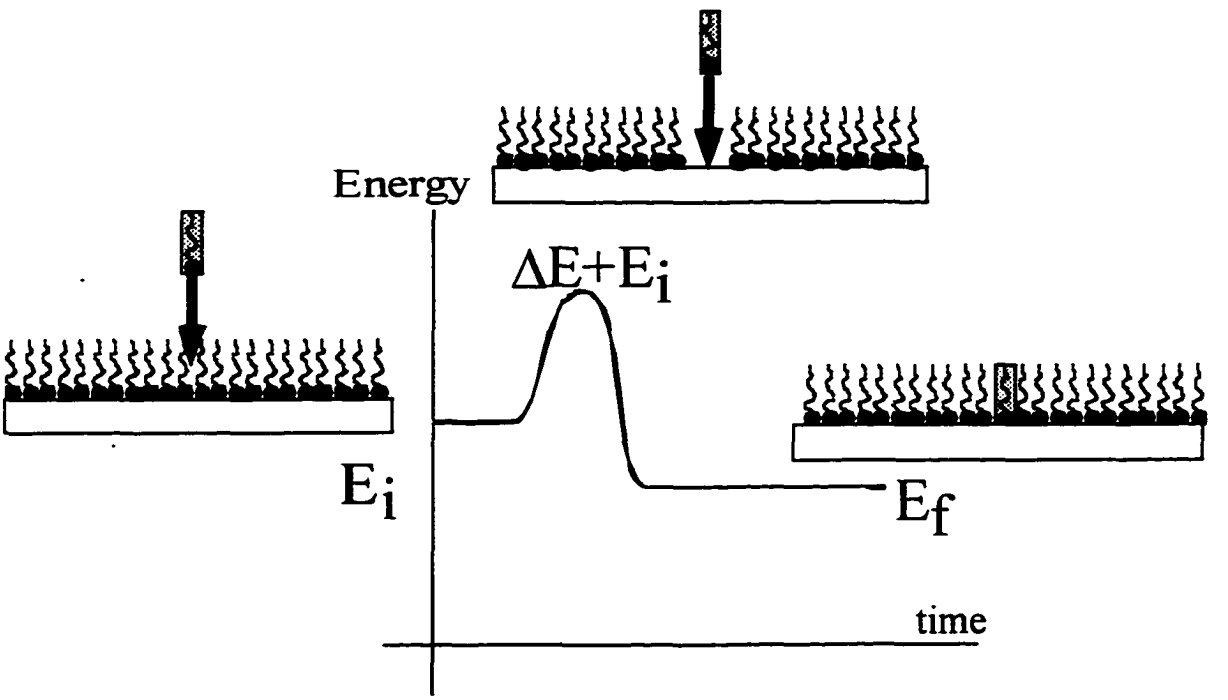

Figure 5.2 The activation energy of adsorption depends on the instantaneous surface coverage, Γ_{ads}

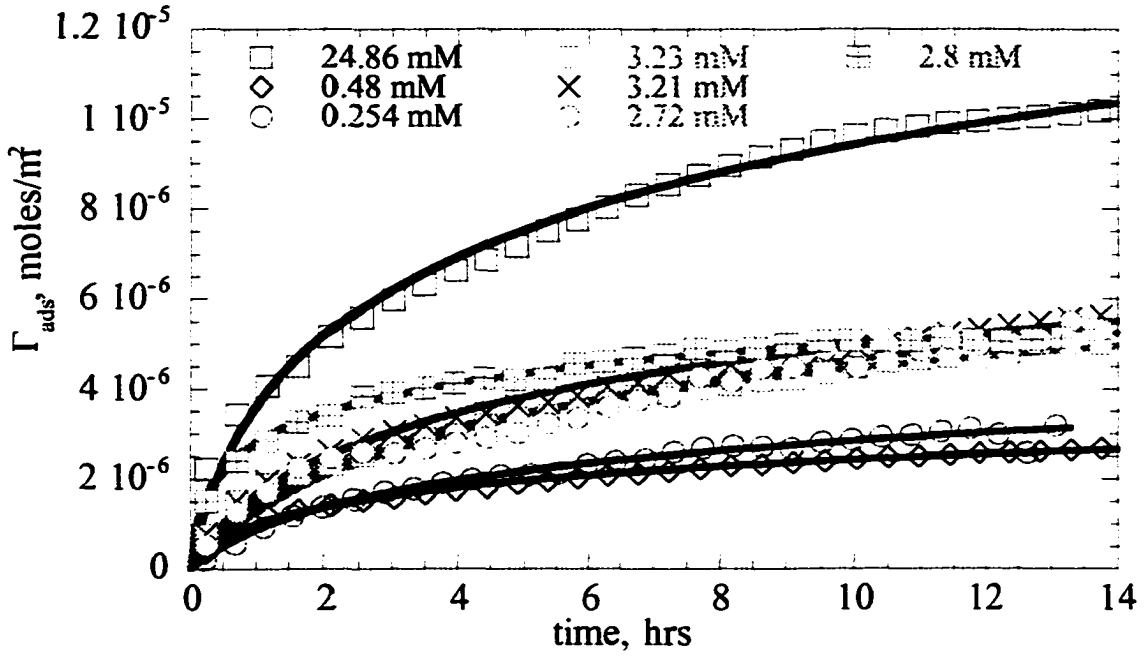

Figure 5.3. Fit of equation 5.6, the activation energy model, to our experimental data. The model describes the experimental data very well.

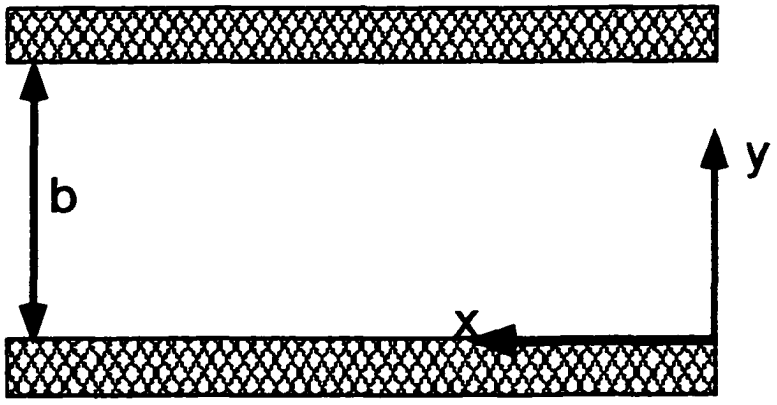

Figure 5.4. Schematic of flow channel with axis notation

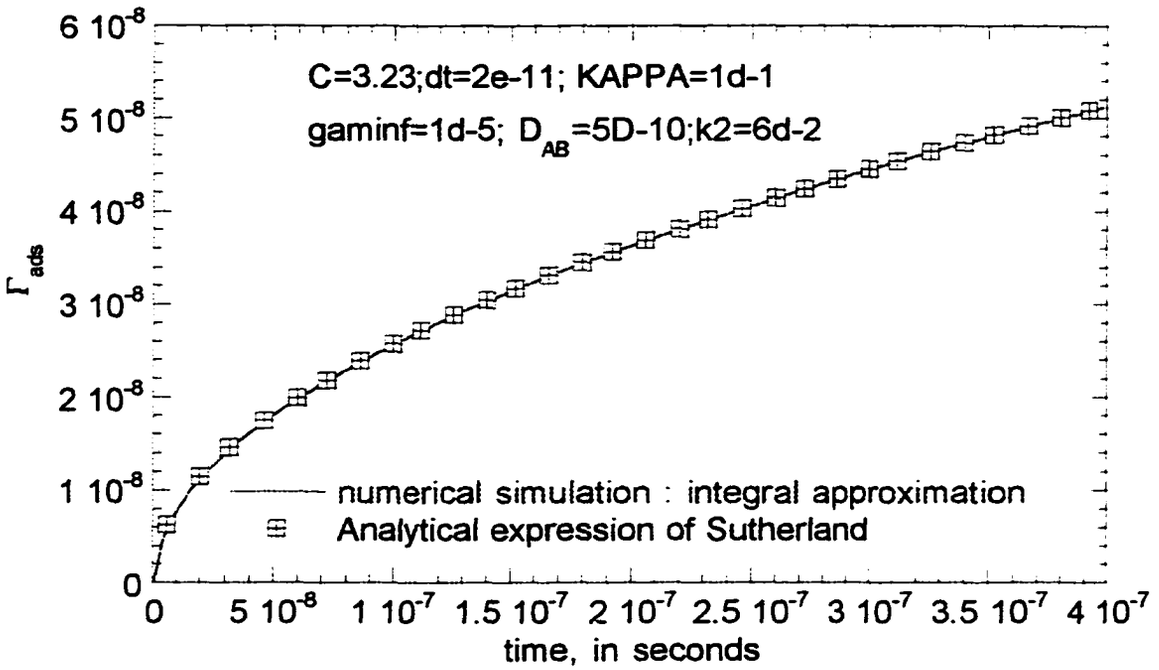

Figure 5.5. Comparison of numerical simulation using integral approximation technique to the analytical expression of Sutherland

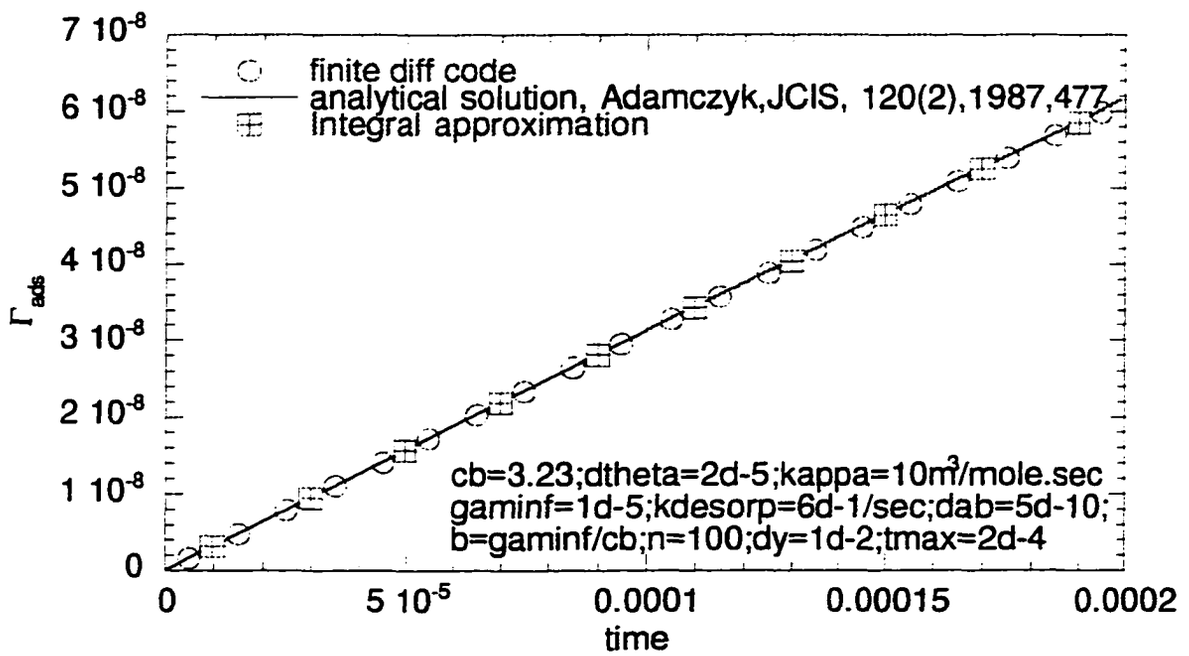

Figure 5.6. Comparison of the numerical simulation results to the analytical expression of Adamczyk (i.e.) equation 5.15

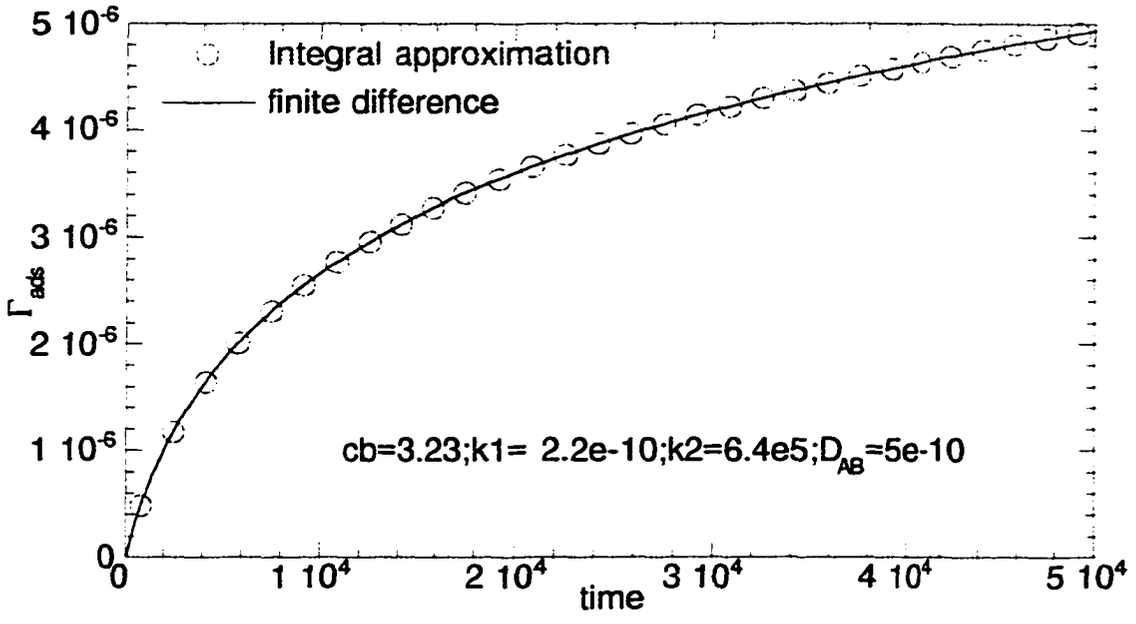

Figure 5.7. Comparison of the two numerical techniques for the solution of the diffusion kinetic equation

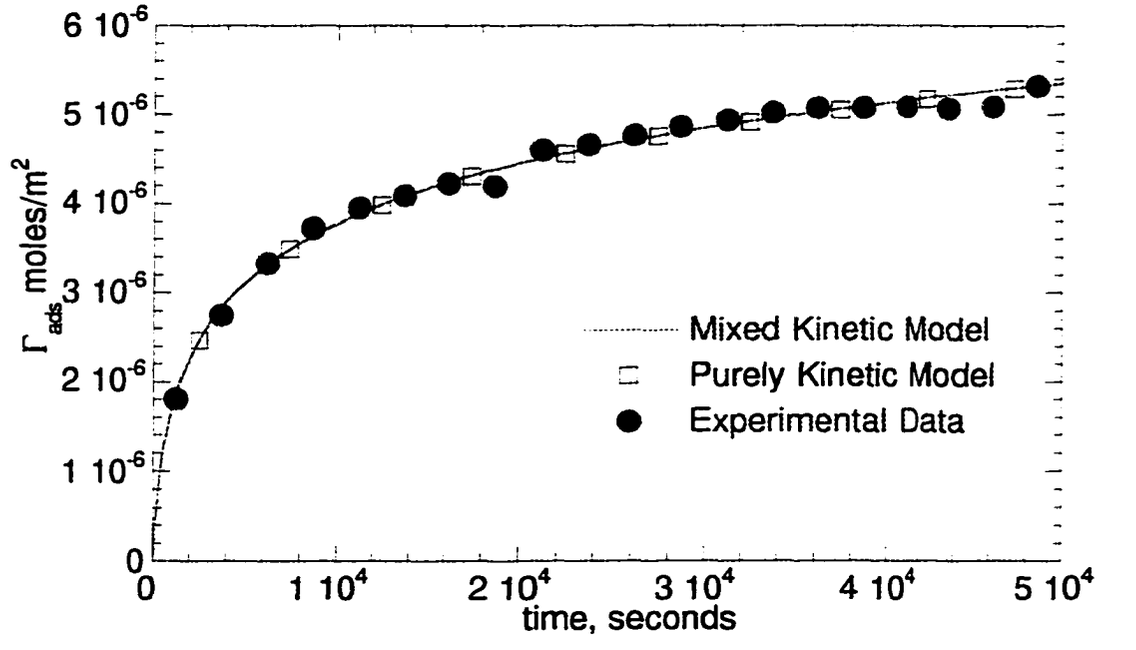

Figure 5.8. Do Mass Transfer limitations really exist? Comparison of the numerical simulation results of purely kinetic, and a mixed kinetic model

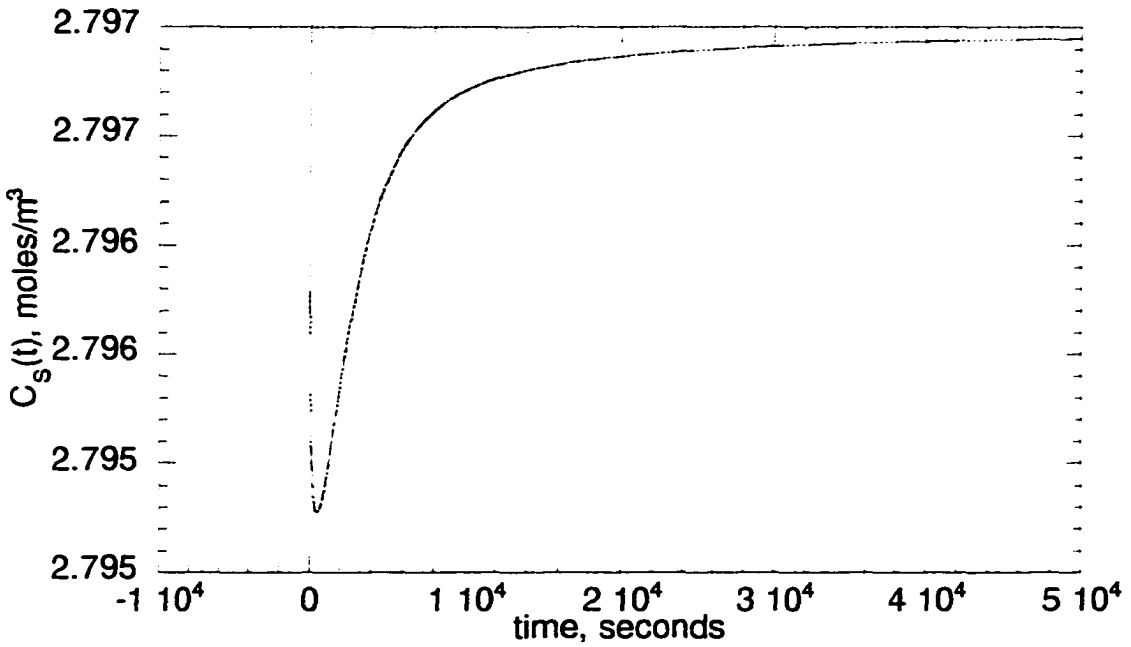

Figure 5.9. The variation of the sublayer concentration with time for the mixed kinetic model. Clearly, $C_S(t)$ is always close to C_{bulk}.

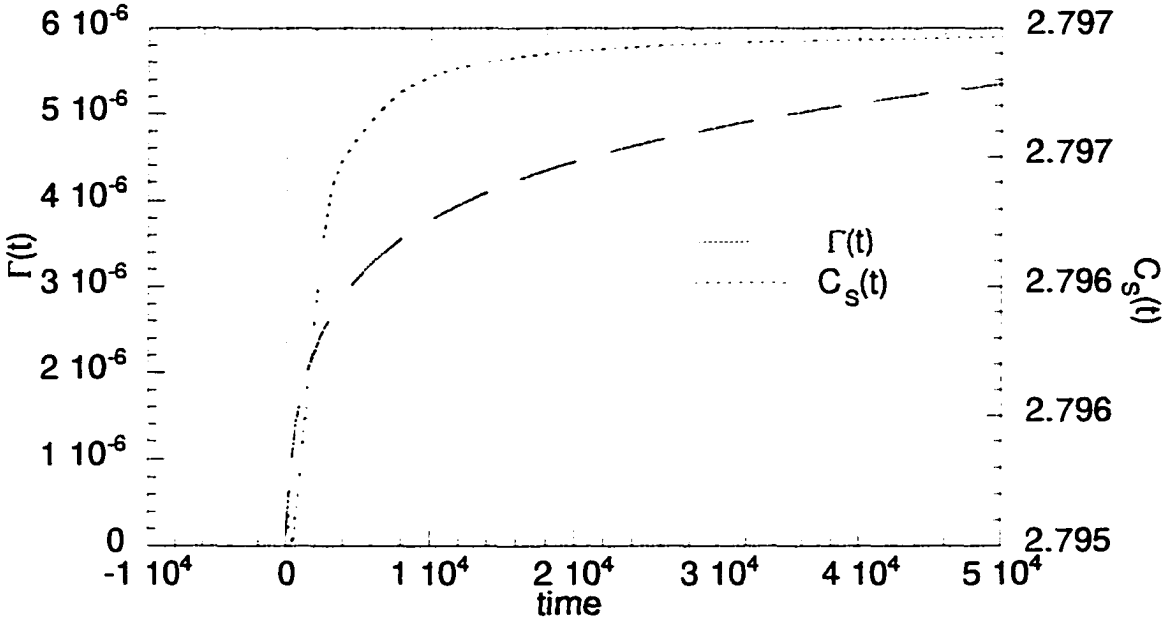

Figure 5.10. Convection-diffusion-kinetic model simulations. The flow effects seen in experiment are not reflected in the numerical simulations.

S. No.	C_{bulk} moles/m^3	Velocity, ml/hr	k_a^1, m/hr	K_2, m^2/mole
1	0.25	0.6	5.51 E-06	9.24 E05
2	0.48	0.2	4.43 E-06	1.43 E06
3	2.72	0.2	6.59 E-07	4.95 E05
4	2.8	1.2	5.62 E-06	1.01 E06
5	3.21	0.2	8.32 E-07	5.62 E05
6	3.23	0.2	7.74 E -07	6.36 E05
7	24.86	0.2	2.90 E-05	3.46 E05

Table 5-1. Coefficients of the purely kinetic model

Chapter 6 Conclusions and recommendations for future study

6.1 Conclusions

Numerous applications involve adsorption of polymers and surfactants on the solid-liquid interface making it necessary to fully comprehend the underlying mechanisms. As described in the previous chapters we have achieved our original goal of investigating the dynamics and the mechanism of the self-assembly of OTS on hydrophilic surfaces. In the next sections we briefly outline the achievements of this project.

- Attenuated total reflection infrared spectroscopy has been successfully used to monitor the self-assembly process in-situ.
- Adsorption experiments for Octadecyltrichlorosilane from their solution in different solvents onto Si/SiO_2 surfaces have been conducted. The data indicate a strong dependence of the rate of adsorption on the concentration of the solution, the time of deposition, the extent of hydration of the substrate surface, the flow rate of the solution across the interface and the solvent used for the adsorption process.
- The sandwiching technique (i.e.) use of a Si wafer/Ge ATR system, has been successfully implemented to increase the useful range of the information available for analysis of the IR spectra.
- The peak characteristic of the methylene bending moment splits with an increase in the surface coverage. This complements the data from the shift in the position

of the asymmetric methylene stretch and is suggestive of the crystalline order occurring in the adsorbed layer with increasing surface coverage.

- We present the first in-situ polarized FTIR-ATR data of OTS self-assembly from solution. The data offer qualitative proof of the interactions existing between the hydrocarbon tails of the OTS molecules, and conformational changes occurring during the self-assembly process.
- In this study, we propose a novel model that describes the adsorption process over the entire time range of the experiment. This model accounts for an activation energy for adsorption, $(E_A)_{ads}$, that varies as a function of the surface coverage. The dependence of $(E_A)_{ads}$ on Γ_{ads} arises due to the van der Waals' interaction between the hydrocarbon chains of the surfactant molecules on the solid surface. As a result of these interactions, a surfactant molecule that adsorbs onto the substrate late in the adsorption process has to spend energy in creating a hole in the existing layer already adsorbed on the substrate. Hence, every incoming surfactant molecule has to overcome an increasingly larger energy barrier in order to adsorb onto the substrate. This energy barrier which is dependent on the surface coverage, assigns a probability for the adsorption of an incoming surfactant to the substrate surface, with the probability being the greatest at the beginning of the process and decreasing as the surface coverage increases. This model is successfully applied to describe the self-assembly of OTS.
- We have also looked at the transport processes involved in the self-assembly process. For the value of the diffusion coefficient being used for monomeric species, the convection-diffusion-kinetic model does not explain the dependence

of the kinetic constants on the flow rates and bulk concentration. The incorporation of a different flow field will not affect the results since, for the value of D_{AB} assumed, the sub-layer concentration always remains close to the bulk value.

- However, if one uses a value of the diffusivity that is substantially lower than the ones used for monomeric species, mass transfer effects in the the self-assembly process may be incorporated. This suggests that the self-assembly process cannot be modeled with the assumption of simple surfactant-like behavior.

6.2 Recommendations

The work done in this project has created new avenues for a variety of questions to be addressed.

- Study of the kinetics of self-assembly of mixed surfactant systems.
- Study of effects of temperature on the self-assembly of OTS.
- Incorporating the reaction of the surfactant species in the bulk that results in the formation of polymeric species into the mathematical model.
- Investigation of the nature of the species in the bulk, polymeric vs. monomeric.
- Chromatography studies to evaluate the kinetic constants in the bulk.
- Performing the adsorption studies where the impinging nature of the flow field can be changed and one can have a flow that enters directly into the adsorption zone. This will facilitate easier comparison of experimental data to the mathematical model.

- Study of the adsorption and interaction at the solid-liquid interface of surfactant species with active head groups. Such materials have applications in areas such as membrane sensors and separation processes.
- Study of adsorption of surfactants that form organized mono or bilayers on the solid-liquid interface. Using ATR spectroscopy questions as surface-adsorbate and adsorbate-adsorbate interactions can be answered. In addition ATR can determine the critical surface coverage at which organization of these molecules take place.
- Successful attempts have shown that ATR can also be used to study adsorption on a metal surface. Thus one can look at the possibility of studying metal-liquid interfaces, that hold a great technological interest in areas such as corrosion protection, and adhesion in polymer-metal systems.
- Finally, study of systems with the solid surface having active groups. Most common material of this kind is paper, and biological tissue. Applications involve food packaging (liquid and solid), delayed drug release, artificial organs in medical applications, and cholesterol removal from blood vessels.

Appendix A Integral Approximation method

In this section we will find the program listing for the program used to solve the diffusion kinetic equation using the integral approximation method suggested by Miller et al.[122]. This program allows the user to choose between whether they want to do the fitting routine using diffusion or without. The user supplies a data file that has the experimental data points and initial guesses for the kinetic constants that are to be fitted. In addition to the sections listed here several other sub routines that are part of a package, MINPACK, are used to successfully accomplish the fitting routine. The actual program is given below.

```
      program fitcomposite_linear

c     driver for fitting one of two models to data, either with diffusion or
c     without. The program uses the minpk routine hybrd to solve the system of
c     non-linear equations instead of newt when diffusion is a parameter. There
c     is no gamma infinity that is considered, likewise, no desorption either.
c     the linear correction to activation energy is used to fit data.

      implicit none
      real*8 gamth,csub,alpha
      real*8 cb,dab,dt,kappa,k2
      real*8 gamexpt(200),time(200),gamexp
      integer*4 adslen,j,y,interplen,choice
      character*20 insitudata,results

c     variable declaration for driver routine for minpack fits for LMDIF

      integer*4 m,n,maxfev,mode,nprint,info,nfev,ldfjac,ipvt(3)
      real*8 ftol,xtol,gtol,epsfcn,factor,fnorm,enorm,dpmpar
      real*8 x1(3),fvec1(50000),diag(3),fjac(50000,3),qtf(3)
      real*8 wa1(3),wa2(3),wa3(3),wa4(50000)

c     end of variable declaration for driver routine for minpack fits

      common /data1/gamth(50000),csub(50000),gamexp(50000)
      common /data2/y
      common /data/dt,kappa,k2,cb,dab,alpha
      common /data3/choice
      external fcn
      external func
```

```
      namelist /pdata/cb,dt,kappa,k2,dab,alpha
      open(1,file='fitcomposite_linear.dat',access='sequential')
      read(1,pdata)
      close(1,status='keep')

c     units
c     pressure,p                :    dynes/cm
c     molar gas constant,r      :    nm/kmole/k
c     temperature,t             :    k
c     bulk solution conc.,cb    :    moles/m^3
c     diffusivity,d,x(3)        :    m^2/sec
c     time step,dt              :    sec
c     rate constant,kappa,x(1)  :    m/sec
c     area to be created,da,x(2)  :  m^2/molecules
c     avagadro number,na          :  molecules/mole
c     surface coverage,gamma      :  moles/m^2
c     gamexpt  :    the surface coverage as is from the adsorbdata file
c     time     :    time step in the adsorbdat file
c     gamexp   :    interpolated surface coverage for uniform dt, read from file
c     adslen   :    number of records in insitudata file
c     interplen :   number of records in interpdata file
c     gam      :    the surface coverage at air/water from pi-a isotherm
c     pres     :    the surface pressure corresponding to the surface coverage, gam
c     arrlen   :    number of records in pi-a isotherm data file
c     gamth    :    the surface coverage calculated from model
c     insitudata:   name of the data file containing the insitu ft-ir data
c     interpdata:   name of the data file containing interpolated ft-ir data

c     this section reads in randomly spaced (x,y) data from a file, adsorbdata and
c     linearly interpolates the y data for an evenly spaced x, defined by user.

c     reading in gamexpt, the unevenly spaced data

c     write(*,*)'enter the name of the adsorption data file,*.dat'
c     read*,insitudata
      insitudata="may12.dat"
      open(4,file=insitudata)
      adslen=1
3     read(4,*,end=4) time(adslen),gamexpt(adslen)
      adslen=adslen+1
      goto 3
4     adslen=adslen-1

c     write(*,*)'enter the bulk concentration, cb'
c     read*, cb
c     write(*,*)'enter the name of the results file,*.dat'
c     read*,results
      results="fitcomp_linear.res"
      open(2,file=results,status='new')

c     interpolating and writing it gamexpt into the evenly spaced, gamexp
```

```
      interplen=1
      gamexp(1)=0
5     interplen=interplen+1
      if (((interplen-1)*dt).le.time(adslen))     then
          call locate(time,adslen,dfloat((interplen-1)*dt),j)
          gamexp(interplen)=(gamexpt(j)*(time(j+1)-dfloat
     *    ((interplen-1)*dt))+gamexpt(j+1)*(dfloat((interplen-1)*dt)
     *    -time(j)))/ (time(j+1)-time(j))
          goto 5
      endif
      interplen=interplen-1
c     end of interpolation

c     entering choice for fit with diffusion, or without

      write(*,*)'enter choice for fit with diffusion(2), or without(1)'
      read*,choice

c     start of minpack, lmdif subroutine
      if (choice.eq.1) then
        n=2
        x1(1)=kappa
        x1(2)=k2
      else
        n=3
        x1(1)=kappa
        x1(2)=k2
        x1(3)=dab
      endif

      m=interplen
      ldfjac=interplen+1
      ftol=dsqrt(dpmpar(1))
      xtol=dsqrt(dpmpar(1))
      gtol=0.0
      maxfev=300*(n+1)
      epsfcn=0.d0
      mode=1
      factor=1.d2
      nprint=0
      call lmdif(fcn,m,n,x1,fvec1,ftol,xtol,gtol,maxfev,epsfcn,diag,
     *           mode,factor,nprint,info,nfev,fjac,ldfjac,ipvt,qtf,
     *           wa1,wa2,wa3,wa4)
      fnorm=enorm(m,fvec1)

c     writing results to file

      write(2,10) fnorm,nfev,info,(x1(j),j=1,n)

      if (choice.eq.2) then
```

```
      write(2,*) 'time gamth csub gamexp'
      do 7 y=1,interplen
      write(2,8) (y-1)*dt,gamth(y),csub(y),gamexp(y)
8      format(4(g13.6,1x))
7      continue
   elseif (choice.eq.1) then
      write(2,*) 'time gamth gamexp'
      do 17 y=1,interplen
      write(2,18) (y-1)*dt,gamth(y),gamexp(y)
18      format(3(g13.6,1x))
17      continue
   endif

   write(*,10) fnorm,nfev,info,(x1(j),j=1,n)
10    format ('#',5x,31h final l2 norm of the residuals,d15.7 /
   *        '#',5x,31h number of function evaluations, i10 /
   *        '#',5x,15h exit parameter,16x,i10 /
   *        '#',5x,27h final approximate solution / '#',5x,3d15.7/)
   end


   subroutine fcn(m,n1,x1,fvec1,iflag)
   implicit none
   integer*4 m,n1,iflag
   real*8 x1(n1),fvec1(m)
   real*8 gamth,csub,gamexp
   real*8 cb,dab,dt,kappa,k2,alpha,temp,error
   integer*4 y,count,choice

c    minpack routine for solution of n nonlinear equations in
c    n variables : will be using hybrid subroutine
c    fvec has been changed to fnlvec
c    fcn has been changed to func

   integer j,n,maxfev,ml,mu,mode,nprint,info,nfev,ldfjac,lr
   double precision xtol,epsfcn,factor,fnorm
   double precision x(2),fnlvec(2),diag(2),fjac(2,2),r1(3),qtf(2),
  *            wa1(2),wa2(2),wa3(2),wa4(2)
   double precision enorm,dpmpar

   external func
   common /data1/gamth(50000),csub(50000),gamexp(50000)
   common /data2/y
   common /data/dt,kappa,k2,cb,dab,alpha

   common /data3/choice

   count=0
   if(iflag.ne.0) goto 5
c    write(*,*)'nprint is positive'
   return
```

```
5    continue
     if (choice.eq.1) goto 9
     kappa=x1(1)
     k2=x1(2)
     dab=x1(3)

c    minpk routine for solving the system of two non-linear equations

     n=2
     ldfjac = n+1
     lr = n*(n+1)/2
c
c    set xtol to the square root of the machine precision.
c    unless high precision solutions are required,
c    this is the recommended setting.
c
     xtol = dsqrt(dpmpar(1))
c
     maxfev = 20000
     ml = n-1
     mu = n-1
     epsfcn = 0.d0
     mode = 2
     do 20 j = 1, n
       diag(j) = 1.d0
  20   continue
     factor = 1.d2
     nprint = 0

c
     gamth(1)=0
     csub(1)=cb
     do 7 y=2,m

          x(1)=gamth(y-1)
          x(2)=csub(y-1)

          call hybrd(func,n,x,fnlvec,xtol,maxfev,ml,mu,epsfcn,diag,
     *         mode,factor,nprint,info,nfev,fjac,ldfjac,
     *         r1,lr,qtf,wa1,wa2,wa3,wa4)

          fnorm = enorm(n,fnlvec)
          gamth(y)=x(1)
          csub(y)=x(2)
          fvec1(y)=gamexp(y)-gamth(y)
7    continue
     goto 15

c    end of section for diffusion inclusive fit

c    start of section for non-diffusion fit
```

```
9     kappa=x1(1)
      k2=x1(2)
c     minpk routine for solving the system of two non-linear equations

      n=1
      ldfjac = n+1
      lr = n*(n+1)/2
c
c     set xtol to the square root of the machine precision.
c     unless high precision solutions are required,
c     this is the recommended setting.
c
      xtol = 1d-3*dsqrt(dpmpar(1))
c
      maxfev = 20000
      ml = n-1
      mu = n-1
      epsfcn = 0.d0
      mode = 2
      do 21 j = 1, n
        diag(j) = 1.d0
   21   continue
      factor = 1.d2
      nprint = 0
      gamth(1)=1d-20

      error=0d0
      do 6 y=2,m

c         temp=log(1+kappa*cb*k2*(y-1)*dt)/k2
        x(1)=gamth(y-1)

        call hybrd(func,n,x,fnlvec,xtol,maxfev,ml,mu,epsfcn,diag,
     *       mode,factor,nprint,info,nfev,fjac,ldfjac,
     *       r1,lr,qtf,wa1,wa2,wa3,wa4)

        fnorm = enorm(n,fnlvec)
        gamth(y)=x(1)
        fvec1(y)=gamexp(y)-gamth(y)
        error=error+(gamth(y)-temp)**2
6     continue
c     write(*,*)count,dsqrt(error)
15    count=count+1
      write(*,*) count
          return
      end


      subroutine func(n,x,fnlvec,iflag)
      implicit none
```

```
      integer*4 n,iflag,y,i
      real*8 fnlvec(n),x(n),pi,gamexp,sum
      real*8 gamth,csub
      real*8 cb,dab,dt,kappa,k2,alpha
      common /data1/gamth(50000),csub(50000),gamexp(50000)
      common /data2/y
      common /data/dt,kappa,k2,cb,dab,alpha


      if(iflag.ne.0) goto 5
c     write(*,*)'nprint is positive'
      return
5     continue

      pi= 3.14159265359

c     kinetic model, that includes diffusion effects. employs the trapezoid rule
c     for evaluation of the integrals.
      if (n.eq.1) goto 4
      sum=0
      do 3 i=2,y-1
3     sum=sum+(csub(y+1-i)+csub(y-i))*(sqrt(float(i))-sqrt(float(i-1)))

      fnlvec(1)=x(1)-dsqrt(dab*dt/pi)*
     *      (2*cb*sqrt(float(y-1))-sum-csub(y-1)-x(2))
      fnlvec(2)=x(1)-kappa*dt*exp(-k2*x(1))*x(2)-gamth(y-1)
      goto 6
4     fnlvec(1)=x(1)-kappa*cb*dt*exp(-k2*x(1))-gamth(y-1)
c4    fnlvec(1)=x(1)-(log(1+kappa*cb*k2*(y-1)*dt))/k2
6     return
      end

      subroutine locate(xx,n,x,j)
c     given an array xx of length n, and given a value x, returns a value j
c     such that x is between xx(j) and xx(j+1). xx must be monotonic, either
c     increasing or decreasing, j=0, or j=n is returned to indicate that x is
c     out of range.
      implicit none
      integer*4 j,n
      real*8 x,xx(n)
      integer*4 jl,jm,ju
      jl=0
      ju=n+1
10    if(ju-jl.gt.1)then
        jm=(ju+jl)/2
       if((xx(n).ge.xx(1)).eqv.(x.ge.xx(jm)))then
        jl=jm
       else
        ju=jm
       endif
      goto 10
```

```
endif
if(x.le.xx(1))then
  j=1
else if(x.ge.xx(n))then
  j=n-1
else
  j=jl
endif
  return
end
```

Appendix B Implicit Alternating-Direction (IAD) method[129]

B.1 Finite-difference formulation

The convection-diffusion equation that is of interest to us was discussed earlier in chapter 5. It is repeated below:

$$\frac{\partial C(x,y,t)}{\partial \theta} + Y(1-Y)\frac{\partial C(x,y,t)}{\partial X} = \frac{1}{Pe}\frac{\partial^2 C(x,y,t)}{\partial Y^2} \tag{1}$$

with the following boundary and initial conditions:

$$\theta = 0,\ C = 0 \quad for all\ Y, X > 0 \tag{2}$$

$$X = 0,\ C = 1 \quad for all\ Y, \theta \tag{3}$$

$$Y = 1,\ C = 1 \quad for all\ X, \theta \geq 1 \tag{4}$$

The above PDE will have to be converted to finite difference form so as to enable the solution using the ADI algorithm that is described in the next paragraph. The first and second derivatives are approximated by the difference formula as given below:

$$\frac{\partial C_{ij}}{\partial x} = \frac{C_{i+1,j} - C_{i-1,j}}{2\Delta x};\ \frac{\partial^2 C}{\partial x^2} = \frac{C_{i+1,j} - 2C_{ij} + C_{i-1,j}}{(\Delta x)^2} \tag{5}$$

The concentration is a function of x,y and t (i.e.), C=C(x,y,t). In this section, the subscript 'i' refers to x direction, and 'j' refers to the y direction. It should be mentioned here that in order to write a FORTRAN code for this method we have used the following notation: the space domain is split into n_x and n_y steps in the x and y directions of step sizes Δx and Δy respectively. In addition, the representation of a distance y is in the form (j-1)Δy, since the array starts from 1..n_y while the distances are from 0..y. We now give a brief introduction to the IAD method.

The IAD method is a numerical method that is a variation of the Crank-Nicholson (C-N) algorithm. It is used to solve a partial differential equation in two dimensions. It is second-order accurate in both time and space, and is unconditionally stable. When using this method, the equations are easier to solve than when one uses the C-N method. It embodies the powerful concept of operator splitting or time splitting. Essentially, the principle is to employ two difference equations, which are used in turn over successive time-steps each of duration $\Delta t/2$. The first equation is implicit only in x-direction and the second is implicit only in the y-direction. In each sub-step, a different dimension is treated implicitly. In this method we will advance in x direction for the first half of the time step and then in the y direction for the next half. Thus if $\bar{C}_{ij}$ is an intermediate value at the end of the first half time-step (i.e.) X sweep, we have:

$$\frac{\bar{C}_{ij}-C_{ijn}}{\Delta\theta/2}=\frac{1}{Pe}\left[\frac{C_{ij-1n}-2C_{ijn}+C_{ij-1n}}{(\Delta y)^2}\right]+(j-1)\Delta y\left[(j-1)\Delta y-1\right]\left[\frac{\bar{C}_{i-1j}-\bar{C}_{i-1j}}{2\Delta x}\right] \qquad (6)$$

The second half of the time step would be in the y direction (i.e.) Y sweep:

$$\frac{C_{ijn+1}-\bar{C}_{ij}}{\Delta\theta/2}=\frac{1}{Pe}\left[\frac{C_{ij-1n+1}-2C_{ijn+1}+C_{ij-1n+1}}{(\Delta y)^2}\right]+(j-1)\Delta y\left[(j-1)\Delta y-1\right]\left[\frac{\bar{C}_{i-1j}-\bar{C}_{i-1j}}{2\Delta x}\right] \qquad (7)$$

When these equations are written out in full and rearranged, these equations become:

$$r_j\bar{C}_{i-1j}+\bar{C}_{ij}-r_j\bar{C}_{i+1j}=r_2C_{ij-1n}+(1-2r_2)C_{ijn}+r_2C_{ij+1n} \qquad (8)$$

$$-r_2C_{ij-1n+1}+(1+2r_2)\,C_{ijn+1}-r_2C_{ij+1n+1}=-r_j\bar{C}_{i-1j}+\bar{C}_{ij}-r_j\bar{C}_{i+1j} \qquad (9)$$

$$r_j=\frac{\Delta\theta\Delta y}{4\Delta x}(j-1)\left[(j-1)\Delta y-1\right];\ r_2=\left(\frac{1}{Pe}\right)\left(\frac{\Delta\theta}{2(\Delta y)^2}\right) \qquad (10)$$

Equation (5.11) is the simplified form of the equation in the X-sweep, and equation (5.13) is the same for the Y-sweep. For the boundary condition at the surface, the derivative is written as:

$$\left.\frac{\partial C_{ij}}{\partial y}\right|_{y=0} = \frac{C_{i2} - C_{i1}}{\Delta y} = DaC_{i1}exp(-\Gamma) \qquad (11)$$

Equations (5.2) and (9) are now written for i=2..n_x, and j=2..n_y respectively. This will give us a system of tridiagonal equations that can be easily solved. The boundary and initial conditions (2)-(4) are now written in finite difference form. The FORTRAN code for the solution of this PDE is given in the next section.

B.2 FORTRAN Code

```
      program condiffnozerofin

c     implicit director method
c     convection diffusion model
c     the boundary condition at the plate surface has been used to define
c     with a forward difference operator
c     the difference between this and condiffreal8nozero.f is that here
c     a different step size has been used for space and another for time
c     with the only difference being that the stability criterion
c     mod(bi)>mod(ai)+mod(ci) is satisfied at all times

c     no gamave, and csub arrays used. just put them in temporary variables
c     from one time step to next

      implicit none
      real*8 ai(2000),bi(2000),ci(2000),di(2000),conc(500,2000)
      real*8 concstar(500,2000),gamave,csub,gamavelast
      real*8 dx,dy,dtheta,theta,concprime(2000),beta
      real*8 l,b,gamdot,pe,da,dab,k1,k2,w,cb,alpha,q,taustar,rj,r2
      real*8 rtsafe,sum,dimmax
      real*8 t0,t1,elapsed

c     the above variables : t1,t0, and elapsed are to calculate process time

      external funcd
      integer i,j,icount,npx1,npy1,nx,ny,temp,facx,facy,tmax,fac1
      common /z1/gamavelast,csub
      common /z3/da,alpha,pe,dtheta
```

```
      namelist /pdata/cb,dtheta,k1,k2,dab,q,b,w,l,dx,dy,facx,facy,tmax
      t0=0d0
      t1=secnds(t0)
      open(1,file='condiffnozerofin.dat',access='sequential'
     *     ,status='unknown')
      read(1,pdata)
      open(2,file='condiffnozerofin.res',status='new')
      open(3,file='condiff_concnozerofin.res',status='new')
      open(4,file='condiffnozerofininit.res',status='new')
      gamdot=6*q*1d-6/(3600*b*b*w)
      pe=gamdot*(b**3)/(l*dab)
      taustar=l/(gamdot*b)
      alpha=k2*b*cb
      da=k1*b/dab
      dimmax=tmax/(dtheta*taustar)
      sum=dimmax/30000
      fac1=int(sum)+1
      write(*,*) gamdot,pe,taustar,alpha,da,dimmax,k1,k2,dtheta,q,dx,dy,cb
      write(2,20) gamdot,pe,taustar,alpha,da,dimmax,k1,k2,dtheta,q,dx,dy,cb
      write(3,20) gamdot,pe,taustar,alpha,da,dimmax,k1,k2,dtheta,q,dx,dy,cb
      write(4,20) gamdot,pe,taustar,alpha,da,dimmax,k1,k2,dtheta,q,dx,dy,cb
      nx=1/dx
      ny=1/dy
      npx1=nx+1
      npy1=ny+1
      r2=dtheta/(2*pe*dy*dy)
      theta=0d0
      icount=1
      gamave=0d0
      gamavelast=0d0
      csub=1d0

c     set initial values

     do 33 i=2,npx1
     do 33 j=1,npy1
     conc(i,j)=1d0
     concstar(i,j)=1d0
33    continue

c     entering time loop
c     setting boundary values

4     do 3 j=1,npy1
      conc(1,j)=1d0
      concstar(1,j)=1d0
3     continue
      do 31 i=1,npx1
      conc(i,npy1)=1d0
      concstar(i,npy1)=1d0
31    continue
```

```
c    writing the concentration values into the file
c    the first few data points are written onto a different results file

     if (icount.le.3*fac1*facy) then
     write(*,*),'icount=',icount
     write(4,*) theta*taustar,gamave/k2,csub*cb
     endif

c    selectively writing data onto file

     if ((icount.eq.1).or.(mod(icount,facy*fac1).eq.0)) then
     write(*,*),'icount=',icount
     write(3,201) theta
     write (3,202) conc(1,1),(conc(1,j*facy),j=1,ny/facy),conc(1,npy1)
     do 15 i=1,nx/facx
     write (3,202) conc(i*facx,1),(conc(i*facx,j*facy),j=1,ny/facy),
    *conc(i*facx,npy1)
15   continue
     write(3,*)
     write(3,*)
     write(2,*) theta*taustar,gamave/k2,csub*cb
     endif

     theta=theta+dtheta
     icount=icount+1
     sum=0d0

c    use of the implicit form in describing the flux condition at the \
c    adsorption surface (i.e.)
c    dc/dy=da*c(i,1)*exp(-gamave(icount-1))
c    (c(i,2)-c(i,1))/dy=da*c(i,1)*exp(-gamave(icount-1))
c    c(i,2)/(1+beta)=c(i,1)

     beta=dy*da*exp(-gamavelast)

c    perform calcualtions over successive time steps

c    compute temperatures at end of half time increment (implicit by columns)
c    X SWEEP

     do 8 j=2,ny
     rj=(dtheta*dy/(4*dx))*(j-1)*((j-1)*dy-1)
     do 7 i=2,nx
     ai(i)=rj
     bi(i)=1d0
     ci(i)=-rj
          if (dabs(bi(i)).lt.(dabs(ai(i))+dabs(ci(i)))) then
             write(*,*) 'xsweep, taudxdy error',i
                  pause
          endif
```

```
      if (j.ne.2) then
          di(i)=r2*(conc(i,j+1)+conc(i,j-1))+(1-2*r2)*conc(i,j)
      else
          di(i)=conc(i,2)*((r2/(1+beta))+1-2*r2)+conc(i,3)*r2
           endif
7     continue
      di(nx)=di(nx)+rj*concstar(npx1,j)
           di(2)=di(2)-rj*concstar(1,j)
      call tridag1(2,nx,ai,bi,ci,di,concprime)
      do 9 i=2,nx
      concstar(i,j)=concprime(i)
9     continue
8     continue

c     compute temperatures at the end of the whole time increment (implicit by rows)
c     Y SWEEP

      do 10 i=2,nx
      do 11 j=2,ny
      rj=(dtheta*dy/(4*dx))*(j-1)*((j-1)*dy-1)
      ai(j)=-r2
      bi(j)=1+2*r2
      ci(j)=-r2
           if (dabs(bi(j)).lt.(dabs(ai(j))+dabs(ci(j)))) then
              write(*,*) 'ysweep, taudydx error',j
                   pause
           endif
      di(j)=concstar(i,j)+rj*(concstar(i+1,j)-concstar(i-1,j))
11    continue
      bi(2)=bi(2)-r2/(1+beta)
           di(ny)=di(ny)+r2*conc(i,npy1)
      call tridag1(2,ny,ai,bi,ci,di,concprime)
      do 12 j=2,ny
      conc(i,j)=concprime(j)
12    continue
      conc(i,1)=conc(i,2)/(1+beta)
      sum=sum+conc(i,1)
10    continue
      csub=(sum+conc(1,1)+conc(npx1,1))/npx1
      gamave=rtsafe(funcd,gamavelast,1d3,1d-6)
           gamavelast=gamave
      if ((dtheta*icount*taustar).le.tmax) goto 4
201   format('at a time theta=',g15.8//)
202   format(32g15.8)
20    format('gamdot=',g15.8/'pe=',g15.8/'taustar=',g15.8/'alpha=',g15.8
     *    /'da=',g15.8/'dimmax=',i10/'k1=',g15.8/'k2=',g15.8/'dtheta=',
     *    g15.8/'q=',g15.8/'dx=',g15.8/'dy=',g15.8/'cb=',g15.8)
           elapsed=secnds(t1)
           write(*,*) 'total time in secs = ',elapsed
      end
```

```
      subroutine tridag1(low,high,a,b,c,d,vec)
      implicit none
      integer high,low,n
      real*8 a(high-low+1),b(high-low+1),c(high-low+1),d(high-low+1)
      real*8 vec(high-low+1)
c     the value of n should be atleast high-low+1
      parameter (n=2000)
      real*8 bet,gam(n)
      integer j
      if(b(low).eq.0.)pause 'tridag: rewrite equations'
      bet=b(low)
      vec(low)=d(low)/bet
      do 11 j=low+1,high,1
       gam(j)=c(j-1)/bet
       bet=b(j)-a(j)*gam(j)
       if(bet.eq.0.)pause 'tridag failed'
       vec(j)=(d(j)-a(j)*vec(j-1))/bet
11    continue
      do 12 j=high-1,low,-1
       vec(j)=vec(j)-gam(j+1)*vec(j+1)
12    continue
      return
      end

      subroutine funcd(rtsafe,f,df)
      implicit none
      real*8 rtsafe,f,df,gamavelast,csub,da,alpha,pe,dtheta
      common /z1/gamavelast,csub
      common /z3/da,alpha,pe,dtheta
      f=rtsafe-gamavelast-dtheta*da*alpha*csub*exp(-rtsafe)/pe
      df=1+dtheta*da*alpha*csub*exp(-rtsafe)/pe
      return
      end


      function rtsafe(funcd,x1,x2,xacc)
      implicit none
      integer maxit
      real*8 rtsafe,x1,x2,xacc
      external funcd
      parameter (maxit=1000)
      integer j
      real*8 df,dx,dxold,f,fh,fl,temp,xh,xl
      call funcd(x1,fl,df)
      call funcd(x2,fh,df)
      if((fl.gt.0..and.fh.gt.0.).or.(fl.lt.0..and.fh.lt.0.))pause
     *    'root must be bracketed in rtsafe'
      if(fl.eq.0.)then
       rtsafe=x1
       return
```

```
      else if(fh.eq.0.)then
        rtsafe=x2
        return
      else if(fl.lt.0.)then
        xl=x1
        xh=x2
      else
        xh=x1
        xl=x2
      endif
      rtsafe=.5*(x1+x2)
      dxold=abs(x2-x1)
      dx=dxold
      call funcd(rtsafe,f,df)
      do 11 j=1,maxit
        if(((rtsafe-xh)*df-f)*((rtsafe-xl)*df-f).ge.0..or. abs(2.*
     *      f).gt.abs(dxold*df) ) then
          dxold=dx
          dx=0.5*(xh-xl)
          rtsafe=xl+dx
          if(xl.eq.rtsafe)return
        else
          dxold=dx
          dx=f/df
          temp=rtsafe
          rtsafe=rtsafe-dx
          if(temp.eq.rtsafe)return
        endif
        if(abs(dx).lt.xacc) return
        call funcd(rtsafe,f,df)
        if(f.lt.0.) then
          xl=rtsafe
        else
          xh=rtsafe
        endif
11    continue
      pause 'rtsafe exceeding maximum iterations'
      return
      end
```

Appendix C Nomenclature

A	integrated absorption
α	absorption coefficient
C_{bulk}	bulk solution concentration
C_i	interfacial concentration
d_e	effective thickness
d_p	penetration depth
ε	molecular emmisivity, molar absorptivity
E_0	electric field amplitude at the interface, in the rarer medium
E_{0i}	electric field amplitude at the interface, in the i-direction
$E_\perp$	electric field amplitude of the perpendicular polarization
$E_{\|\|}$	electric field amplitude of the parallel polarization
Γ_i	Surface excess, Surface Coverage
η	Refractive index
φ	angle of refraction
ℓ	film thickness
N	number of reflections
θ	angle of incidence
R	reflectivity

Bibliography

1) Bigelow, W. C.; Pickett, D. L.; Zisman, W. A. *Journal of Colloid and Interface Science* **1947**, *1*, 513-538.

2) Sagiv, J. *J. Amer. Chem. Soc.* **1980**, *102*, 92-98.

3) Cohen, S. R.; Naaman, R.; Sagiv, J. *J. Phys. Chem.* **1986**, *90*, 3054-3056.

4) Gun, J.; Iscovici, R.; Sagiv, J. *J. Colloid Interface Sci.* **1984**, *101*, 201-213.

5) Gun, J.; Sagiv, J. *J. Colloid Interface Sci.* **1986**, *112*, 457-472.

6) Maoz, R.; Sagiv, J. *J. Colloid Interface Sci.* **1984**, *100*, 465-496.

7) Ulman, A. *An Introduction to Ultrathin Organic Films, from Langmuir-Blodgett to Self-Assembly*; Academic Press: San Diego, 1991.

8) Schlotter, N. E.; Porter, M. D.; Bright, T. B.; Allara, D. L. *Chemical Physics Letters* **1986**, *132*, 93-98.

9) Allara, D. L.; Nuzzo, R., G. *Langmuir* **1985**, *1*, 45-52.

10) Allara, D. L.; Nuzzo, R. G. *Langmuir* **1985**, *1*, 52-66.

11) Bain, C. D.; Troughton, B. E.; Tao, Y.-T.; Evall, J.; Whitesides, G. M.; Nuzzo, R. G. *J. Am. Chem. Soc.* **1989**, *111*, 321-335.

12) Finklea, H. O.; Robinson, L. R.; Blackburn, A.; Richter, B.; Allara, D. L.; Bright, T. *Langmuir* **1986**, *2*, 239-244.

13) Carson, G.; Granick, S. *Journal of Applied Polymer Science* **1989**, *37*, 2767-2772.

14) Sagiv, J.; Ziona, N.; Rubinstein, I.; le-Zion, R.; Steinberg, S.; Shanzer, A.; Tor, Y. *Ionic Recognition and Selective Response in SAM membranes on electrodes*; Yeda Research and Development Company Limited, Rehovot, Israel: Israel, 1990.

15) Steinberg, S.; Tor, Y.; Sabatani, E.; Rubinstein, I. *J. Am. Chem. Soc.* **1991**, *113*, 5176-5182.

16) Steinberg, S.; Rubinstein, I. *Langmuir* **1992**, *8*, 1183-1187.

17) Swalen, J. D. *Annu. Rev. Mater. Sci.* **1991**, *21*, 373-408.

18) Edelman, P. G.; Wang, J. *Biosensors and Chemical Sensors; Optimizing Performance Through Polymeric Materials*; ACS: Altanta, 1992; Vol. 487, pp 332.

19) DePalma, V.; Tillman, N. *Langmuir* **1989**, *5*, 868-872.

20) Meyer, E.; Overney, R.; Brodbeck, D.; Howald, L.; Lüthi, R.; Frommer, J.; Güntherodt, H.-J. *Physical Review Letters* **1992**, *69*, 1777-1780.

21) Helbert, J. N.; Hughes, H. G. *Organosilanes as process compatible adhesion promoters for resist materials*; Mittal, K. L., Ed.; Plenum: New York, NY, 1981, pp 499-508.

22) Nawrocki, J.; Buszewski, B. *Journal of Chromatography* **1988**, *449*, 1-24.

23) Abel, E. W.; Pollard, F. H.; Uden, P. C.; Nickless, G. *Journal of Chromatography* **1966**, *22*, 23.

24) van Roosmalen, A. J.; Mol, J. C. *Journal of Physical Chemistry* **1979**, *83*, 2485-2488.

25) Kallury, K. M. R.; Krull, U. J.; Thompson, M. *Analytical Chemistry* **1988**, *60*, 169.

26) Angst, D. L.; Simmons, G. W. *Langmuir* **1991**, *7*, 2236-2242.

27) Le Grange, J. D.; Markham, J. L.; Kurkjian, C. R. *Langmuir* **1993**, *9*, 1749-1753.

28) Silberzan, P.; Léger, L.; Ausserré, D.; Benattar, J. J. *Langmuir* **1991**, *7*, 1647-1651.

29) Wasserman, S. R.; Tao, Y.-T.; Whitesides, G. M. *Langmuir* **1989**, *5*, 1074-1087.

30) Ulman, A. *Advanced Materials* **1990**, *2*, 573-582.

31) Tripp, C. P.; Hair, M. L. *Langmuir* **1992**, *8*, 1120-6.

32) Banga, R.; Yarwood, J.; Morgan, A. M. *Langmuir* **1995**, *11*, 618-622.

33) Karpovich, D. S.; Blanchard, G. J. *Langmuir* **1994**, *10*, 3315-3322.

34) Pan, W.; Durning, C. J.; Turro, N. J. *Langmuir* **1996**, *12*, 4469-4473.

35) Peterlinz, K. A.; R., G. *Langmuir* **1996**, *12*, 4731-4740.

36) Chen, S. H.; Frank, C. W. *Langmuir* **1989**, *5*, 978-987.

37) Chen, S. H.; Frank, C. W. *n-Alkanoic Acid Self-Assembled Monolayer Adsorption Kinetics*; Scheuing, D. R., Ed.; American Chemical Society: Boston, 1990, pp 160-176.

38) Kessel, C. R.; Granick, S. *Langmuir* **1991**, *7*, 532-538.

39) Gaines, G. L. *Insoluble monolayers at Liquid-Gas Interfaces*; InterScience: New York, 1966.

40) Beredjick, N.; Burlant, W. J. *Journal of Polymer Science: Part A-1* **1970**, *8*, 2807-2818.

41) Brinker, C. J.; Scherer, G. W. *Sol-Gel Science, The Physics and Chemistry of Sol-Gel Processing*; Academic Press, Inc.: New York, 1990.

42) Ariga, K.; Okahata, Y. *Journal of the American Chemical Society* **1989**, *111*, 5618-5622.

43) Lindén, M.; Slotte, J. P.; Rosenholm, J. B. *Langmuir* **1996**, *12*, 4449-4454.

44) Sjöblom, J.; Stakkestad, G.; Ebeltoft, H.; Friberg, S. E.; Claesson, P. *Langmuir* **1995**, *11*, 2652-2660.

45) Cheng, S. S.; Scherson, D. A.; Sukenik, C. N. *J. Am. Chem. Soc.* **1992**, *114*, 5436-5437.

46) Kellar, J. J.; Cross, W. M.; Miller, J. D. *Applied Spectroscopy* **1990**, *44*, 1508-1512.

47) Kellar, J. J.; Cross, W. M.; Miller, J. D. *Applied Spectroscopy* **1989**, *43*, 1456-1459.

48) Couzis, A.; Gulari, E. *Langmuir* **1993**, *9*, 3414-21.

49) Couzis, A.; Gulari, E. *Macromolecules* **1994**, *27*, 3580-3588.

50) Green, J.-B. D.; McDermott, M. T.; Porter, M. D. *J. Phys. Chem.* **1996**, *100*, 13342-13345.

51) Guyot-Sionnest, P.; Superfine, R.; Hunt, J. H.; Shen, Y. R. *Chemical Physics Letters* **1988**, *144*, 1-5.

52) Buck, M.; Grunze, M.; Eisert, F.; Fischer, J.; Träger, F. *Journal of Vacuum Science and Technology. A.* **1992**, *10*, 926-929.

53) Hines, M. A.; Todd, J. A.; Guyot-Sionnest, P. *Langmuir* **1995**, *11*, 493-497.

54) Bain, C. D.; Davies, P. B.; Ward, R. N. *Langmuir* **1994**, *10*, 2060-2063.

55) DeBono, R. F.; Loucks, G. D.; Manna, D. D.; Krull, U. J. *Canadian Journal of Chemistry* **1996**, *74*, 677-688.

56) Harrick, N. J. *Internal Reflection Spectroscopy*; Interscience Publishers: New York, 1967.

57) Colthup, N. B.; Daly, L. H.; Wiberley, S. E. *Introduction to Infrared and Raman Spectroscopy*; Third ed.; Academic Press: New York, 1990.

58) Sperline, R. P.; Muralidharan, S.; Freiser, H. *Langmuir* **1987**, *3*, 198-202.

59) Sperline, R. P.; Muralidharan, S.; Freiser, H. *Appl. Spectr.* **1986**, *40*, 1019-1022.

60) Couzis, A. *Adsorption of polymers and surfactants from solution onto the solid-liquid interface*; The University of Michigan, 1992.

61) Couzis, A.; Gulari, E. *Acs Symp. Ser* **1992**, *501(Mixed Surfactant Syst.)*, 354-65.

62) Higashiyama, T.; Takenaka, T. *Journal of Physical Chemistry* **1974**, *78*, 941-947.

63) Kuzmenka, D. J.; Granick, S. *Coll. Surf.* **1988**, *31*, 105-116.

64) Mielczarski, J. A.; Mielczarski, E. *J. Phys. Chem.* **1995**, *99*, 3206-3217.

65) Sperline, R. P.; Freiser, H. *Langmuir* **1990**, *6*, 344-7.

66) Hair, M. L.; Tripp, C. P. *Colloids and Surfaces A: Physiochemical and Engineering Aspects* **1995**, *105*, 95-103.

67) Tripp, C. P.; Kazmaier, P.; Hair, M. L. *Langmuir* **1996**, *12*, 6402-6406.

68) Tripp, C. P.; Hair, M. L. *Langmuir* **1995**, *11*, 1215-19.

69) Tripp, C. P.; Hair, M. L. *Langmuir* **1992**, *8*, 1961-1967.

70) Tripp, C. P.; Hair, M. L. *Langmuir* **1991**, *7*, 923-927.

71) Claassen, W. C. M.; Dieleman, J. *J. Vac. Sci. Technol. B* **1987**, *5*, 1450-1452.

72) Iwamoto, R.; Ohta, K. *Applied Spectroscopy* **1984**, *38*, 359-365.

73) Ohta, K.; Iwamoto, R. *Applied Spectroscopy* **1985**, *39*, 418-425.

74) Ohta, K.; Iwamoto, R. *Analytical Chemistry* **1985**, *57*, 2491-99.

75) Tompkins, H. G. *Applied Spectroscopy* **1974**, *28*, 335.

76) Kumar, V.; Krishnan, S.; Steiner, C.; Maldarelli, C.; Couzis, A. *Journal of Physical Chemistry, B:* **1998**, *102*, 3152-3159.

77) Smith, A. L. *Applied Infrared Spectroscopy*; Interscience: New York, 1979.

78) Harrick, N. J.; Beckmann, K. H. *Internal Reflection Spectroscopy*; Interscience Publishers: New York.

79) Griffiths, P. R. *Chemical Infrared Fourier Transform Spectroscopy*; Interscience: New York, 1975.

80) Hair, M. L. *Infrared Spectroscopy in Surface Chemistry*; Marcel Dekker, INC.: New York, 1967.

81) Diem, M. *Introduction to Modern Vibrational Spectroscopy*; Wiley-Interscience: New York, 1993.

82) Parikh, A. N.; Allara, D. L.; Azouz, I. B.; Rondelez, F. *J. Phys. Chem.* **1994**, *98*, 7577-7590.

83) Jang, W.-H.; Miller, J. D. *The Journal of Physical Chemistry* **1995**, *99*, 10272-10279.

84) Porter, M. D.; Bright, T. B.; Allara, D. L.; Chidsey, C. E. D. *Journal of American Chemical Society* **1987**, *109*, 3559-3568.

85) Sperline, R. P.; Song, Y.; Freiser, H. *Langmuir* **1992**, *8*, 2183-2191.

86) Sperline, R. P.; Song, Y.; Freiser, H. *Langmuir* **1994**, *10*, 37-44.

87) Kellar, J. J.; Young, C. A.; Knutson, K.; Miller, J. D. *Journal of Colloid and Interface Science* **1991**, *144*, 381-389.

88) Laibinis, P. E.; Whitesides, G. M.; Allara, D. L.; Tao, Y.-T.; Parikh, A. N.; Nuzzo, R. G. *J. Am. Chem. Soc.* **1991**, *113*, 7152-7167.

89) Kimura, F.; Umemura, J.; Takenaka, T. *Langmuir* **1986**, *2*, 96-101.

90) Fang, J.; Knobler, C. M. *The Journal of Physical Chemistry* **1995**, *99*, 10425-10429.

91) Barton, S. W.; Goudot, A.; Rondelez, F. *Langmuir* **1991**, *7*, 1029-1030.

92) Samha, H.; DeArmond, M. K. *Langmuir* **1993**, *9*, 1927-1929.

93) Bourdieu, L.; Daillant, J.; Chatenay, D.; Colson, D. *Physical Review Letters* **1994**, *72*, 1502-05.

94) Kirchnerová, J.; Cave, G. C. B. *Canadien Journal of Chemistry* **1976**, *54*, 3909-3916.

95) Dubault, A.; Casagrande, C.; Veyssie, M. *Journal of Physical Chemistry* **1975**, *79*, 2254-2259.

96) Meller, P.; Peters, R.; Rinsdorf, H. *Colloid Polymer Science* **1989**, *267*, 97-107.

97) Baraton, M. I.; Jaffrezic, N.; Quintard, P. *J. Molec. Struc.* **1992**, *267*, 353-358.

98) Wasserman, S. R.; Whitesides, G. M.; Tidswell, I. M.; Ocko, B. M.; Pershan, P. S.; Axe, J. D. *J. Am. Chem. Soc.* **1989**, *111*, 5852-5861.

99) Schwartz.D.K.; Steinberg.S.; Israelachvili.J.; Zasadzinski.J.A.N. *Physical Review Letters* **1992**, *69*, 3354-57.

100) Britt, D. W.; Hlady, V. *J. Coll. Interface Sci.* **1996**, *178*, 775-784.

101) Bierbaum, K.; Grunze, M.; Baski, A. A.; Chi, L. F.; Schrepp, W.; Fuchs, H. *Langmuir* **1995**, *11*, 2143-2150.

102) McGovern, M. E.; Kallury, K. M. R.; Thompson, M. *Langmuir* **1994**, *10*, 3607-14.

103) Allara, D. L.; Parikh, A. N.; Rondelez, F. *Langmuir* **1995**, *11*, 2357-2360.

104) Banga, R.; Yarwood, J.; Morgan, A. M.; B., E.; Kells, J. *Thin Solid Films* **1996**, *284-285*, 261-266.

105) Banga, R.; Yarwood, J.; Morgan, A. M.; B., E.; Kells, J. *Langmuir* **1995**, *11*, 4393-4399.

106) Kumar, N.; Steiner, C.; Maldarelli, C.; Couzis, A. *Langmuir* **1998**, *Under Preparation.*

107) Tripp, C. P.; Hair, M. L. *Langmuir* **1995**, *11*, 149-155.

108) Xu, S.; Cruchon-Dupeyrat, S. J. N.; Garno, J. C.; Liu, G.-Y.; Jennings, G. K.; Yong, Y.-H.; Laibinis, P. E. *Journal of Chemical Physics* **1998**, *108*, 5002-5012.

109) Adamson, A. W. *Physical Chemistry of Surfaces*; Second ed.; Interscience Publishers: New York, 1967.

110) Biebuyck, H. A.; Bain, C. D.; Whitesides, G. M. *Langmuir* **1994**, *10*, 1825-1831.

111) Zhao, X.; Kopelman, R. *Journal of Physical Chemistry* **1996**, *100*, 11014-11018.

112) Folkers, J. P.; Laibinis, P. E.; Whitesides, G. M. *Langmuir* **1992**, *8*, 1330-1341.

113) Offord, D. A.; Griffin, J. H. *Langmuir* **1993**, *9*, 3015-3025.

114) MacRitchie, F.; Alexander, A. E. *Journal of Colloid Science* **1963**, *18*, 453-457.

115) MacRitchie, F. *Chemistry At Interfaces*; Academic Press: New York, 1989.

116) Kumar, V. *2-Dimensional assembly of surfactants at the solid/water and air/water interfaces*; City College and Graduate Centre of City University of New York: New York, 1998.

117) Chang, C. H.; Frances, E. I. *Colloids and Surfaces* **1992**, *69*, 189-201.

118) Ward, A. F. H.; Tordai, L. *The Journal of Chemical Physics* **1946**, *14*, 453-461.

119) Sutherland, K. L. *Aust. J. Sci. Res., Ser. A* **1952**, *5*, 683.

120) Adamczyk, Z.; Petlicki, J. *Journal of Colloid and Interface Science* **1987**, *118*, 20-49.

121) Adamczyk, Z. *Journal of Colloid and Interface Science* **1987**, *120*, 477-485.

122) Miller, R.; Kretzchmar, G. *Advances in Colloid and Interface Science* **1991**, *37*, 97-121.

123) Lok, B. K.; Cheng, Y.-L.; Robertson, C. R. *Journal of Colloid and Interface Science* **1983**, *91*, 104-116.

124) Shibata, C. T.; Lenhoff, A. M. *Journal of Colloid and Interface Science* **1992**, *148*, 485-507.

125) Kim, D.; Cha, W.; Beissinger, R. L. *Journal of Colooid and Interface Science* **1993**, *159*, 1-8.

126) Filippov, L. K. *Journal of Colloid and Interface Science* **1995**, *174*, 32-39.

127) Filippov, L. K. *Journal of Colloid and Interface Science* **1996**, *182*, 330-347.

128) Filippov, L. K.; Filippova, N.L. *Journal of Colloid and Interface Science* **1997**, *189*, 1-16.

129) Carnahan, B.; Luther, H. A.; Wilkes, J. O. *Applied Numerical Methods*; Wiley: New York, 1969.

130) Lin, S.-Y.; McKeigue, K.; Maldarelli, C. *Langmuir* **1991**, *7*, 1055-1066.

IMAGE EVALUATION
TEST TARGET (QA-3)

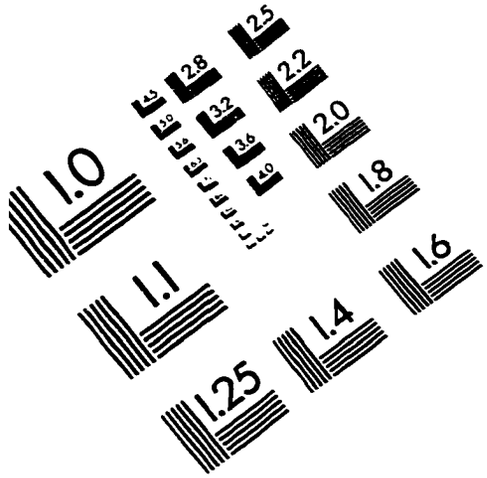

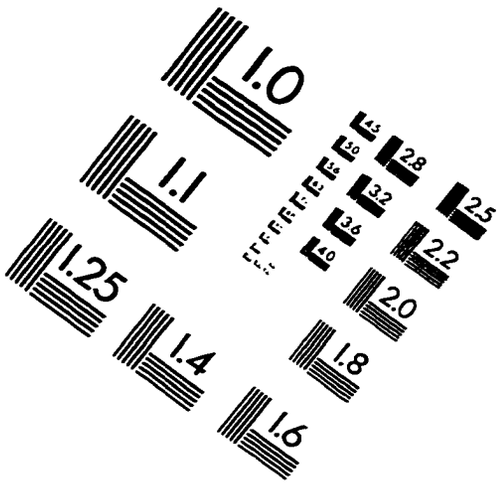

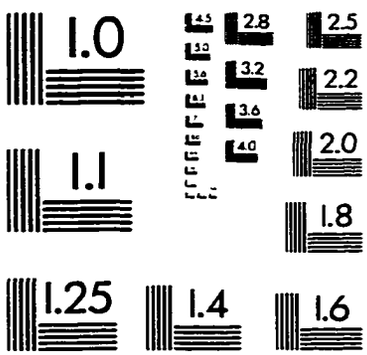

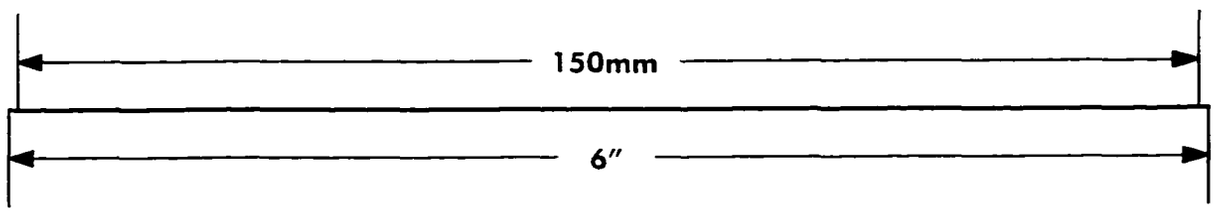

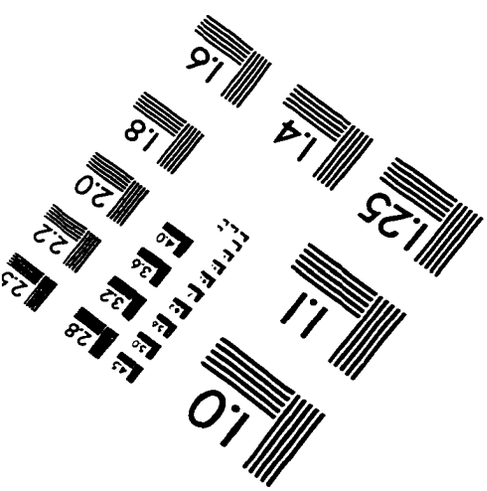

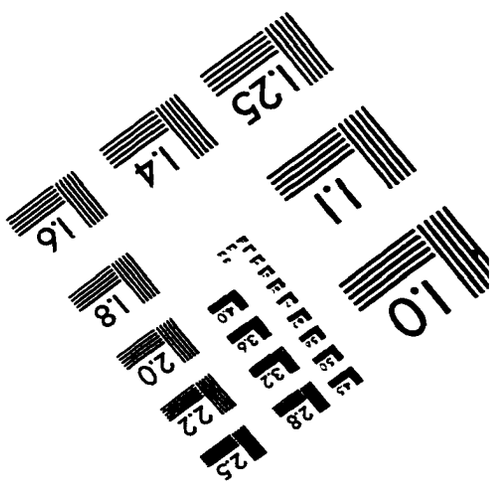

APPLIED IMAGE, Inc
1653 East Main Street
Rochester, NY 14609 USA
Phone: 716/482-0300
Fax: 716/288-5989